Advanced Restraint Systems (ARS)

Final Report

CAMP

Advanced Restraint Systems

Ford   GM

Mercedes-Benz

Advanced Restraint Systems

DISCLAIMER

This publication is distributed by the U.S. Department of Transportation, National Highway Traffic Safety Administration, in the interest of information exchange. The opinions, findings, and conclusions expressed in this publication are those of the authors and not necessarily those of the Department of Transportation or the National Highway Traffic Safety Administration. The United States Government assumes no liability for its contents or use thereof. If trade names, manufacturers' names, or specific products are mentioned, it is because they are considered essential to the object of the publication and should not be construed as an endorsement. The United States Government does not endorse products or manufacturers.

Technical Report Documentation Page

1. Report No. DOT HS 811 794A	2. Government Accession No.	3. Recipient's Catalog No.	
4. Title and Subtitle Advanced Restraint Systems (ARS) Final Report		5. Report Date July 2013	
		6. Performing Organization Code	
7. Author(s) Stephen Cassatta, Mark Cuddihy, Mark Huber, Matthias Struck, Para Weerappuli and Mike Scavnicky		8. Performing Organization Report No.	
9. Performing Organization Name and Address Crash Avoidance Metrics Partnership on behalf of the Advanced Restraint Systems Consortium 27220 Haggerty Road, Suite D-1 Farmington Hills, MI 48331		10. Work Unit No. (TRAIS)	
		11. Contract or Grant No. DTNH22-05-H-01277	
12. Sponsoring Agency Name and Address National Highway Traffic Safety Administration 1200 New Jersey Avenue, SE. Washington, DC 20590		13. Type of Report and Period Covered	
		14. Sponsoring Agency Code	
15. Supplementary Notes			

16. Abstract

This report presents a summary of the work performed during the Advanced Restraint Systems (ARS) project. The primary objective of this effort was to evaluate the potential benefit of using pre-crash information associated with two unique crash configurations (one vehicle-to-vehicle scenario and one vehicle-to-object scenario) to tailor an advanced restraint system to the occupant and crash type. The project work encompassed the Computer Aided Engineering (CAE) analysis of these two crash modes, as well as the identification, development, integration and physical evaluation of a prototype advanced restraints system within a targeted baseline vehicle environment. For each mode, injury assessments were made for the small, mid-size, and large driver and passenger occupants in either a combination of CAE and vehicle testing or with solely CAE analysis. With three different occupants and two crash modes at two different speeds, 24 different "load cases," 12 for the driver and 12 for the passenger, were studied. This project was conducted by the Crash Avoidance Metrics Partnership (CAMP) ARS Consortium (Ford Motor Company, General Motors, and Mercedes-Benz).

17. Key Word Restraints Systems, Tunable Restraints, Computer-Aided Engineering, Sled Testing, Vehicle Crash Testing		18. Distribution Statement Document is available to the public from the National Technical Information Service www.ntis.gov	
19. Security Classif. (of this report)	20. Security Classif. (of this page)	21. No. of Pages 109	22. Price

Form DOT F 1700.7 (8-72)   Reproduction of completed page authorized

Executive Summary

Restraint system technologies (e.g., air bags, seat belts, seats, etc.) are continually advancing and are a major contributor to mitigating crash fatalities and other related injuries. However, a significant number of crash injuries still occur, and efforts are ongoing to further improve restraint effectiveness.

Pre-crash technologies and vehicle integrated crash avoidance systems are becoming more prevalent in the U.S. fleet. These sensor-based systems may in future years offer an opportunity to fine-tune restraint systems by providing additional environmental information. Given this restraint system technological advancement, manufacturers could then merge the pre-crash sensing information into the overall vehicle system development cycle, thereby enhancing vehicle crashworthiness and enabling further reduction in vehicular injury.

With National Traffic Highway Safety Administration (NHTSA) project sponsorship through NHTSA Cooperative Agreement No. DTNH22-05-H-01277, Project Order 0003, a unique, pre-competitive Advanced Restraint Systems (ARS) Project was initiated in August 2007. It was conducted by the Crash Avoidance Metrics Partnership (CAMP) ARS Consortium (ARSC) whose participants are Ford Motor Company (Ford), General Motors (GM) and Mercedes-Benz. The major objective of this multi-year project was to evaluate the potential benefit of using pre-crash information associated with two unique crash test configurations to tailor an advanced restraint system to the occupant and the crash type.

The ARS project definition and management plan included many highly successful elements. As mentioned previously, cooperative project management, engineering technical leadership and work plan task responsibilities were co-owned by the three project participants: Ford, GM, and Mercedes-Benz. Regular informal project interface and updates were shared with NHTSA as well as their contractor, the Volpe National Transportation Systems Center (Volpe). Interim project reports and management briefings were held with the ARS Consortium Participants and NHTSA. The ARS Consortium leveraged additional resources for project engineering as well as financial and program management; outside expertise for test vehicle procurement, build and measurement; an independent testing laboratory for vehicle testing and documentation; as well as a restraint systems supplier with demonstrated development capability in component part design and development and in advanced Computer Aided Engineering (CAE) design and analysis.

The project technical approach consisted of a nine-task work plan. The initial tasks focused on analysis of existing field crash injury data and determination of the predominant field crash types in which serious head, chest, and lower extremity injuries occurred. The data was filtered to include only events which have high occurrence of Abbreviated Injury Scale (AIS) 2+ injuries in the field, and in which an advanced restraints system could be enhanced by a pre-crash sensing system input. This subset became the population of crashes and occupants that may primarily benefit from advanced restraint systems. Concurrently, discovery sessions were held with restraint system suppliers to identify available advanced restraint technologies which were then

combined and configured into overall driver- and passenger-specific vehicle restraint systems for future study and analysis.

The field data analysis, anticipated pre-crash sensing input, advanced restraint system capability assessments, investigative CAE studies, and discussions with NHTSA led to the identification of two ARS project crash modes: (1) vehicle-to-vehicle impact simulated with a moveable deformable barrier (MDB) to stationary vehicle (delta-v = 35/25mph); and (2) vehicle-to-object impact represented by centerline pole impact (v = 35/25mph). These four crash modes are abbreviated MDB25, MDB35, Pole25 and Pole35 in the figures that appear later in this summary. For each mode, injury assessments were made for the small, mid-size and large driver and passenger occupants in either a combination of CAE and vehicle testing or with solely CAE analysis. With three different occupants and two crash modes at two different speeds, 24 different "load cases," 12 for the driver and 12 for the passenger, were identified.

The final project work encompassed the CAE analysis of these two crash modes, as well as the identification, development, integration and physical evaluation of the prototype advanced restraints systems within a targeted baseline vehicle environment. A series of vehicle crash tests with the Prototype Vehicle Platform (PVP) were completed to establish baseline characteristics. These baseline tests provided the basis for the development of CAE system models which included an instrument panel, seats, body sheet metal, door trim, A- and B-pillars, knee bolsters, a glove box and the steering column. From an occupant performance standpoint, the baseline PVP restraint system performed well in the baseline tests, making it challenging for the ARS Project to demonstrate improved performance with advanced restraint systems, particularly at the lower speed conditions.

A single restraint supplier, TK Holdings, Inc. (Takata) was selected to participate in the ARS project. Takata was responsible for not only the development and prototyping of the advanced restraint system components, but they were also responsible for the system-level CAE used to supplement the component design and to identify the optimized restraint system parameters.

In selecting the components for the advanced restraint system, the primary philosophy was to employ restraints that minimized forward pelvic movement as much as possible, and, assuming a full suite of pre-crash information was available (including occupant size and weight, seating position, crash type and severity), utilize adaptive features in the advanced restraint system to provide maximum tunability over the full range of occupants and load cases. The ARS components with responses that could be tailored based on pre-crash information selected for study within the ARS Project were:

- Driver Air Bag (DAB) with active vent (Takata Programmable Venting Module (PVM))

- Passenger Air Bag (PAB) with active vent (Takata PVM)

- D-Shape Head Side Air Bag (HSAB)

- Knee Air Bag (KAB)

- Motorized Seat Ramp (MSR) (simulated by a fixed steel structure)

- Motorized Seat Belt (MSB)
- Dual-stage, Switchable Load Limiting Retractor
- Retractor Pretensioner (RPT)
- Outboard Seat Belt Lap Anchor Pretensioner (LPT)

To aid in the ARS hardware development, component and sled testing was conducted. This included the development of a new sled test methodology to simulate the higher speed MDB-to-vehicle crash mode. Sled equivalent CAE models were also developed to aid in refining ARS components and to gain further confidence in occupant response predictions (with special emphasis on the large occupant).

For each of the 24 load cases, a CAE Design of Experiments (DOE) was conducted to identify the "optimal" settings for the tunable parameters of the advanced restraint system. This led to a recommended ARS configuration for each of the 24 load cases. The project assumed availability of pre-crash sensing data and a vehicle system algorithm which then defined restraint deployment timing and thresholds. The DOE and restraint component testing results were encouraging and suggested that the optimized advanced restraint system would show an overall occupant performance benefit for both test modes and speeds.

During the final several months of the project, full vehicle crash tests were conducted for 10 of the 24 load cases with the corresponding recommended ARS configurations for both the driver and passenger. The execution of the test protocol for the two modes was shown to be repeatable, with measured speeds and final change in velocity. Furthermore, injury metrics were gathered for all Anthropomorphic Test Devices (ATD), with limited data errors. Data from these vehicle tests, along with the CAE analysis for the remaining 14 load cases, provided an overall comparison of the performance of the PVP baseline restraint system to that of the advanced restraint system.

A combined "occupant injury measure" was calculated by estimating the risk of AIS3+ and AIS2+ injury for the head, chest, and lower extremities. The estimated risk is based on test data or CAE predictions for the HIC15, chest deflection, axial femur loads, and upper and lower axial tibia loads. The injury risk estimates for these body regions are combined independently in the following manner:

$$\text{Occupant Injury Measure (AIS3+, all ATDs)}$$
$$= (1-(1-p(HIC15)) \times ((1-p(ChDefl)) \times (1-p(\max(Femur)_{left,right})))^{AIS3+}$$

For the AIS2+ occupant injury measures, two different equations were used, depending on the ATD:

$$\text{Occupant Injury Measure (AIS2+, 5}^{th}\text{ and 50}^{th}\text{ Hybrid III)}$$
$$= (1-(1-p(HIC15)) \times ((1-p(ChDefl)) \times (1-p(\max(Femur)_{left,right})) \times$$
$$(1-p(\max(UprTib)_{left,right})) \times (1-p(\max(LwrTib)_{left,right})))^{AIS2+}$$

Occupant Injury Measure (AIS2+, 95th Hybrid III)

$$= (1-(1-p(HIC15)) \times ((1-p(ChDefl)) \times (1-p(\max(Femur)_{left,right})))^{AIS2+}$$

These equations use the peak values recorded between the left and right legs for the femur and tibia axial forces. A summary of the AIS3+ and AIS2+ occupant injury measures for the driver associated with both restraint systems is provided in Figures ES1 and ES2, respectively, while the same comparison is provided for the passenger in Figures ES3 and ES4.
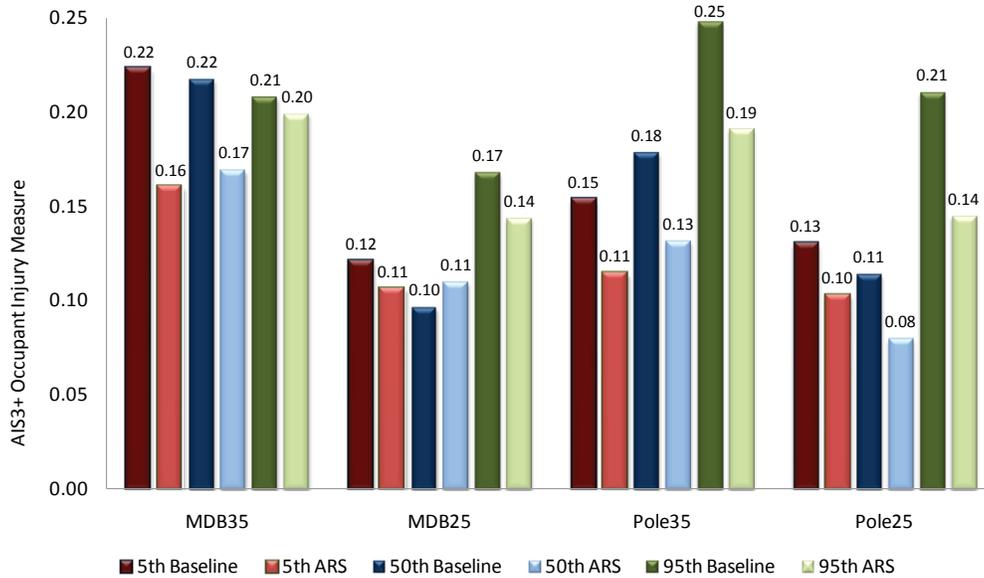
Figure ES1 – Combined AIS3+ Occupant Injury Measure, PVP Versus ARS, All Drivers
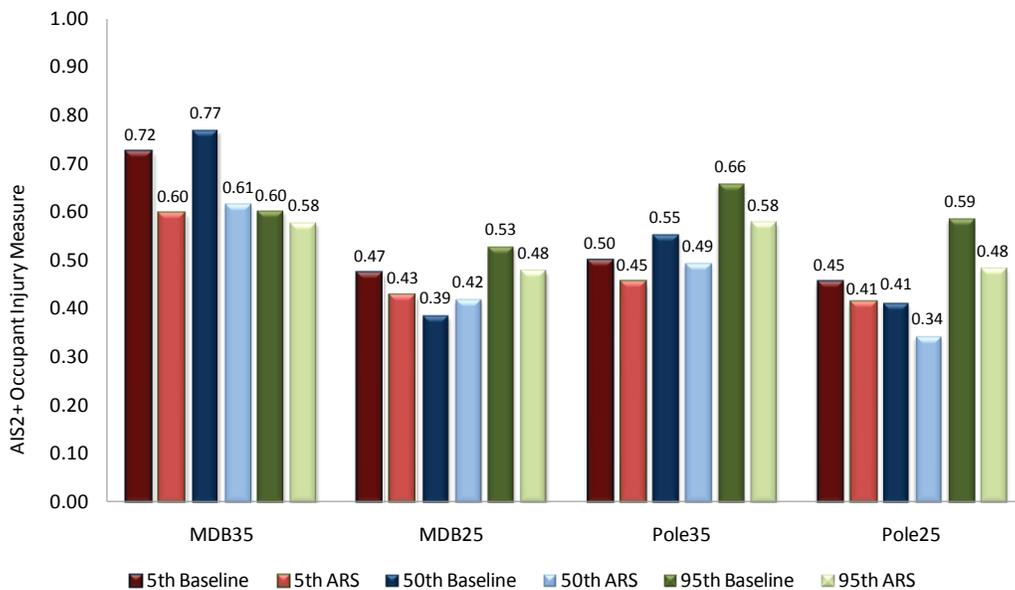
Figure ES2 – Combined AIS2+ Occupant Injury Measure, PVP Versus ARS, All Drivers
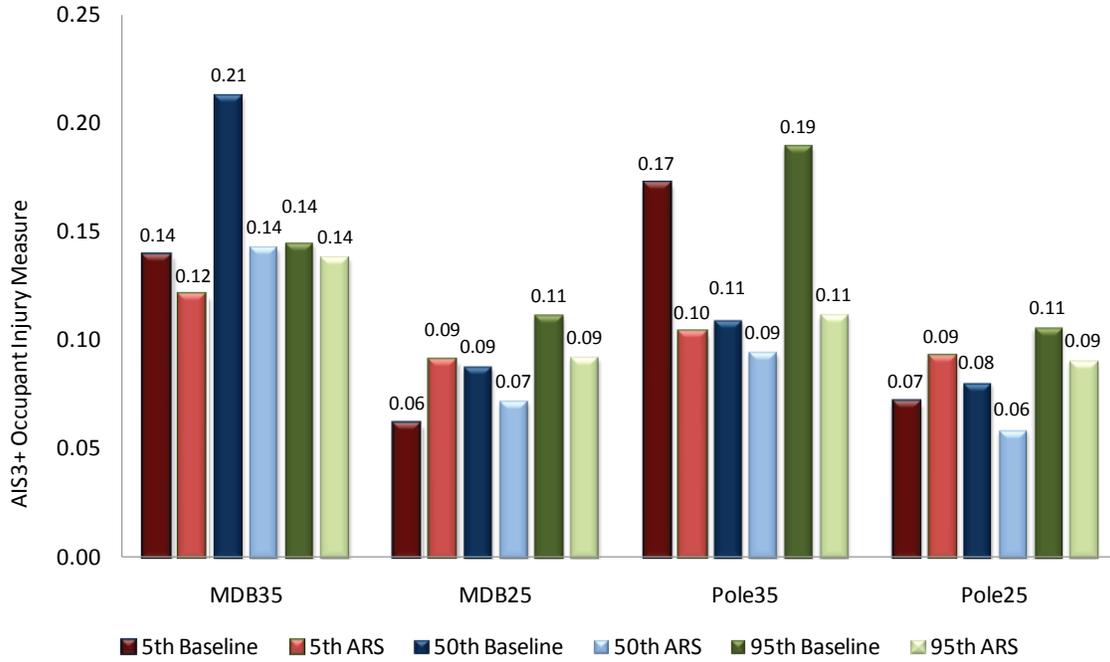
Figure ES3 – Combined AIS3+ Occupant Injury Measure, PVP Versus ARS, All Front-Outboard Passengers
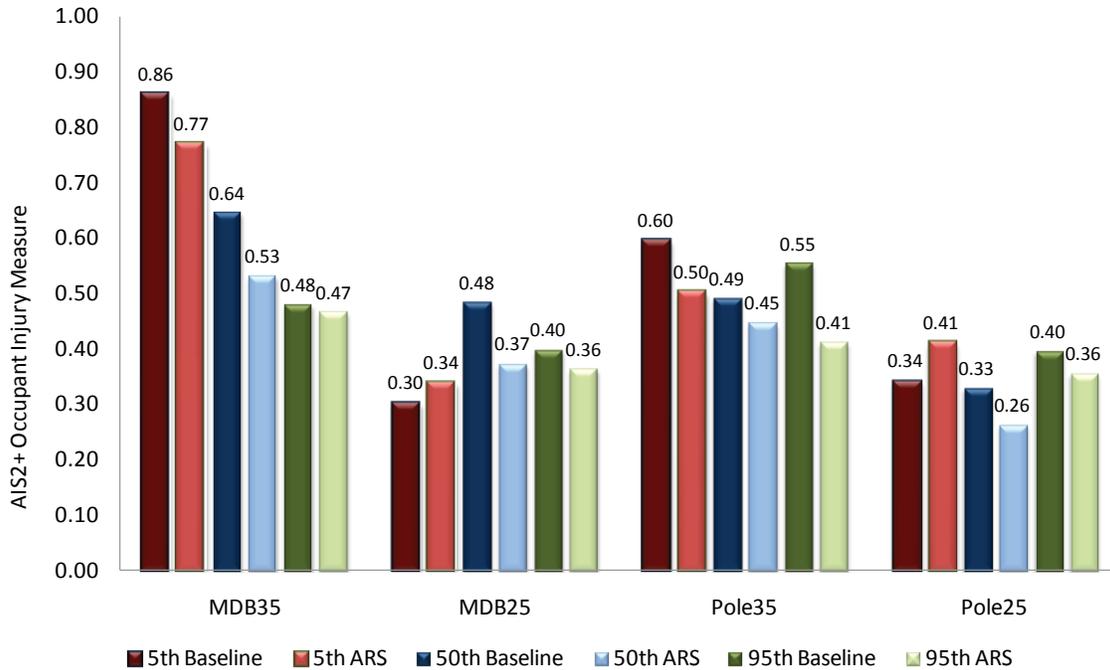
Figure ES4 – Combined AIS2+ Occupant Injury Measure, PVP Versus ARS, All Front-Outboard Passengers

Regional injury metrics for the head, chest and lower extremities were not in all cases lower than the measured baseline responses, and for higher energy tests, intrusion significantly limited the ability of the advanced restraint system to improve the lower extremity performance results. However, the overall occupant injury reduction benefit with a tailorable advanced restraint system was demonstrated for both test modes at the higher impact speeds; whereas for the lower speed conditions, the baseline versus advanced restraint system performance was comparable with an overall benefit not clearly shown.

By scope and definition, this project is limited by the test and analysis conducted; crash injury data collected; as well as conclusions drawn from prior engineering studies and field accident data. For example, the baseline vehicle performed well and was the only vehicle architecture evaluated. Thus, the applicability of these results to other vehicle architectures across the fleet is unknown. Also, vehicle manufacturers consider structural response, compartment / occupant packaging and interior component construction, and these are tuned coincidently for several crash modes with the restraint performance tuned and optimized accordingly. Thus, the "retrofitting" of hardware onto the existing project vehicle architecture may limit the potential benefit of the restraint system configurations evaluated. Significantly more research of test and field data analysis of baseline vehicle restraints systems available to consumers today are necessary to extrapolate and predict overall real-world benefit potential with advanced restraint systems.

The ARS Project met its deliverables and also provided tangible occupant performance data through the use of unique test modes and advanced restraint system configurations. Furthermore, research data was collected from which future studies might be configured.

Table of Contents

List of Figures

List of Tables

List of Acronyms

AIS	Abbreviated Injury Scale
ARS	Advanced Restraint System
ARSC	Advanced Restraint Systems Consortium
ATD	Anthropomorphic Test Device
CAE	Computer Aided Engineering
CAMP	Crash Avoidance Metrics Partnership
CDS	Crashworthiness Data System
CG	Center of Gravity
CMM	Coordinate Measuring Machine
DAB	Driver Air Bag
DLT	Dynamic Locking Tongue
DOE	Design of Experiments
EA	Energy Absorbing
FARS	Fatality Analysis Reporting System
FE	Finite Element
FEA	Finite Element Analysis
FLx	Female Lower Extremity
FMVSS	Federal Motor Vehicle Safety Standard
FSP	Front Seat Passenger
GES	General Estimates System
HIC	Head Injury Criteria
HIC15	Head Injury Criterion 15 ms
HIII	Hybrid III (Anthropomorphic Test Device)
HIII 5F	Hybrid III 5th Percentile Female ATD
HIII 50M	Hybrid III 50th Percentile Male ATD
HIII 95M	Hybrid III 95th Percentile Male ATD
HSAB	Head Side Air Bag
HYGE	Hydraulically Controller Gas Energized
IARV	Injury Assessment Reference Value
IAV	Injury Assessment Value
IEA	Intelligent Energy Absorbing
IIHS	Insurance Institute for Highway Safety
IP	Instrument Panel

KAB	Knee Air Bag
LPT	Lap Anchor Pretensioner
LTAP-OD	Left Turn Across Path – Opposite Direction
MADYMO	MAthematical DYnamic MOdeling
MAIS	Maximum Abbreviated Injury Scale
MDB	Moving Deformable Barrier
MSB	Motorized Seat Belt
MSR	Motorized Seat Ramp
MY	Model Year
NASS	National Automotive Sampling System
NCAP	New Car Assessment Program
NHTSA	National Highway Traffic Safety Administration
ODB	Offset Deformable Barrier
OIM	Occupant Injury Measure
PAB	Passenger Air Bag
PDOF	Principal Direction of Force
PVM	Programmable Venting Module
PVP	Prototype Vehicle Platform
RPT	Retractor Pretensioner
RTI	Revised Tibia Index
Takata	TK Holdings, Inc.
THOR-FLx	THOR Female Lower Extremity (NHTSA Advanced ATD)
THOR-Lx	THOR Male Lower Extremity (NHTSA Advanced ATD)
TRC	Transportation Research Center, Inc.
TTO	Time-to-Open
Volpe	Volpe National Transportation Systems Center
USDOT	U.S. Department of Transportation

1   Introduction and Project Background

Restraint system technologies (e.g., air bags, seat belts, seats, etc.) are continually advancing and are a major contributor to mitigating crash fatalities and other related injuries. However, a significant number of crash injuries still occur, and efforts are ongoing to further improve restraint effectiveness.

Pre-crash technologies and vehicle integrated crash avoidance systems are becoming more prevalent in the U.S. fleet. These sensor-based systems may in future years offer opportunity to further tune restraint systems by providing additional environmental information. Given this restraint system technological advancement, manufacturers could then merge the pre-crash sensing information into the overall vehicle system development cycle, thereby enhancing vehicle crashworthiness and enabling further reduction in vehicular injury.

With National Traffic Highway Safety Administration (NHTSA) project sponsorship through NHTSA Cooperative Agreement No. DTNH22-05-H-01277, Project Order 0003, a unique, pre-competitive Advanced Restraint Systems (ARS) project was initiated in August 2007. It was conducted by the Crash Avoidance Metrics Partnership (CAMP) ARS Consortium (ARSC) whose participants are Ford Motor Company (Ford), General Motors (GM), and Mercedes-Benz. The major objective of this multi-year project was to evaluate the potential benefit of using pre-crash information associated with two unique crash configurations to tailor an advanced restraint system to the occupant and the crash type.

The ARS project definition and management plan included many highly successful elements. As mentioned previously, cooperative project management, engineering technical leadership and work plan task responsibilities were co-owned by the three project participants: Ford, GM, and Mercedes-Benz. Regular informal project interface and updates were shared with NHTSA as well as their contractor, Volpe. Interim project reports and management briefings were held with the ARS Consortium Participants and NHTSA. The ARS Consortium leveraged additional resources for project engineering as well as financial and program management; outside expertise for test vehicle procurement, build and measurement; an independent testing laboratory for vehicle testing and documentation; as well as a restraint systems supplier with demonstrated development capability in component part design and development as well as in advanced Computer Aided Engineering (CAE) design and analysis.

The project technical approach consisted of a nine task work plan. Overall, the ARS Project met its deliverables and also provided tangible occupant performance data through the use of unique test modes and advanced restraint system configurations. Furthermore, research data was collected from which future studies might be configured. This report summarizes the key findings from the individual ARS Project tasks, including a detailed description of the investigated two crash test modes and the identification, development, integration and assessment of an advanced restraint system designed to utilize pre-crash information to tailor its response to a specific crash mode, crash speed and occupant size.

2   Field Data Analysis

Under Task 2 of the ARS Project, the predominant crash types, injury frequency and injury severity were identified from several major crash databases: National Automotive Sampling System (NASS)/Crashworthiness Data System (CDS) and General Estimates System (GES), and the Fatality Analysis Reporting System (FARS) databases. In-depth reviews of these databases were conducted in an effort to provide guidance on two key project objectives. The first of these objectives, the creation of two unique frontal crash test configurations and procedures, was influenced by some of the crash characteristics observed in the field. The second project objective, the assessment of the potential benefit of an adaptive advanced restraint system that can be tailored based on pre-crash information, required an understanding of the types of injuries that were occurring in the field.

A key driver towards achieving both of these objectives was a statistical analysis of the NASS/CDS database that was completed by the U.S. Department of Transportation (USDOT). The frontal crashes in the database were filtered according to the following criteria:

- Belted drivers and front-seat passengers age 13 and older (FSP 13+)

- No pedestrian or pedalcyclist crashes

- No motorcycle crashes

- No animal impacts

- Vehicles from model years 1998 and later (MY98+)

At a high level, the NASS/CDS analysis yielded five different crash scenarios from which two unique crash test procedures were developed, one vehicle-to-object test and one vehicle-to-vehicle test. These scenarios are listed in Table 1.

Table 1 - Crash Scenarios: NASS/CDS Analysis

Vehicle-to-Object Pre-Crash Scenarios and Impact Types	
Pre-Crash Scenario	**Obstacle**
Road Departure	Structure
Road Departure	Pole, Tree

Vehicle-to-Vehicle Pre-Crash Scenarios and Impact Types	
Pre-Crash Scenario	**Impact Types**
Opposite Direction	Front-to-Front
Rear-End	Front-to-Rear
Left Turn Across Path - Opposite Direction	Front-to-Front

For the vehicle-to-object crash scenarios associated with road departure, injuries during impacts to objects such as trees or poles were significantly larger in number than those in crashes involving off-road impacts to "structures." In addition, it was assumed that a pole or tree had the potential to be detected and differentiated from a pre-crash sensing perspective compared to the more generic "vehicle-to-structure" category which would include objects such as guard rails, buildings, wooden fences and other highway infrastructure. Consequently, focus regarding the vehicle-to-object test configuration turned to a pole impact simulation.

For the vehicle-to-vehicle crash scenario, the injuries in front-to-rear impacts were fewer in number compared to the front-to-front crashes. With this in mind, the front-to-front crashes were further analyzed to determine key characteristics that could potentially be simulated in the laboratory.

The Left Turn Across Path - Opposite Direction (LTAP-OD) pre-crash scenario resulted in off-axis impacts and accounted for 69 percent of the vehicle-to-vehicle dataset. The angle of impact for the front-to-front crashes in general was clustered tightly around 180°, yet also included an off-axis longitudinal component in the majority of the cases, up to ± 15 degrees principal direction of force (PDOF) as shown in Figure 1.
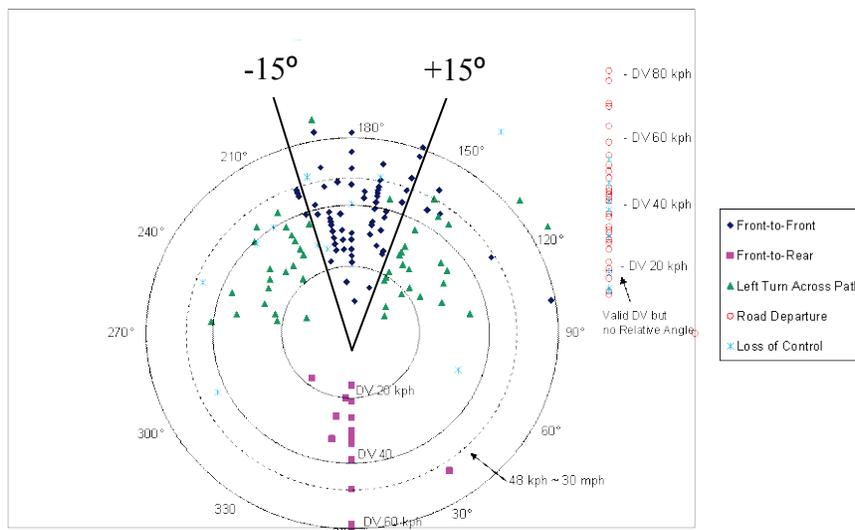
Figure 1 - Subject Vehicle Delta-V and Angle of Incidence Relative to Subject Vehicle (Unweighted), Head, Chest and Lower Extremity Injuries

The NASS/CDS analysis also looked at the delta-v recorded for each of the two broad categories of crashes (vehicle-to-object and vehicle-to-vehicle). Figure 2 provides the cumulative distribution of drivers in pole/tree crashes by delta-v while Figure 3 provides the same analysis for vehicle-to-vehicle crashes. In addition, Figure 4 plots the lateral delta-v for this same dataset. Note that a larger lateral delta-v was more common in the vehicle-to-vehicle crashes than in the vehicle-to-object crashes.
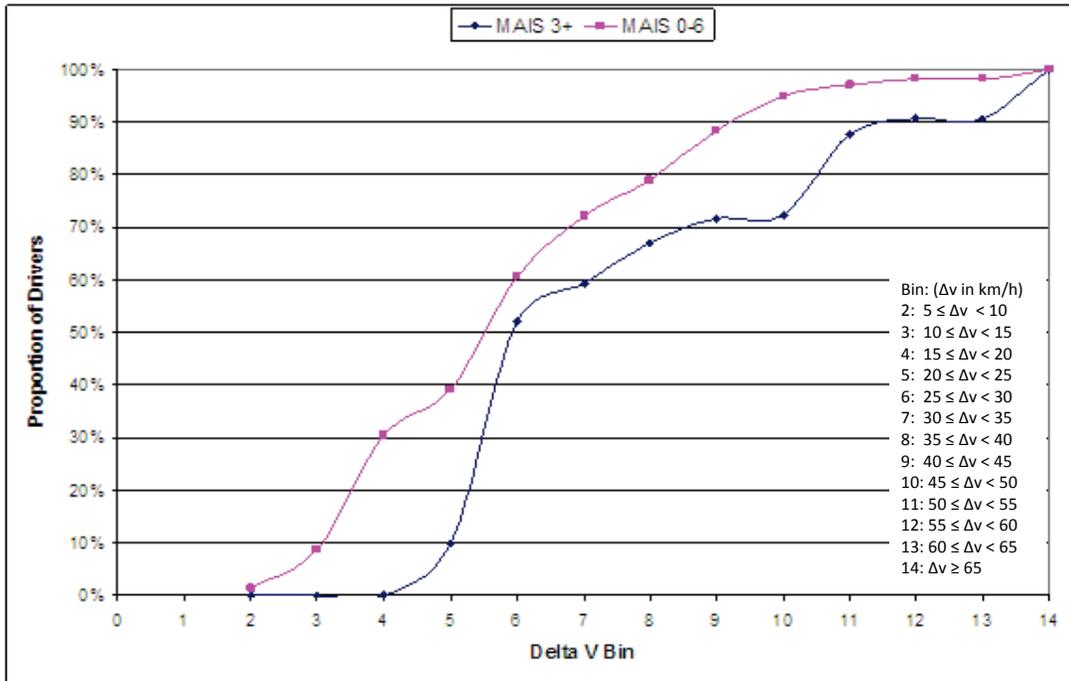
Figure 2 - Cumulative Distribution of Drivers in Pole/Tree Crashes by Delta-V
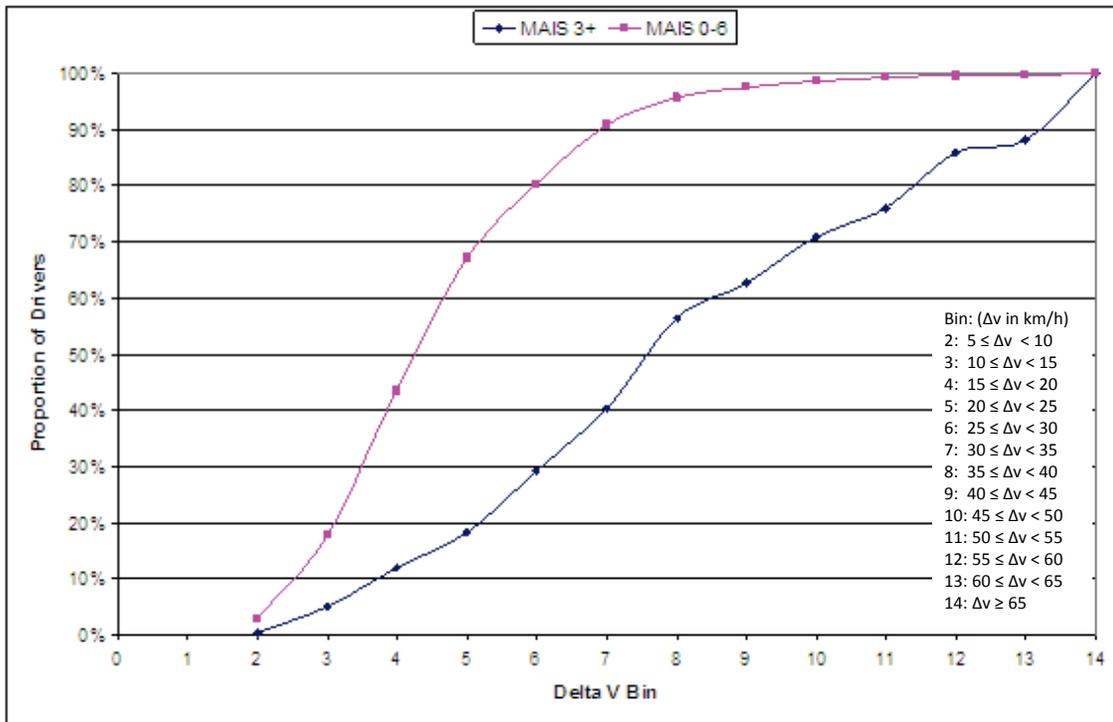
Figure 3 - Cumulative Distribution of Drivers in Vehicle-to-Vehicle Crashes by Delta-V
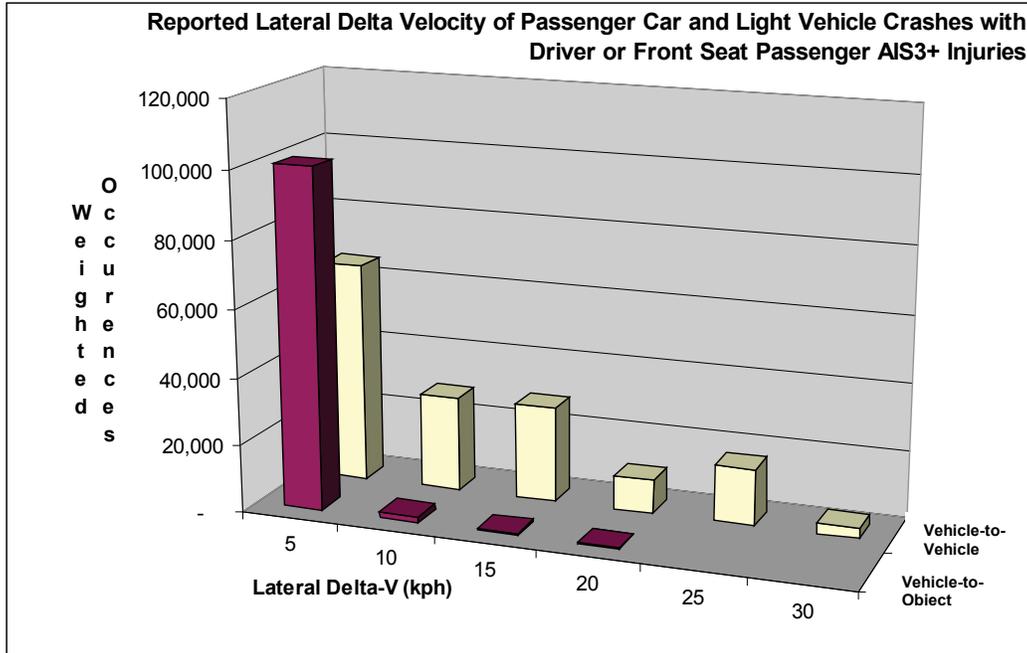
**Figure 4 - Lateral Delta-V Distribution for Vehicle-to-Vehicle and
Vehicle-to-Object Impacts**

From an injury perspective, the NASS/CDS analysis provided insight into the injury severity and the associated body region for both categories of crashes. Table 2 provides a summary of the maximum known injury level on the Abbreviated Injury Scale (AIS) (i.e., Maximum AIS, or MAIS), as well as the associated body region, for restrained occupants in towed MY98+ vehicles involved in frontal-damage, single-impact, vehicle-to-object crashes.

**Table 2 – Maximum AIS Injury Summary for Vehicle-to-Object Crashes
(NASS/CDS Analysis, Percentages Based on Weighted Data)**

Driver							Front Seat Passenger Age 13 Years and Older					
Body Region	MAIS 1 Minor %	MAIS 2 Moderate %	MAIS 3 Serious %	MAIS 4 Severe %	MAIS 5 Critical %	MAIS 6 Maximum %	Body Region	MAIS 1 Minor %	MAIS 2 Moderate %	MAIS 3 Serious %	MAIS 4 Severe %	MAIS 5 Critical %	MAIS 6 Maximum %
Head	4	3	2	3	15	0	Head	0	19	0	0	6	
Face	14	11	12	17	15	0	Face	13	13	24	0	6	
Neck	4	21	2	0	1	0	Neck	3	0	0		13	
Thorax	12	20	25	21	18	0	Thorax	16	14	21	0	19	
Abdomen	6	8	2	17	15	0	Abdomen	6.0	0	3.3		19	
Spine	10	2	8	6	3	0	Spine	23	6	2	0	13	
Upper Extremity	31	8	35	16	17	0	Upper Extremity	14	26	24	0	6	
Lower Extremity	20	27	14	19	17	0	Lower Extremity	25	23	26	0	19	
Sum %	100	100	100	100	100	0	Sum %	100	100	100	0	100	

In a similar manner, the vehicle-to-vehicle crashes were analyzed to better understand the injury trends. These results, based on restrained occupants in towed MY98+ vehicles involved in frontal-damage, single impact, vehicle-to-vehicle crashes, are summarized in Table 3.

Table 3 – Maximum AIS Injury Summary for Vehicle-to-Vehicle Crashes
(NASS/CDS Analysis, Percentages Based on Weighted Data)

Driver							Front Seat Passenger Aged 13 Years and Older						
Body Region	MAIS 1 Minor %	MAIS 2 Moderate %	MAIS 3 Serious %	MAIS 4 Severe %	MAIS 5 Critical %	MAIS 6 Maximum %	Body Region	MAIS 1 Minor %	MAIS 2 Moderate %	MAIS 3 Serious %	MAIS 4 Severe %	MAIS 5 Critical %	MAIS 6 Maximum %
Head	3	8	7	8	37	39	Head	1	3		10	100	100
Face	13	2	1				Face	15	1	9	1		
Neck	3	0.1	0.1				Neck	7	0.01				
Thorax	13	3	12	67	53	34	Thorax	16	21	15	89		
Abdomen	6	1	2	15	7		Abdomen	11	1	9			
Spine	13	3	2	3	4	27	Spine	18	5	1			
Upper Extremity	29	12	22				Upper Extremity	17	13	43			
Lower Extremity	19	71	53	7			Lower Extremity	15	56	22			
Sum %	100	100	100	100	100	100	Sum %	100	100	100	100	100	100

To supplement the statistical analysis, the ARSC conducted an in-depth analysis of the details for a subset of the NASS-CDS cases. The prescreened cases for investigation were provided by Volpe, who eliminated cases that were not survivable, incomplete, etc. The case numbers were provided to the ARS team in an MS Excel file, and the team examined the data for each case using NHTSA's online case viewer. Additional cases were eliminated upon closer inspection of the crash data, for the reasons of insufficient data, not the correct crash mode, and unique modes that were not applicable to the study. For example, frontal impacts with no frame engagement (FL--, FR--) are classified as frontal impacts in the database but in many cases result in A pillar contact with predominant side impact damage and injury. Some of the Center Pole/Tree impact cases would likely limit the effectiveness of the restraints due to losses in passenger compartment integrity, so they were excluded from the study. A total of 246 cases were selected for review providing further details for the injuries occurring in these field events. Figure 5 provides a count summary of the AIS3+ injuries and their corresponding body regions for the 246 cases.

AIS 3+ INJURIES BY BODY REGION (246 CASES)
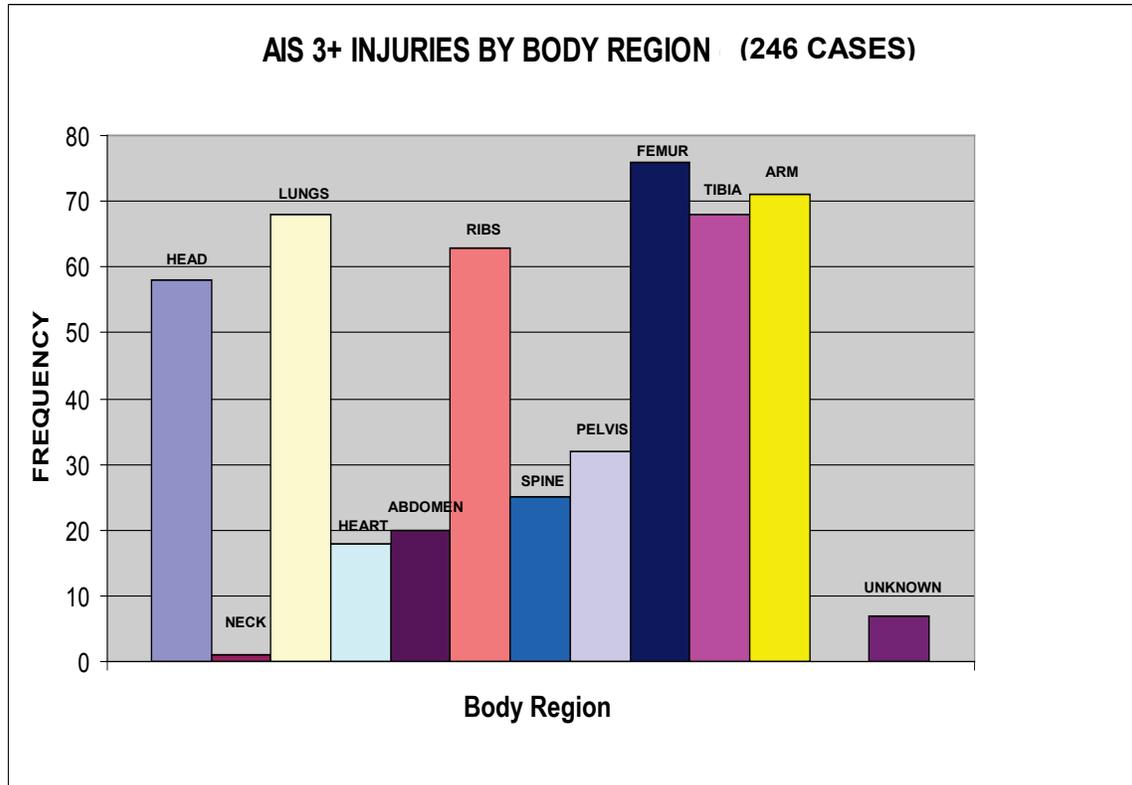
Figure 5 - Injury Counts by Body Region (All Events, In-depth Analysis)

In the in-depth analysis, lower extremity injuries (including the pelvis, femur and tibia) were predominant in all crash modes. The next most frequently injured body region was the chest, which included ribs, heart and lungs. Additionally, multiple impact events were noted in many of the vehicle-to-object crashes. In these cases, the occupant position in the secondary event may not be on the seat due to the occupant movement resulting from initial impact with a sign post, mailbox or other obstacle. In many crash cases, an initial impact preceded the primary impact event believed to have caused the AIS 3+ injury.

Overall, the statistical and in-depth field data analyses provided direction for the ARS Project with respect to the key project objectives. With respect to the creation of two unique frontal crash test configurations and procedures, two crash modes were identified, vehicle-to-object and vehicle-to-vehicle. Additionally, some of their key characteristics were studied. The injury data provided insight into the types of adaptive advanced restraint systems that may offer opportunity to reduce the overall field injury.

3   Test Methodology Development

With the crash modes of interest defined based on field data, the ARSC's next step was to pick a vehicle to use as a Prototype Vehicle Platform (PVP) and determine two ARS Project crash modes (one vehicle-to-vehicle mode and one vehicle-to-object mode) based on CAE (Computer-Aided Engineering) analysis. These modes were to be used to evaluate the effectiveness of the pre-crash activated restraint system proposals.

In order to choose the vehicle platform, the team considered the following criteria:

1. A "mid-sized" class vehicle

2. A vehicle that would facilitate "retrofitting" of advanced restraint components

3. Demonstrated structural integrity and safety performance in the standard crash test modes, including Federal Motor Vehicle Safety Standard (FMVSS) No. 208 and IIHS frontal offset test

The ARSC team considered a number of potential vehicles and chose a U.S., mid-sized, sedan, along with its associated CAE model, as the PVP for the study. The vehicle chosen is from the 1998 Model Year and received a "good" rating in the IIHS Frontal ODB test and a "5-Star" rating for driver and passenger in U.S. NCAP frontal impact tests. For the vehicle crash testing, the team decided to purchase used vehicles and developed criteria for purchase. For the CAE studies, the team obtained two computer models of the PVP, a Finite Element Analysis (FEA) model created in RADIOSS V4.1 and a MAthematical DYnamic MOdeling (MADYMO) occupant system sled model.

Using the PVP FEA model, several crash pulses were generated for use in model validation. Table 4 lists the crash pulses that were studied.

Table 4 - CAE Crash Pulses Generated

Crash Mode Number	Description of Crash Mode
1	U.S. Frontal New Car Assessment Program (NCAP)
2	IIHS Frontal Offset Deformable Barrier (ODB)
3	40% overlap, 15 deg. PDOF, car-to-car both cars @ 35 mph
4	50% overlap, 15 deg. PDOF, car-to-car both cars @ 35 mph
5	65% overlap, 15 deg. PDOF, car-to-car both cars @ 35 mph
6	80% overlap, 15 deg. PDOF, car-to-car both cars @ 35 mph
7	Center pole impact, 10" diameter @ 30 mph
8	Center pole impact, 10" diameter @ 35 mph
9	Center pole impact, 10" diameter @ 40 mph

The crash pulses were used as input to a MADYMO occupant model to estimate occupant responses for a 50th percentile male Hybrid III (HIII) Anthropomorphic Test Device (ATD) model. The HIII ATD was seated in the driver position with the seat at the

mid-position of the fore-aft travel and with the seat height full down. Several modifications were made to the MADYMO model to improve its response in an offset vehicle-to-vehicle mode as follows:

1. The driver door was added to the model to better simulate the occupant kinematics during the offset vehicle-to-vehicle modes. (For clarity, the door is not shown in Figure 6.)

2. The steering wheel was modified with force-deflection curves in the lateral direction to better represent steering wheel deformation when subjected to lateral forces from the occupant.
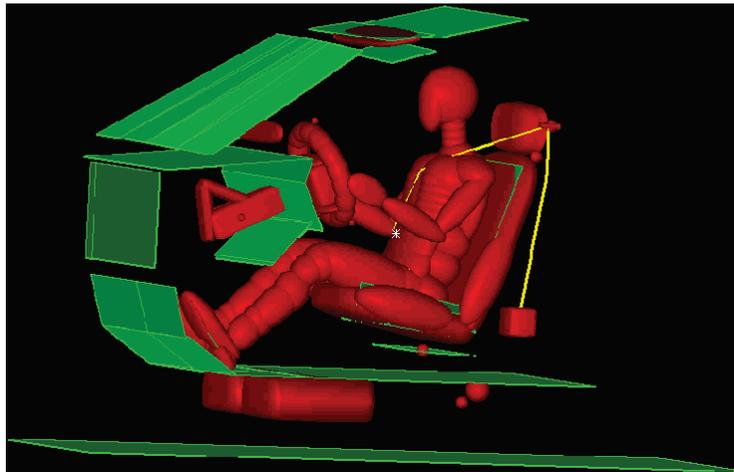
Figure 6 - CAE Front Occupant System MADYMO Model

The MADYMO model was modified for the vehicle-to-vehicle, offset, oblique mode, but was not specifically tuned and optimized with these selected set-up configurations. Therefore, the resulting occupant data could only be used to estimate trends for responses which might be measured in actual vehicle tests. For the vehicle-to-vehicle mode, the estimated x and y acceleration pulses, as well as the estimated pitch, yaw, and floorpan intrusion, were all input into the occupant model. Subject to these inputs, the occupant responses of the HIII 50th percentile driver occupant in the mid-seating position were obtained.

The pole test simulation showed that the highest speed impact was the most severe in terms of the ATD injury metrics. However, at higher speeds the challenge of tuning vehicle characteristics to influence ATD injury numbers becomes less dependent on restraining devices and more dependent on structural response. However, structural modifications were beyond the scope of the project. The intrusions for the pole impacts at 35 mph and 40 mph were simulated and are shown with respect to the current IIHS guidelines for rating occupant compartment intrusion (40 mph vehicle to IIHS ODB) in Figures 7 and 8.
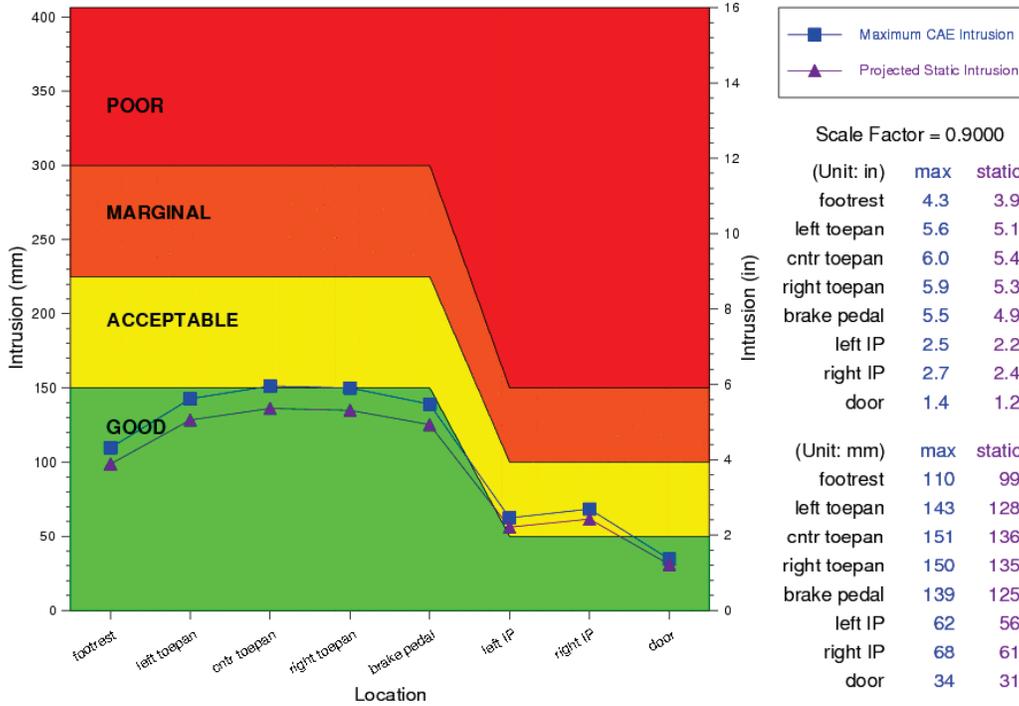
**Figure 7 - Interior Compartment Intrusions for the 35 mph Centerline Pole Impact
Plotted with IIHS Guidelines for Rating Occupant Compartment Intrusion
(40 mph ODB)**
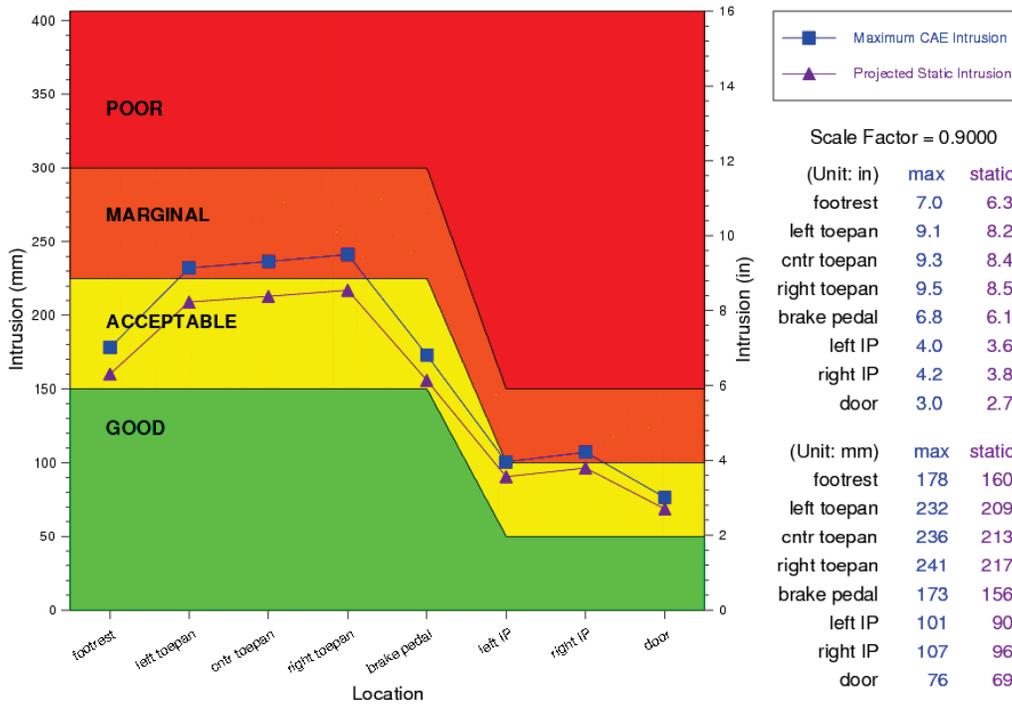
**Figure 8 - Interior Compartment Intrusions for the 40 mph Centerline Pole Impact
Plotted With IIHS Guidelines for Rating Occupant Compartment Intrusion
(40 mph ODB)**

The results of the intrusion simulation study showed that the 35 mph centerline pole resulted in intrusion within the 40 mph vehicle to barrier IIHS ODB "good" region. The 40 mph centerline pole intrusion simulation predicted intrusion in the 40 mph vehicle to barrier IIHS ODB "acceptable" and "marginal" regions. Thus, in an effort to minimize the role intrusion may play in the measured ATD responses, the ARSC and NHTSA jointly agreed to specify the vehicle-to-pole test at 35 mph into a 10-inch diameter stationary rigid pole. This decision is further supported by the data in Figure 2 which shows that for vehicle-to-object frontal crashes, approximately 90 percent of the MAIS3+ injured drivers and 98 percent of all drivers (MAIS 0-6) were involved in a crash with a recorded delta-v of 35 mph or less. The vehicle-to-pole impact point is at the front longitudinal centerline (see Figure 9).
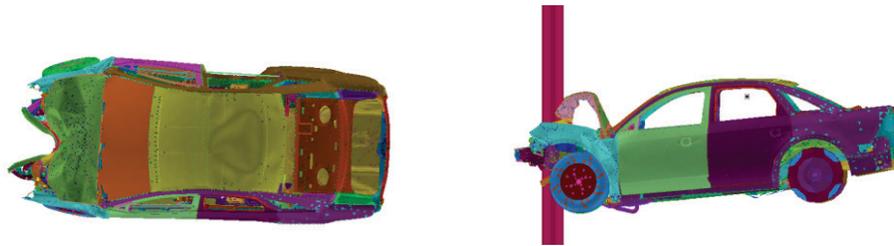
Figure 9 - Top and Side View of PVP Centerline Pole at 35 mph

In order to determine the test mode for the vehicle-to-vehicle test, a CAE study was performed with a constant 35 mph velocity change, an overlap between 40-80 percent, 15 degree angle, and the 50th percentile male ATD seated in the driver position. The vehicle-to-vehicle CAE results are shown in Table 5. Typically, a smaller overlap led to more rotation of the ATD and to more intrusion, whereas a higher overlap resulted in a stiffer pulse. The 15 ms Head Injury Criterion (HIC15), chest acceleration, chest deflection, and right lower extremity revised tibia index (RTI) all increased along with increasing overlap. The femur loads were all less than 15 percent of the Injury Assessment Reference Value (IARV) of 10 kN, thus, the femur loads were considered negligible for determining the worst-case overlap.

Table 5 - CAE Simulated Occupant Responses for Different Overlap Vehicle-to-Vehicle Impacts

50th Male HIII Occupant Response	Overlap			
	40%	**50%**	**65%**	**80%**
HIC 15	204	239	350	588
Chest Deflection (mm)	29	30	34	36
Chest Accel – 3ms (g)	40	46	49	49
Left Femur Fz (kN)	1.24	1.27	1.21	0.82
Right Femur Fz (kN)	1.24	1.27	1.21	0.82
RTI - Left	1.08	1.00	1.27	1.21
RTI - Right	1.20	1.20	1.39	1.57

The 80-percent overlap was selected for two primary reasons. The first was that the model results for the various overlaps of vehicle-to-vehicle impacts indicated that the injury assessment values increased with increasing vehicle overlap. The second reason was to limit intrusion effects and better isolate the tailorable restraint effects on ATD responses.

For this project, it was decided to simulate the vehicle-to-vehicle crash mode in a "MDB-to-vehicle" mode by utilizing a moving deformable barrier (MDB) into a stationary vehicle with 80-percent overlap at an oblique impact angle of 15 degrees (Figure 10). Compared to a striking PVP vehicle, the MDB offered the advantage of a uniform crush zone so that changes in the overlap or angle would not have as much effect on the crush characteristics of the MDB. The team added ballast to the MDB so that it would be roughly the same weight as the PVP. At equal weights, the MDB requires an impact speed of 70 mph in order to achieve a 35 mph delta-v for the stationary PVP.

Stationary
Target Delta-V = 35 mph

V ~ 70 mph
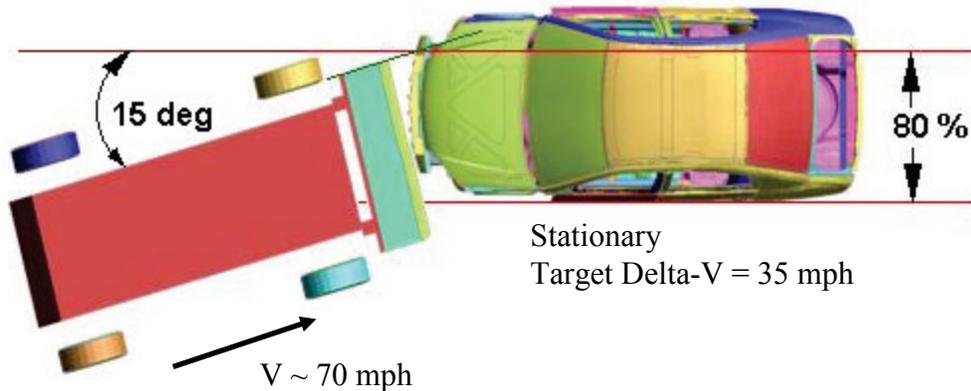
Figure 10 - 15 Degree PDOF, 80-Percent Overlap MDB-to-Vehicle Analysis Setup

The ARSC also considered the relative bumper height in the MDB-to-vehicle mode. Mismatched bumper height prevents the frames from fully engaging, which can cause additional test-to-test variation. Therefore, for the MDB-to-vehicle mode, the bumper height of the MDB was adjusted to the same bumper height (within ± 5 mm) as the PVP vehicle (Figure 11).
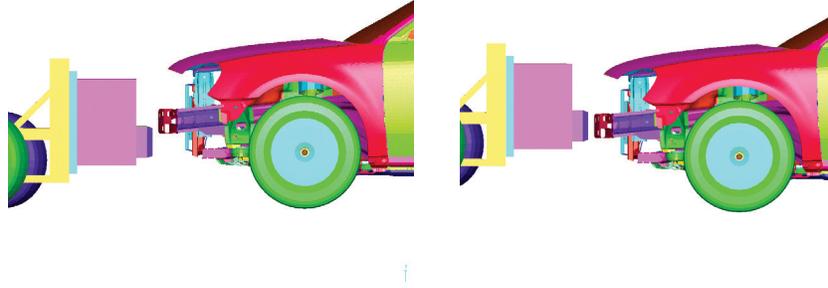
Figure 11 - MDB and Target Vehicle Bumper Alignment

To give an indication of trends in the injury criteria results with respect to delta-v, and to study the potential benefit of tuning an adaptive restraint system based on closing speed, the ARS Project Plan also called for the selection of a lower speed for both crash modes. Based on the NASS/CDS field data analysis of vehicle-to-vehicle crashes, shown earlier in Figure 2, approximately 55 percent of the restrained drivers experiencing an MAIS3+ injury were involved in frontal crashes with a recorded delta-v of 25 mph or less. For all restrained drivers (MAIS 0-6), 95 percent of the crashes recorded a delta-v of 25 mph or less. In a similar analysis of the vehicle-to-object frontal crashes, shown in Figure 3, approximately 65 percent of the MAIS3+ injured drivers and 80 percent of all drivers (MAIS 0-6) were involved in a crash with a recorded delta-v of 25 mph or less. Thus, the lower speeds for both the centerline pole impact and the MDB-to-vehicle impact were chosen at 25 mph. The test modes will be abbreviated in the remainder of this report as MDB35 and MDB25 for the 35 mph and 25 mph MDB-to-vehicle tests, respectively, and similarly Pole35 and Pole25 for the 35 mph and 25 mph vehicle-to-pole tests, respectively.

Measures, such as choosing an MDB over an actual vehicle and matching the bumper heights, were taken to limit variation for this test condition. However, there is inherent variability in full-vehicle crash testing and test-to-test variability must be considered when comparing the performance of different restraint systems and assessing the statistical significance of the results.

4   ATD Criteria for ARS Assessment

The next step in the ARS Project was to define the key ATD injury metrics. Three different sized ATDs were identified to represent the range of occupants in the field – 5th percentile female HIII ATD with THOR-FLx legs, 50th percentile male HIII ATD with THOR-Lx legs, and the 95th percentile male HIII ATD. The THOR legs for the 5th and 50th ATDs were utilized to take advantage of newer, ATD, lower extremity hardware. In the remainder of the report, the 5th percentile female, 50th percentile male, and 95th percentile male ATDs will be referred to as HIII 5F, HIII 50M, and HIII 95M, respectively.

For each of the ATDs, NHTSA identified the key injury assessment values (IAVs) and body regions that would be evaluated at both the AIS2+ and AIS3+ injury levels as shown in Figure 12. These IAVs, and the corresponding injury risk curve equations provided by NHTSA (NHTSA, 2008), are listed in Table 6.
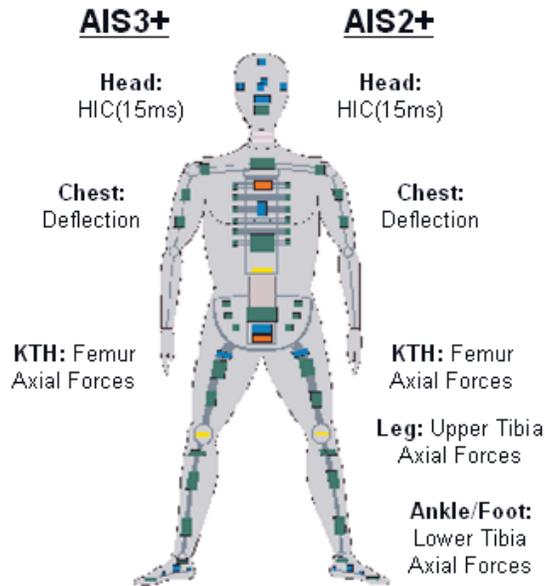
Figure 12 - ARS Assessment Criteria

Table 6 - Injury Risk Curve Equations Provided by the USDOT for Each of the ATDs

Dummy Type	AIS 2+	AIS 3+
HEAD: (HIC15)		
HIII 5F HIII 50M HIII 95M	$\Phi\left(\dfrac{\ln(HIC15)-6.96362}{0.84687}\right)$	$\Phi\left(\dfrac{\ln(HIC15)-7.45231}{0.73998}\right)$
THORAX: Chest Deflection (mm)		
HIII 5F	$\dfrac{1}{1+e^{1.870636-\frac{F}{187}\times10.1657}}$	$\dfrac{1}{1+e^{3.712417-\frac{F}{187}\times10.8774}}$
HIII 50M	$\dfrac{1}{1+e^{1.870636-\frac{F}{229}\times10.1657}}$	$\dfrac{1}{1+e^{3.712417-\frac{F}{229}\times10.8774}}$
HIII 95M	$\dfrac{1}{1+e^{1.870636-\frac{F}{254}\times10.1657}}$	$\dfrac{1}{1+e^{3.712417-\frac{F}{254}\times0.8774}}$
KNEE/THIGH/HIP: Axial Femur Force (KN)		
HIII 5F	$\dfrac{1}{1+e^{5.7949-F\times0.7619}}$	$\dfrac{1}{1+e^{4.9795-F\times0.478}}$
HIII 50M	$\dfrac{1}{1+e^{5.7949-F\times0.5196}}$	$\dfrac{1}{1+e^{4.9795-F\times0.326}}$
HIII 95M	$\dfrac{1}{1+e^{5.7949-F\times0.4091}}$	$\dfrac{1}{1+e^{4.9795-F\times0.257}}$
LEG: Upper Tibia Axial Force (KN)		
HIII 5F	$\dfrac{1}{1+e^{5.6654-F\times1.1374}}$	*Not Available*
HIII 50M	$\dfrac{1}{1+e^{5.6654-F\times0.8189}}$	*Not Available*
HIII 95M	*Not Available*	*Not Available*
ANKLE/FOOT: Lower Tibia Axial Force (KN)		
HIII 5F	$\dfrac{1}{1+e^{4.572-F\times0.9306}}$	*Not Available*
HIII 50M	$\dfrac{1}{1+e^{4.572-F\times0.67}}$	*Not Available*
HIII 95M	*Not Available*	

In addition, the NHTSA proposed a combined "occupant injury measure" at both the AIS2+ and AIS3+ levels. This approach (NHTSA, 2008) uses the injury probabilities for each of the body regions listed in Table 6 to calculate an overall combined injury measure for the occupant in the following manner:

Occupant Injury Measure (AIS3+, all ATDs)
$$= (1-(1-p(HIC15)) \times ((1-p(ChDefl)) \times (1-p(max(Femur)_{left,right})))^{AIS3+}$$

For the AIS2+ occupant injury measure calculations, two different equations were used, depending on the ATD:

Occupant Injury Measure (AIS2+, HIII 5F and HIII 50M)
$$= (1-(1-p(HIC15)) \times ((1-p(ChDefl)) \times (1-p(max(Femur)_{left,right})) \times$$
$$(1-p(max(UprTib)_{left,right})) \times (1-p(max(LwrTib)_{left,right})))^{AIS2+}$$

Occupant Injury Measure (AIS2+, HIII 95M)
$$= (1-(1-p(HIC15)) \times ((1-p(ChDefl)) \times (1-p(max(Femur)_{left,right})))^{AIS2+}$$

These equations use the peak values recorded for either the left and right legs for the femur and tibia axial forces.

For the ARS Project, these ATD injury metrics became the basis for developing the advanced restraint system parameters and for comparing to the baseline performance of the PVP restraint system. In the remainder of the report, the occupant injury measure calculations for AIS3+ and AIS2+ will be abbreviated as OIM-AIS3+ and OIM-AIS2+.

5   ARS Assessment Strategy and Baseline Vehicle Testing

With 2 different crash modes, at 2 different speeds, and 3 different occupant sizes, a total of 24 different "load cases," 12 for the driver and 12 for the right front passenger, were identified. It was not practicable within the constraints of the ARS Project to conduct vehicle-level crash tests for all 24 load cases with both the baseline restraint system and the advanced restraint system. Therefore, an assessment strategy utilizing both analysis and physical testing was developed. The assessment matrix is shown in Table 7. The intent was to use a combination of CAE and actual vehicle crash tests to provide a comparison between the two different restraint systems for each of the 24 load cases.

Table 7 - ARS Project Assessment Matrix

	Test	Restraint	Occupant		
			HIII 5F	**HIII 50M**	**HIII 95M**
Driver	MDB35	Baseline	*Test*	*Test*	CAE
	MDB35	ARS	*Test*	*Test*	CAE
	MDB25	Baseline	*Test*	*Test*	CAE
	MDB25	ARS	CAE	*Test*	CAE
	Pole35	Baseline	CAE	*Test*	CAE
	Pole35	ARS	CAE	*Test*	CAE
	Pole25	Baseline	CAE	*Test*	CAE
	Pole25	ARS	CAE	*Test*	CAE
Right Front Passenger	MDB35	Baseline	*Test*	*Test*	CAE
	MDB35	ARS	*Test*	*Test*	CAE
	MDB25	Baseline	*Test*	*Test*	CAE
	MDB25	ARS	*Test*	CAE	CAE
	Pole35	Baseline	*Test*	CAE	CAE
	Pole35	ARS	*Test*	CAE	CAE
	Pole25	Baseline	*Test*	CAE	CAE
	Pole25	ARS	*Test*	CAE	CAE

Based on the field data analysis, the 95th percentile male population represented a smaller percentage of real-world injuries. Therefore, it was decided to conduct the 95th percentile ATD assessment in CAE. Also, for the vehicle-to-pole crash mode, the 50th percentile ATD driver and 5th percentile female ATD passenger were tested at both speeds, and CAE simulation was conducted for the same modes with the ATD positions reversed. This resulted in six different baseline test configurations. The 5th percentile female ATD was tested in the full-forward seating position while the 50th percentile male ATD was tested in the mid-seat position. For the CAE analysis, the 95th was always placed in its nominal position which was the full rear seating position in the project vehicle.

All vehicle crash tests for the ARS Project were conducted at the Transportation Research Center (TRC) in East Liberty, Ohio. As discussed previously, the vehicle-to-vehicle crash mode was simulated by using a MDB into a stationary vehicle. Originally, the ARSC team investigated using the existing FMVSS No. 214 MDB. However, in order to match the mass of the PVP, over 700 pounds of ballast would need to be added to the cart. The TRC personnel determined that this, along with the intended speed of the test, would result in a significant chance of damage to the cart during the test. The FMVSS No. 301 (Fuel System Integrity) cart was considered as an alternative, since it has a higher mass than the FMVSS No. 214 cart, but it does not have a crushable impact surface. Ultimately, the MDB-to-vehicle tests were conducted with a modified MDB configuration, the FMVSS No. 301 cart with the FMVSS No. 214 deformable barrier mounted to its front. The mounting of the deformable barrier was adjustable in the vertical direction and was adjusted to match the bumper height of the PVP.

For the first baseline MDB-to-vehicle crash test, the total weight of the MDB was 4,000 lbs, while that of the PVP was 4,502 lbs. The maximum tow-speed capability at the test facility was required in an attempt to achieve the delta-v target of 35 mph. This may be a concern if this test mode is attempted at other crash test facilities that may not be capable of achieving these high speeds. It also should be noted that all of the MDB-to-vehicle tests were conducted outdoors. Given the post-impact kinematics of the MDB-to-vehicle test, an indoor facility may be challenged to provide adequate space to conduct this test.

Figure 13 is an overhead photo of the pretest configuration for the first baseline MDB-to-vehicle test (Test #090904), showing the 80-percent offset and 15° oblique angle. The MDB achieved a test speed of 73.4 mph resulting in a measured delta-v for the PVP of 35.8 mph.
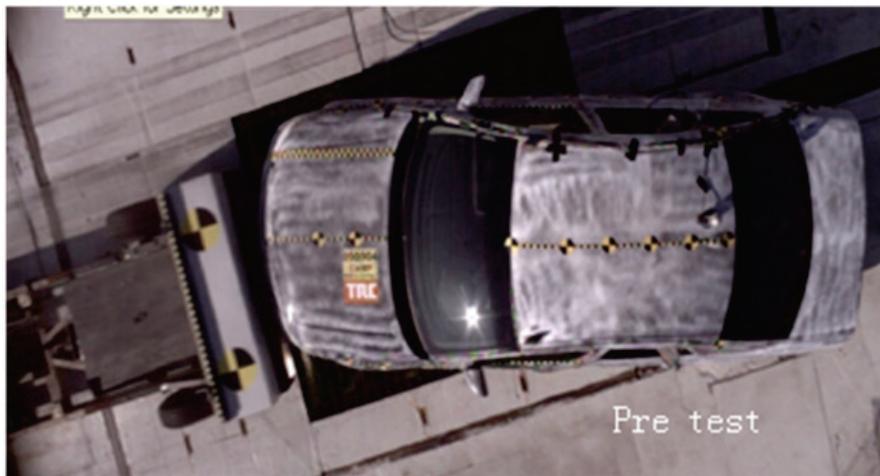
Figure 13 - MDB-to-Vehicle Test Configuration

The second baseline crash test (Test #090922) simulated a vehicle-to-object crash event. A pole test was conducted at a speed of 34.8 mph. The 10-inch pole was aligned with the centerline of the vehicle (see Figure 14).

Figure 14 - Vehicle-to-Pole Test Configuration

Given the reliance on CAE for many of the load cases, it was important to understand the amount of intrusion that was observed in the baseline testing in order to estimate the dynamic intrusion in the CAE models. For each test, a coordinate-measuring machine (CMM) was used to conduct a detailed dimensional analysis of the vehicle by determining the coordinates of a large matrix of reference points pre- and post-test. Figures 15 and 16 show the toepan intrusion measured in the first MDB35 baseline crash test for the driver and passenger sides, respectively (Test #090904), while Figures 17 and 18 provide the same measurements for the first Pole35 baseline crash test (Test #090922). Additional points were tracked at the centerline of the driver seating position, centerline of vehicle, and centerline of passenger seating position from the floorpan to the upper dash for a more complete picture of the intrusion profile.
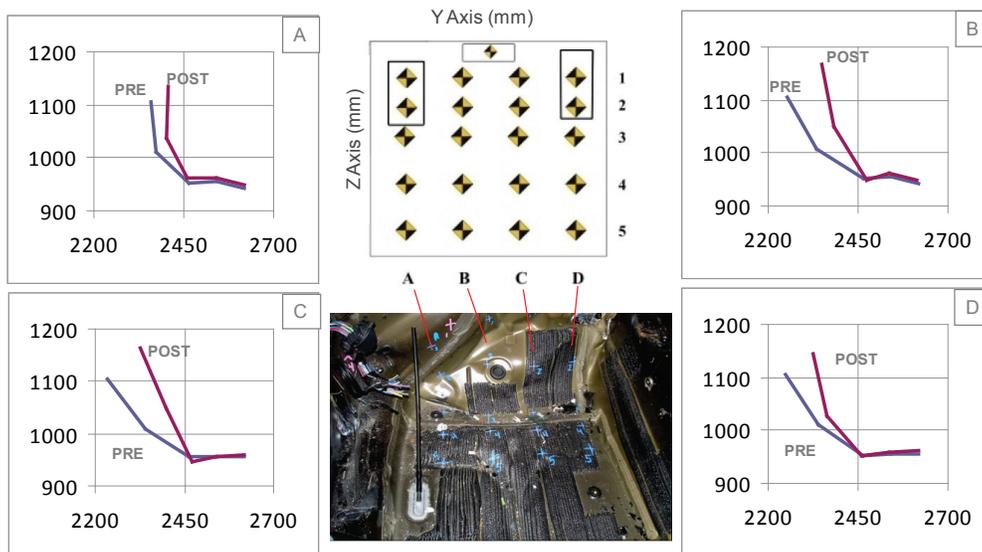
Figure 15 – Driver Side Toepan Intrusion From MDB35 Baseline (Test #090904)
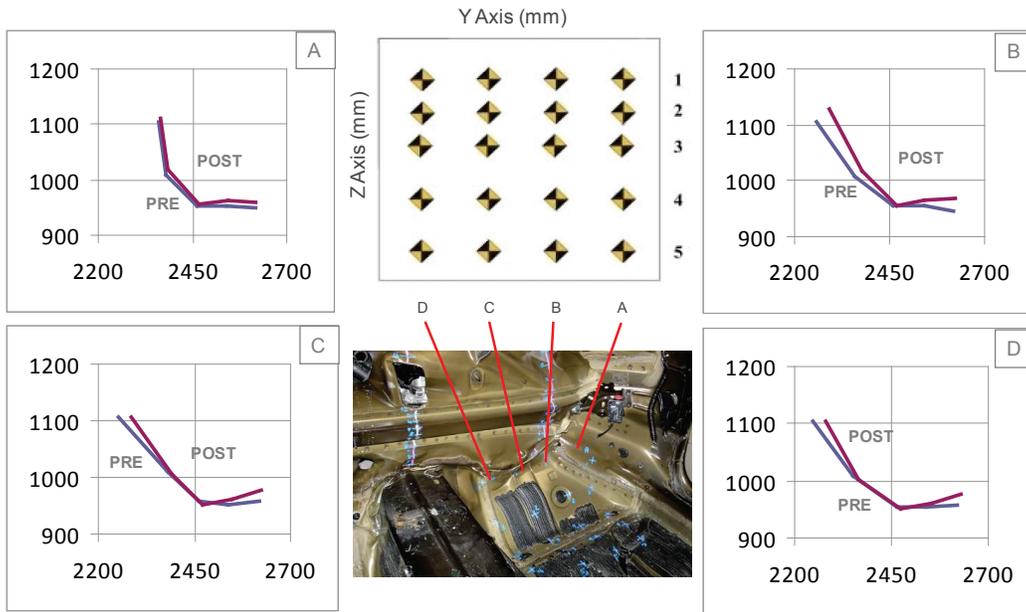
Figure 16 – Passenger Side Toepan Intrusion From MDB35 Baseline (Test #090904)
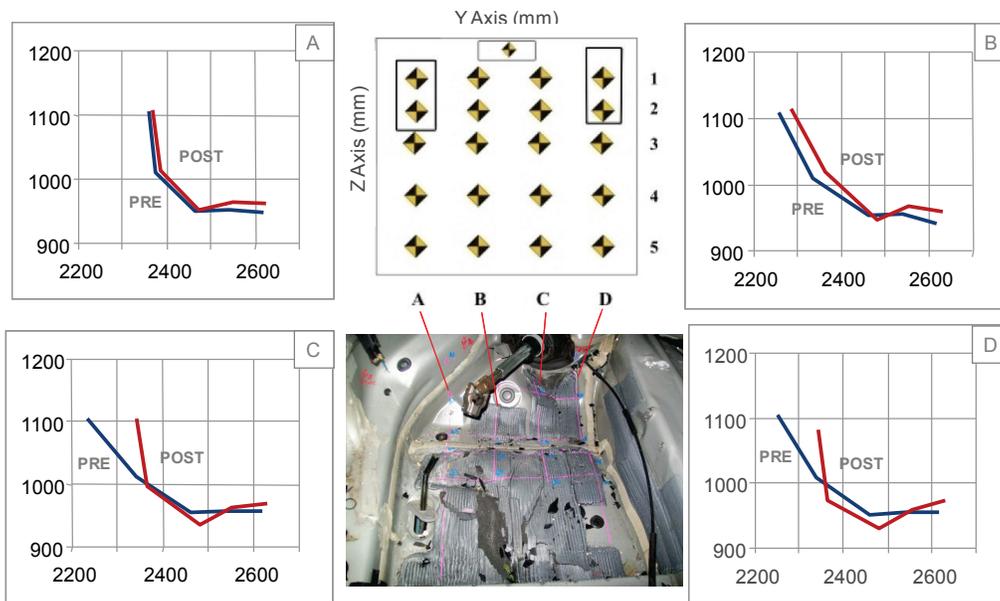
Figure 17 - Driver Side Toepan Intrusion From Pole35 Baseline (Test #090922)
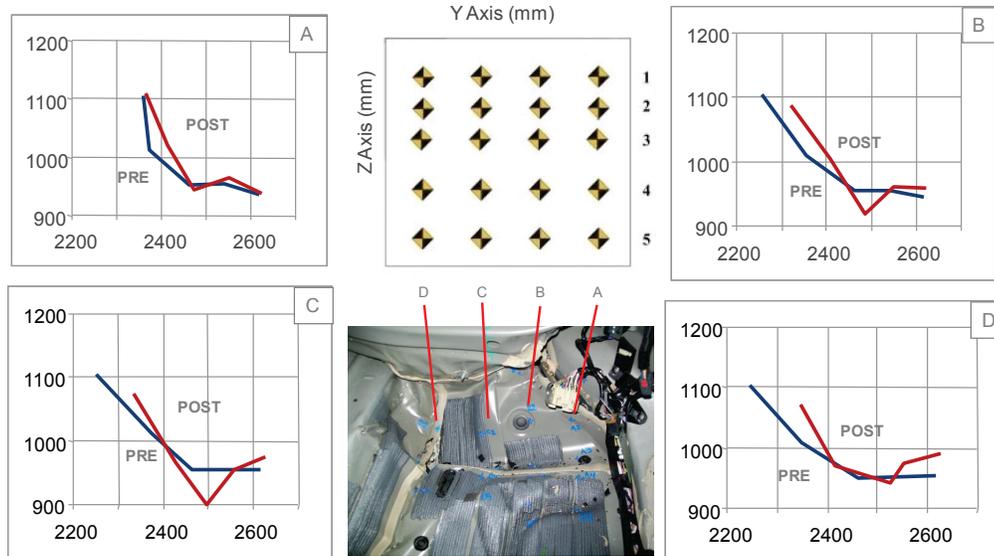
Figure 18 - Passenger Side Toepan Intrusion From Pole35 Baseline (Test #090922)

Overall the pre- to post-test dimensional differences showed significant intrusion for both test modes. The intrusion of the footwell area will add test to test variability, especially for the lower extremities, through differences in interaction with the intruding floorpan and instrument panel. In addition, hardware damage was noted for the right THOR-Lx leg on the driver ATD and for the left THOR-FLx on the passenger ATD in the first MDB-to-vehicle crash test, with nearly one third of the lower leg data channels identified as having recorded questionable data. Also of note was the inability to reproduce intrusion within a Hydraulically Controlled Gas Energized (HYGE) sled environment. HYGE sled testing was conducted during the course of the ARS Project as a development tool for the advanced restraint system. Thus, results from the sled tests, particularly with respect to the lower extremities, were not directly comparable to the physical crash tests.

The final list of baseline vehicle crash tests conducted for the ARS Project is shown in Table 8. The longitudinal acceleration measured at the CG of the vehicle was used to calculate the delta-v. The chart contains the original six load cases and compares the target and final delta-v values. An additional MDB35 test (Test #101027) was conducted to address an anomaly in the passenger side chest deflection measured on the HIII 50M in the initial test (Test #100301). This repeat test resulted in improved data, which was utilized for the baseline comparison.

Table 8 - Baseline Vehicle Crash Test Matrix

Crash Configuration	Test Speed (mph)	Delta-V (mph)	Test Number	Driver	Passenger
MDB35	73.4	35.8	090904	HIII 50M	HIII 5F
Pole35	34.9	39.3	090922	HIII 50M	HIII 5F
MDB35	72.7	38.9	100301	HIII 5F	HIII 50M
MDB25	54.1	24.6	100316	HIII 50M	HIII 5F
Pole25	24.9	29.0	100322	HIII 50M	HIII 5F
MDB25	54.0	26.3	100624	HIII 5F	HIII 50M
MDB35	72.6	35.6	101027	HIII 5F	HIII 50M

Photographs of the PVP after the first baseline MDB-to-vehicle tests and vehicle-to-pole tests at both speeds are provided in Figures 19 and 20, respectively.

Figure 19 - Post-Test Photographs of PVP: MDB35 Test #090904 (Left) and MDB25 Test #100316 (Right)

**Figure 20 - Post-Test Photographs of PVP: Pole35 Test #090922 (Left) and
Pole25 Test #100322 (Right)**

A summary of the key ATD injury measurements is provided for all baseline testing in
Table 9 (driver) and Table 10 (right front passenger). In general, the PVP restraint system
performed well in the baseline tests, with all measured injury values below the
established injury limits specified in FMVSS No. 208. The establishment of this baseline
posed a challenge to the advanced restraint system under development, with limited
opportunities for significant occupant performance improvement in many regions.

**Table 9 - Summary of Driver ATD Injury Assessment for
Baseline Vehicle Crash Tests**

Injury Criteria	MDB35		MDB25		Pole35	Pole25
	HIII 5F (101027)	HIII 50M (090904)	HIII 5F (100624)	HIII 50M (100316)	HIII 50M (090922)	HIII 50M (100322)
HIC (15ms)	192	244	164	109	151	103
Neck NIJ	0.52	0.37	0.41	0.29	0.32	0.34
Chest Deflection (mm)	31	45	26	27	43	30
Chest Accel - 3ms (g)	51	52	39	30	45	36
Left Femur Fz (kN)	5.96	2.78	3.09	2.80	3.81	3.91
Right Femur Fz (kN)	3.92	6.33	1.14	2.02	3.28	3.52
Left Upper Tibia Fz (kN)	2.77	1.88	2.10	1.64	1.60	1.03
Right Upper Tibia Fz (kN)	2.26	2.61	0.54	0.31	0.45	1.02
Left Lower Tibia Fz (kN)	3.54	3.28	2.00	2.20	1.66	1.63
Right Lower Tibia Fz (kN)	3.91	6.38	1.14	1.54	2.32	1.95

**Table 10 - Summary of Passenger ATD Injury Assessment for
Baseline Vehicle Crash Tests**

Injury Criteria	MDB35		MDB25		Pole35	Pole25
	HIII 5F (090904)	HIII 50M (101027)	HIII 5F (100316)	HIII 50M (100624)	HIII 5F (090922)	HIII 5F (100322)
HIC (15ms)	467	630	76	107	632	76
Neck NIJ	0.58	0.36	0.40	0.22	0.38	0.34
Chest Deflection (mm)	20	29	11	26	17	13
Chest Accel - 3ms (g)	47	42	26	27	44	28
Left Femur Fz (kN)	3.44	6.52	1.59	2.81	3.36	2.62
Right Femur Fz (kN)	1.71	3.74	1.93	2.75	1.90	2.03
Left Upper Tibia Fz (kN)	4.46	1.58	1.49	1.75	2.65	1.67
Right Upper Tibia Fz (kN)	2.03	3.03	0.81	1.96	1.57	0.23
Left Lower Tibia Fz (kN)	5.36	2.29	2.17	1.86	2.99	2.51
Right Lower Tibia Fz (kN)	3.07	4.09	1.32	2.43	2.51	0.42

The level of IAVs for the lower speed tests did not indicate a significant risk of injury, especially for the lower extremities. The field data analysis showed that the off-road, lower speed impacts in which AIS2+ or AIS3+ injuries occurred often involved an out-of-position occupant. Since this situation is not recreated in the vehicle crash tests, the crash test data is not representative of all the injuries being observed in the field data. This situation has been documented previously for centerline pole impacts (Insurance Institute for Highway Safety, 2009).

6   Identification and Development of Advanced Restraint System

The initial tasks within the ARS Project provided the background for selecting the advanced restraint system developed under Task 6. In Task 3, a survey of restraint suppliers was conducted to identify potential technology that could be used for future advanced restraint systems and subsequently synthesize countermeasure concepts from this information. During this task, the ARSC Participants agreed that the current, state-of-the-art, pre-crash sensors could not predict an imminent collision with enough reliability to be used to deploy irreversible restraints. It was also agreed that this was unlikely to change in the next three to five years. Thus, the ARSC only pursued the pre-deployment of reversible (motorized) restraint components and focused on using the pre-crash sensor information to identify the crash mode and adapt the restraints system to the identified mode. In Task 4, the restraint technology identified in the supplier survey was evaluated and rated for its potential effectiveness in reducing injuries for the two ARS Project crash modes. The outputs from Task 4 included the identification of four candidate advanced restraint systems (two driver-side systems and two right front passenger systems) from two separate restraints suppliers. Ultimately, a single restraint supplier, TK Holdings, Inc. (Takata) was selected. Takata was responsible for not only the development and prototyping of the advanced restraint system components but also for the system-level CAE used within the component design and the development process used to optimize restraint system parameters.

In selecting the components for the advanced restraint system, the primary philosophy was to employ restraints that minimized forward pelvic movement as much as possible and, assuming a full suite of pre-crash information was available (including occupant size and weight, seating position, crash type and severity), utilize adaptive features in the advanced restraint system to provide maximum tunability over the full range of occupants and load cases. The ARS components with responses that could be tailored based on pre-crash information selected for further study within the ARS Project were:

- Driver Air Bag (DAB) with active vent (Takata Programmable Venting Module (PVM))
- Passenger Air Bag (PAB) with active vent (Takata PVM)
- D-Shape Head Side Air Bag (HSAB)
- Knee Air Bag (KAB)
- Motorized Seat Ramp (MSR) (simulated by a fixed steel structure)
- Motorized Seat Belt (MSB)
- Dual-stage, Switchable Load Limiting Retractor
- Retractor Pretensioner (RPT)
- Outboard Seat Belt Lap Anchor Pretensioner (LPT)

In the following sections, a summary of the development of the key advanced restraint system components is provided.

6.1   Driver Air Bag System and Steering Wheel

6.1.1 Driver Air Bag System

The key adaptive feature of the ARS driver air bag system was an active vent (referred to as a "Programmable Venting Module," or PVM). The PVM mechanism consisted of a pyrotechnically driven steel band that is incorporated onto the driver air bag (DAB) housing. When activated, the band rotates relative to the housing and exposes window openings on the housing, which serves to vent inflator gas for supplemental cushion venting (see Figure 21).
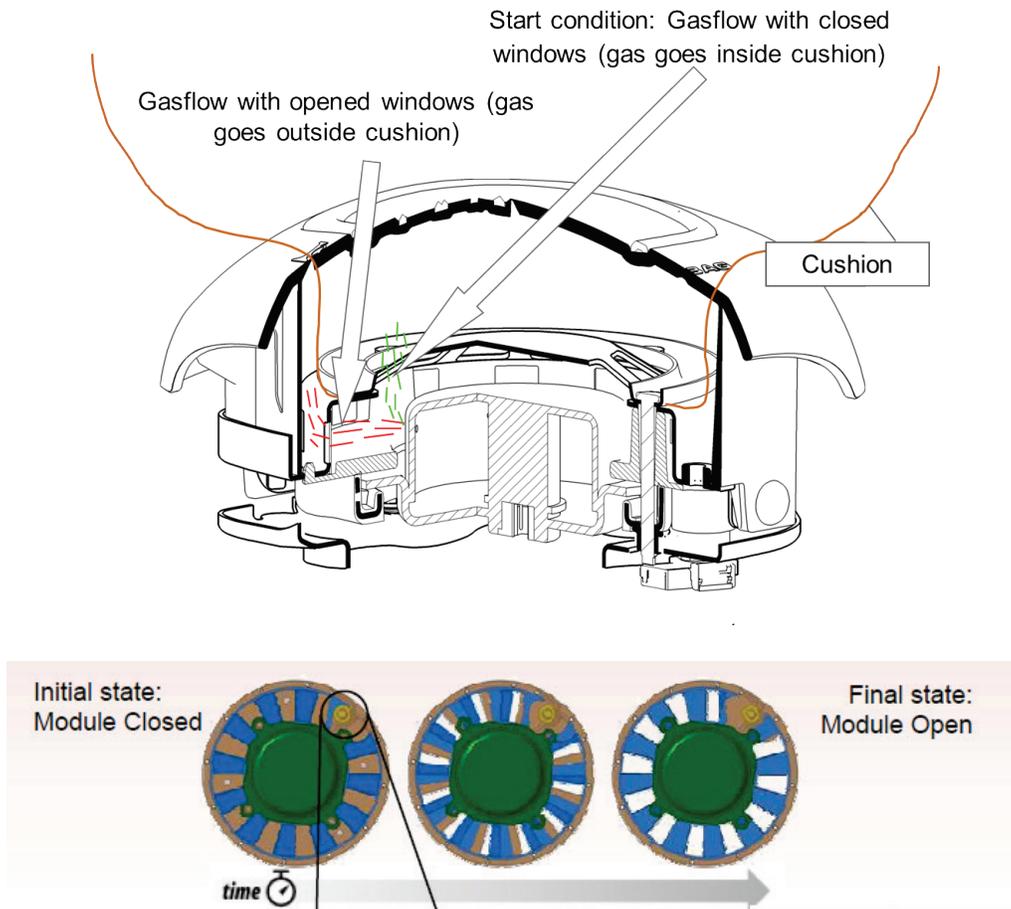
Figure 21 - Driver Air Bag Module With PVM Functionality

Given the good performance in the baseline tests, the overall strategy for the ARS driver air bag development was to mimic some of the key characteristics of the PVP driver air

bag and then to use the PVM functionality to further optimize the performance of the ARS DAB system for each of the 12 driver load cases.

The dual-stage inflator and cushion design of the ARS DAB were determined through CAE analysis and confirmed through component–level, static deployments and pendulum tests, which was then followed by sub-system level sled tests. In each of these assessments, the PVP DAB performance was directly compared to the proposed ARS DAB system, and iterations continued until an optimized inflator and cushion design for the ARS DAB system was achieved. The cushion vent size, a fixed parameter, was determined through CAE analysis. A range of fixed vent sizes was considered (1 x Ø25 mm, 1 x Ø28 mm, 1 x Ø31 mm) with the understanding that the fixed vent chosen needed to be compatible with the range of possible PVM open times. CAE studies were conducted for all of the higher speed load cases (with each of the three ATDs) to identify the appropriate fixed vent size. From this, a fixed vent size of 1 x Ø28 mm was selected. Static and sled testing were also used to identify a cushion fold that provided air bag deployment kinematics and steering wheel coverage per target specifications.

The PVM mechanism was evaluated via pendulum component tests and the resulting data were used to correlate the component DAB CAE model. Figure 22 shows representative deceleration versus time responses and the effect of opening the PVM at various times.
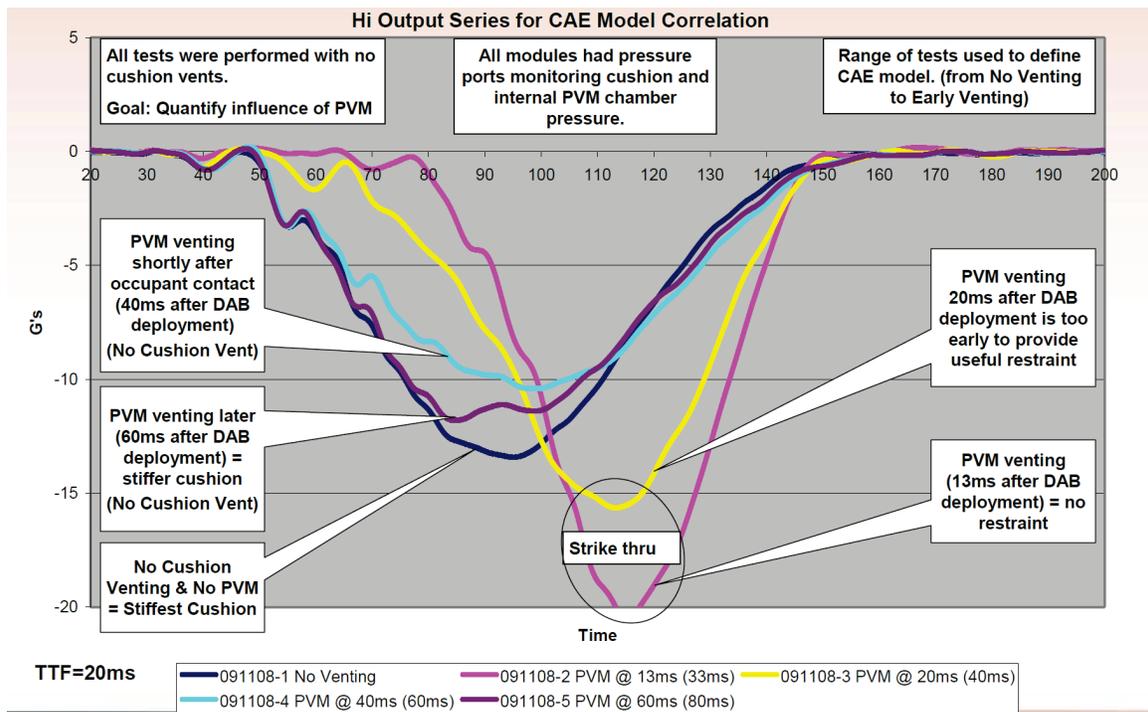
Figure 22 - Pendulum Testing Illustrating the Effect of Various PVM Open Times on Response

One critical aspect of the PVM function is that opening the PVM mechanism prior to the bag achieving its "bag full" condition significantly hinders the filling time and ultimate

pressure attainable by the air bag when full. This is illustrated by the yellow and magenta curves above in Figure 22. As a result of CAE optimization studies, the minimum PVM activation time was set at 30 ms from initiation of the primary stage of the inflator which ensured the bag achieved its fully inflated condition prior to activation.

6.1.2 Steering Wheel

Incorporating the ARS cushion, inflator, and PVM mechanism into the PVP driver air bag cover and housing was not practical. Therefore, Takata used a surrogate ARS module to facilitate integration of the key ARS DAB sub-components. This in turn drove the need for a surrogate steering wheel, to which the ARS DAB mated. Like the PVP steering wheel, the ARS surrogate steering wheel was a 4-spoke wheel with a die cast aluminum armature (see Figure 23). To attach the surrogate ARS steering wheel to the PVP steering column, bridging collars were fabricated.

Figure 23 - PVP Steering Wheel (Left) and ARS Surrogate Steering Wheel (Right)

To compare the stiffness of the surrogate ARS steering wheel to the PVP steering wheel, and to facilitate steering wheel component CAE model correlation, impact tests were conducted. In these tests, a 34 kg free-motion torso was launched at 6.7 m/s and impacted the steering wheel. The torso deceleration was recorded. Impacts were conducted on the lower rim at 6 o'clock and on the upper rim at 12 o'clock (the steering wheel was turned 180 degrees). Deceleration vs. time responses of the torso impact to the PVP and ARS steering wheels were analyzed and the ARS steering wheel was found to be slightly "softer" than the PVP steering wheel. This was accounted for in the CAE model and was deemed to be a relatively insignificant factor relative to the other ARS system parameters.

6.2   Passenger Air Bag System

The design and development of the ARS PAB system was done in a very similar manner to the approach adopted for the ARS DAB system. As was the case with the ARS DAB, an active vent (PVM) was the key adaptive feature for the ARS PAB system. The PVM mechanism consists of a pyrotechnically-driven steel slide plate that translates relative to the housing and exposes window openings on the housing, venting inflator gas away from the air bag (Figure 24).

Initial state: PVM closed   Final state: PVM opened
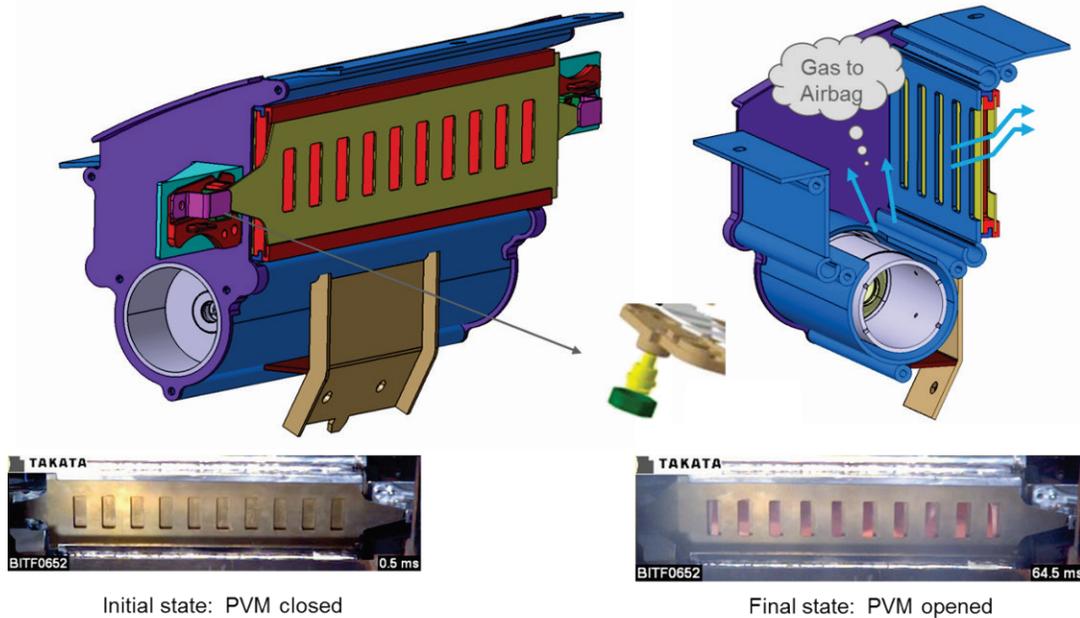
Figure 24 - Passenger Air Bag Module With PVM Functionality

The dual-stage inflator and cushion design for the ARS PAB system were tuned to yield equivalent performance with the PVP PAB system. This was accomplished initially through CAE analysis and confirmed via static deployments, linear impactor tests and sled tests. The fixed cushion vent size was again determined through a CAE analysis of the higher speed load cases with the understanding that the fixed vent chosen had to be compatible with the range of possible PVM open times. Three vent sizes were studied (2 x Ø64mm, 2 x Ø68mm, 2 x Ø72mm), with the smaller vent sizes of 2 x Ø64mm selected. Finally, the cushion fold was determined though an evaluation of the ARS PAB deployment kinematics through a number of static and sled tests.

As was the case with the ARS DAB PVM, a range of potential PVM activation times was studied in a series of component-level tests (for the PAB, a linear impactor was used). From this study, the minimum PVM activation time was set at 35 ms from initiation of the primary stage of the inflator to ensure the bag achieved its full condition prior to activation of the PVM.

6.3   D-Shape Head Side Air Bag System

Given the angularity of the MDB-to-vehicle crash mode, and the anticipated ATD kinematics associated with the test configuration in general, one of the ARS components studied was the "D-shape" Head Side Air Bag (HSAB) system. Compared to a standard head side air bag, the D-shape HSAB includes a bend that allows the cushion to extend further inboard into the occupant compartment as illustrated in Figure 25. Conceptually, the benefit of the D-shape construction is to support the driver's head in an effort to keep him/her centered on the restraint system as the post-impact kinematics of the PVP in the MDB-to-vehicle crash mode cause the driver to move forward and outboard relative to their initial seating position. Additionally, the extended cushion coverage associated with the D-shape HSAB design serves to provide inflated coverage forward in the A-pillar area, and serves to potentially mitigate injuries associated with off-axis rebound caused by the angular impact.

Cross-section on B pillar   ①
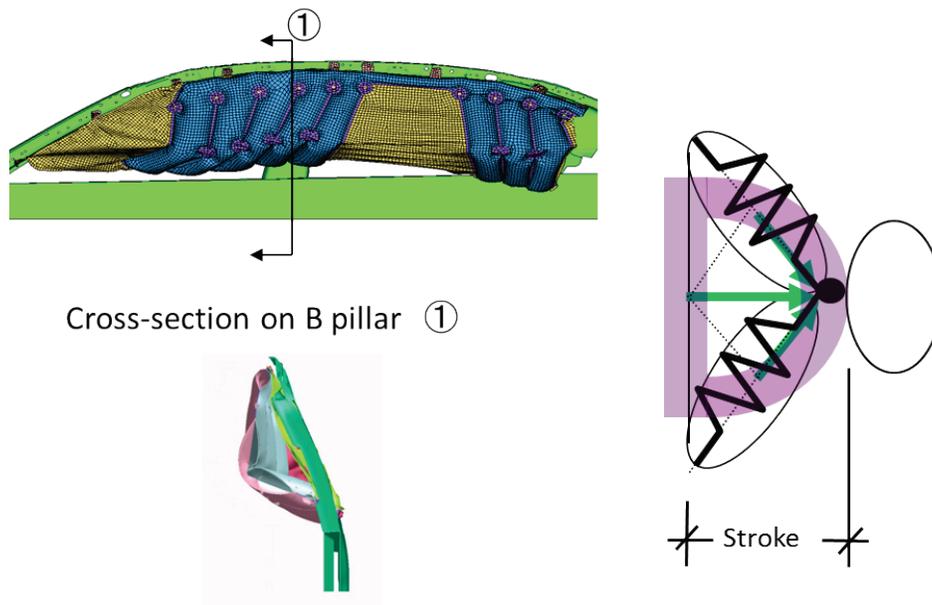
Figure 25 - D-Shape HSAB Design

The development of the ARS D-Shape HSAB involved several design iterations intended to minimize seat belt interaction with the deploying HSAB, provide sufficient inflated coverage area, ensure the cushion would position sufficiently inboard to provide lateral support to the ATD's head, and identify a suitable inflator output for the final cushion size. The design was evaluated via static deployment testing, linear impactor testing and sled testing. Figure 26 shows a deployed D-shape HSAB.

Figure 26 - D-Shape HSAB (HIII 50M)

Given the driver ATD kinematics observed in the baseline MDB-to-vehicle crash tests and the associated IAVs measured, the D-Shape HSAB was ultimately omitted from the final ARS CAE optimization studies and the subsequent final ARS crash tests. In the baseline tests, the ATD remained largely centered on the driver air bag. IAVs measured during the rebound phase did not represent a significant risk of injury. Although not used in the final ARS system, any potential benefit of the D-shape HSAB may be realized in crashes involving more offset and angularity.

6.4   Knee Air Bag

The intrusion associated with the two crash test modes, especially at the higher speeds, posed a significant challenge to mitigate the risk of lower extremity injuries. In an effort to achieve this, the ARS Project employed a strategy of minimizing the forward pelvis movement and providing cushioning to the knee bolster area via a knee air bag (KAB). The baseline PVP was not equipped with a KAB. Therefore there were no packaging accommodations for the KAB. The KAB was mounted to the instrument panel below the bolsters, pointing downwards. This arrangement is referred to as an "ultra-low" mount KAB or downward deploying KAB.

The initial development of the ARS KAB focused on the specification of the overall cushion geometry and inflator output. CAE analysis, static deployments, pendulum tests, and sled tests were used to evaluate the suitability of each design under study.

The first step in the development process was to define the cushion shape. Cushion design options were prototyped and inflated using compressed air to evaluate the overall shape and coverage. The initial inflator output was specified based on the volume of the cushion. Next, the preferred cushion options were evaluated via static testing. Figure 27 shows a typical static deployment test setup.
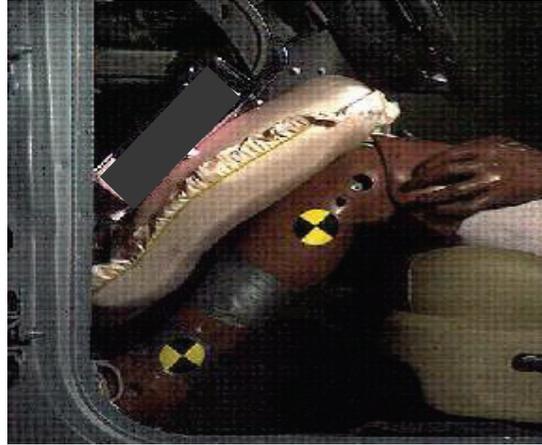
Figure 27 – Driver Side KAB Static Deployment (HIII 50M)

To characterize the energy absorbing capability of the ARS KAB, and to generate a data set for component model CAE correlation, impact pendulum tests were also conducted (see Figure 28).

Figure 28 - ARS KAB Shown in a Pendulum Test Fixture

The final design for the ARS KAB design was influenced by the results of sled testing. Changes to the inflator output and cushion design were implemented to reduce the likelihood of knee strike-through.

For the final ARS KAB system level sled testing and the ensuing ARS vehicle crash tests, the KAB cushion was positioned in the pre-deployed (unfolded) state prior to the test as shown in Figure 29. A pre-positioned KAB was used to yield a repeatable, reliable position of the KAB cushion. This was judged within the scope of the ARS Project given the study intent is to understand the potential energy absorbing (EA) benefits of the KAB. The pre-deployed position ensured that the cushion was in the proper position to cover the knees, especially for the full-forward sitting 5th percentile female, whose knee gap to the instrument panel was nominally less than 35 mm.

Figure 29 - Pre-Positioned ARS KAB, Prior to Inflation (HIII 50M)

6.5   Motorized Seat Ramp

A Motorized Seat Ramp (MSR) was selected for inclusion in the ARS system as part of the strategy to minimize forward excursion of the pelvis. Packaged in the seat cushion, the MSR is an electrically-actuated, reversible device that uses pre-crash information to determine whether or not activation is required. When activated, the motor drives a ramp that extends upwards in the seat cushion, to engage the lower thighs and, thus, provide supplemental pelvic restraint.

The geometry of the MSR was recommended by Takata and the initial development of the MSR for the ARS Project focused on defining the preferred MSR ramp angle and fore-aft location on the PVP seat. This was accomplished through CAE analysis. A simple PVP sled model was constructed and the effect on forward pelvic movement and femur loads was evaluated with the HIII 5F, HIII 50M, and HIII 95M for various positions and ramp angles of the MSR. From the CAE study, it was concluded that the seat ramp angled at 30 degrees placed directly below the H-point had the greatest effect on minimizing forward pelvic movement and reducing femur loads.

To facilitate hardware re-use, a surrogate seat ramp was used to represent the MSR in the "activated" condition. Figure 30 shows the surrogate MSR installed onto the baseline PVP seat. The seat ramp attached to the seat frame using the four existing bolts found on the PVP seat. The seat ramp design was common for both the driver and passenger sides of the vehicle.
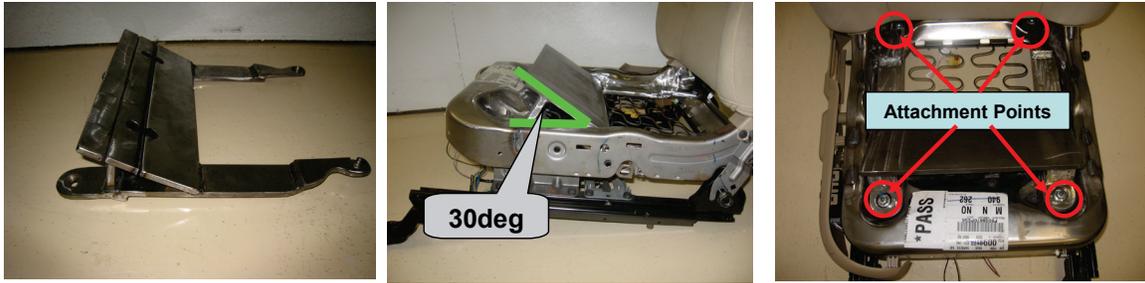
Figure 30 - Fabricated MSR Seat Ramp on PVP Seat

The activation of the seat ramp in the seat cushion may raise the occupant's pelvis. To control for this potential source of variation, the ATD's H-point in the ARS seat was monitored to maintain a target z-coordinate within 20 mm of the comparable position in the baseline seat. There were some ARS tests in which z-coordinate deviations required that the seat cushion be modified to maintain the target H-point position.

6.6 Seat Belt System

6.6.1 Motorized Seat Belt (MSB)

The Motorized Seat Belt (MSB) is an element of the seat belt retractor whereby an electric motor reverse-winds the spool pre-crash to take seat belt slack out of the system. Its activation requires pre-crash sensing information. There are three, primary, real-world potential benefits of the MSB. First, the MSB serves to provide a haptic warning to the occupant when a crash is imminent, which can alert the driver to begin evasive maneuvering or braking. Second, the MSB may reduce the occupant's forward-movement during an emergency braking situation and thus decrease out-of-position potential. Third, it may remove seat belt webbing slack to help the restraint system achieve increased restraining benefit if, in fact, a crash event occurs.

For all load cases in the ARS Project, the test protocol required that the ATDs be nominally seated with all seat belt slack removed. Thus, the design of the study was such that the potential real-world benefits of the MSB could not be evaluated, and the MSB feature was omitted from the ARS seat belt content.

6.6.2 Dual-Stage, Switchable Load Limiting Retractor

The ARS seat belt retractor featured a pyrotechnically-activated, switchable, dual-stage, adaptive load limiter device, referred to as an Intelligent Energy Absorber (IEA). Standard load-limiting retractors have one energy absorbing load that must cover the range of occupant sizes in all crash scenarios. Adaptive load limiting, provided by the dual-stage device, allows three load-limiting levels to cover the full range of occupant sizes in all crash scenarios: a "high" load level, a "low" load level, and a "stepped" load level going from the high load threshold to the low load threshold as shown in Figure 31. The time at which the load level is stepped down is a tunable parameter and can be adjusted by using pre-crash sensing information that can classify the occupant and crash type.
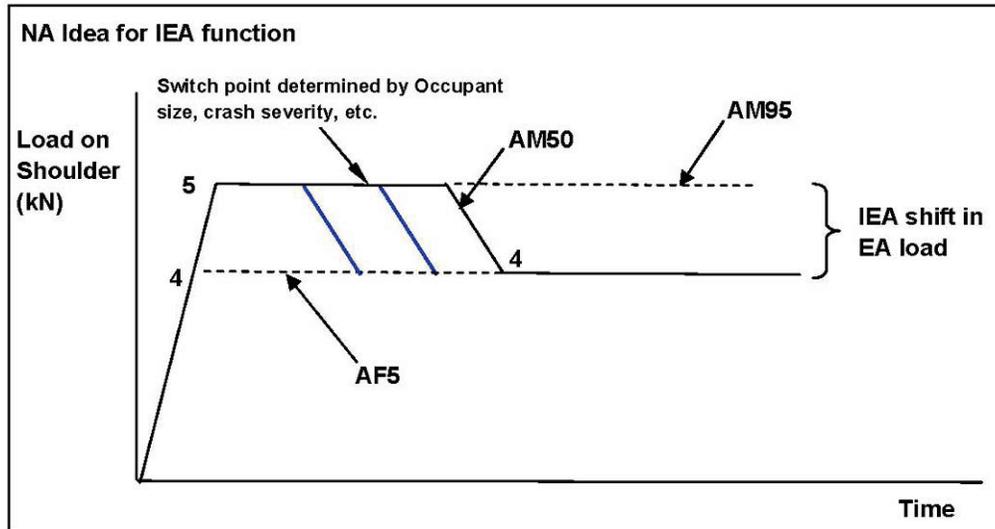
**Figure 31 - Load Curve Scenarios for the Dual-Stage,
Adaptive Load Limiter Device**

The IEA load limiter device contained two torsion bars thus allowing for two levels of load limiting. By design, the load limiting must always be switched from a "high" load to a "low" load. The switch time is determined by the sensing system and the step-down in the load limiter occurred over a short time interval after the signal is received.

Three torsion bar combinations were studied for the ARS Project (denoted as "high/low" based on loads measured at the retractor):

- 4.55/2.45 kN
- 4.20/2.10 kN
- 3.85/1.75 kN

The torsion bar combinations, while tunable, were selected from an inventory of readily available hardware. Since the available options represented a large enough range of EA levels suitable for the load cases under study, no other load limiter combinations were considered.

The initial CAE optimization study determined the best settings for the "fixed" ARS parameters, including the preferred load limiter combination. For the ARS Project, the 3.85/1.75kN torsion bar combination was selected. As a fixed parameter, the torsion bar combination could not be varied across load cases. The only parameter that was varied in the optimization studies was the torsion bar switch time.

6.6.3 Retractor Pretensioner (RPT)

The ARS seat belt system incorporated a "dual-pretensioning" strategy with pyrotechnic pretensioners at the retractor and outboard anchor. As a "tunable" parameter, the retractor pretensioner was considered from a "deploy/no deploy" perspective, while the pretensioner output and stroke were fixed variables.

6.6.4 Lap Anchor Pretensioner (LPT)

A lap anchor pretensioner was included as part of the ARS system. As illustrated in Figure 32, the outboard portion of the lap belt is attached to the anchor, and the pretensioner is pyrotechnically activated to cinch the lap belt down.

Cinch direction

Lap portion of belt attached here

Direction of piston movement, which pulls cable attached to anchor
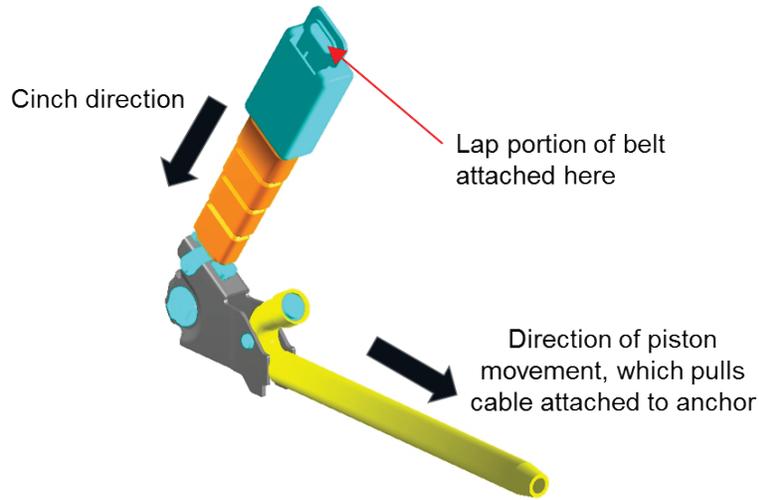
Figure 32 - Lap Anchor Pretensioner

The "tunable" parameter for the LPT was the deployment time relative to the retractor pretensioner. Two potential tuning conditions were evaluated: simultaneous deployment of both pretensioners, or a deployment of the LPT 6 ms after the RPT. The delay of 6 ms between the retractor pretensioner deployment and lap anchor pretensioner deployment represented the time at which the RPT had completed its webbing pay-in phase. As was the case with the RPT, the LPT output and stroke were fixed variables, representing a current production design.

6.6.5 Dynamic Locking Tongue

The Dynamic Locking Tongue (DLT) is a feature of the tongue that under normal conditions functions as a standard, free-falling latch. However, when the lap portion of the seat belt is loaded during a crash event from the pretensioner and/or from the occupant's forward movement, the DLT locks to prevent webbing from slipping from the shoulder to the lap portion of the seat belt. The net effect is to isolate the lap and shoulder sections of the seat belt. Figure 33 illustrates components of the dynamic locking tongue.
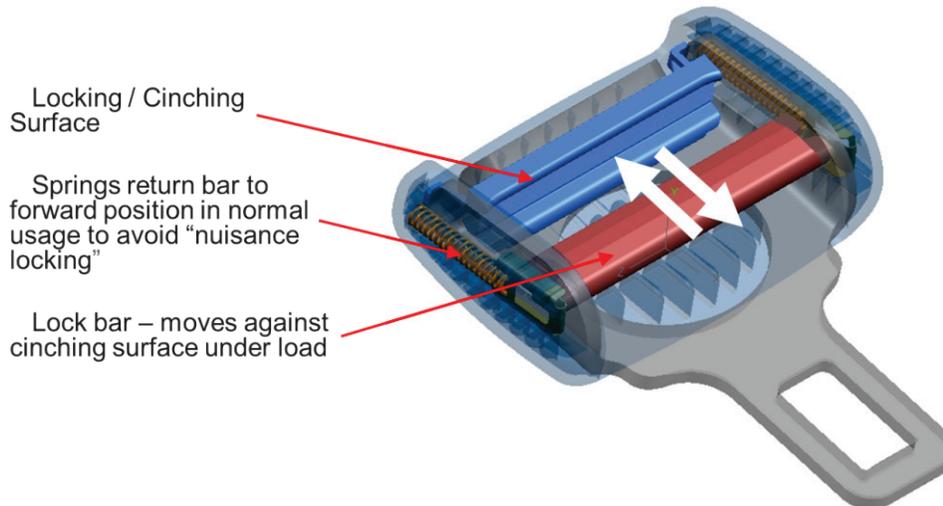
Figure 33 - Dynamic Locking Tongue (DLT)

One potential benefit of the DLT is that it helps better restrain the occupant's pelvis, since the lap portion of the seat belt cannot slip through the tongue as the occupant moves forward. The improved pelvic restraint could, in theory, help mitigate femur and tibia loads. Another potential benefit is that the load at the lap, which is typically high, cannot be transmitted to the shoulder portion of the seat belt, which in turn may help mitigate chest deflection.

For the ARS Project, the DLT was considered a "fixed parameter" and was included in the seat belt content for all load cases.

6.7   Sled Testing

Two different types of sled test methodologies were utilized during the ARS component development.

6.7.1 Sled Testing with NCAP Pulse

The first method used a 35mph NCAP pulse with the PVP sled buck positioned at 0 degrees (no angularity was simulated). Four series of sled tests were conducted by Takata, of which the primary goal was to confirm the functionality and integrity of the ARS components prior to sled or vehicle testing conducted at TRC. Over the course of these sled series, a methodical approach was taken whereby components of the ARS system were introduced systematically to ensure the effect of each component could be isolated for evaluation.

6.7.2 Sled Simulation of MDB-to-Vehicle Test

A second sled methodology was developed to simulate the 35 mph delta-v MDB-to-vehicle crash test. The sled tests were conducted at TRC and utilized their HYGE sled system. A rigidized PVP sled buck (Figure 34) was mounted to an interface frame that could be adjusted in 5-degree increments of yaw. This adjustability was necessary in order to simulate the 15-degree oblique impact of the MDB-to-vehicle baseline test. It was also necessary to identify an appropriate sled metering pin - a component of the

HYGE actuator that controls the flow of gas required to propel the sled buck with the desired acceleration pulse. After several trial runs, a sled pin was identified that produced an acceleration pulse that closely matched the vehicle pulse from MDB35 Test #090904 and was consequently selected for further study.

Figure 34 - PVP Sled Buck

Four series of sled tests were conducted using this methodology with the following primary objectives:

- Provide hardware learning cycles to verify functionality to specification of ARS components

- Observe trends in key ATD injury criteria in comparing baseline PVP restraint system to ARS

- Generate system-level sled data to cross-check CAE models prior to conducting full-scale CAE DOE optimization runs

As shown previously in Table 7, the assessment of the 95th percentile male and the potential benefit offered by the advanced restraint system for a larger occupant was determined exclusively through CAE. However, the 95th Hybrid III ATD was tested in the sled environment and the data was important input for the CAE predictions.

A primary sled test limitation was the inability to simulate the dynamic intrusion observed in the vehicle tests. Intrusion likely plays a role in lower leg/foot injury mechanisms. In analyzing the sled test results, emphasis was placed on the ATD upper body kinematics and responses, recognizing that learning with respect to the lower body ATD responses would be limited in the sled environment. Pelvis forward movement

relative to the PVP baseline was the primary metric for evaluating the potential for lower extremity injury mitigation on the sled.

6.7.2.1 TRC Sled Test Series #1

The primary objectives of the first sled test series were to assess correlation with the MDB-to-vehicle test (Test #090904) and to establish baseline performance for all three ATDs in both seating positions. A total of five tests were conducted in this series as described in Table 11.

Table 11 - Test Matrix for TRC Sled Test Series #1

Test Number	Sled Angle (deg)	Driver ATD	Passenger ATD
S100212	15	HIII 50M	HIII 5F
S100217	10	HIII 50M	HIII 5F
S100219	10	HIII 50M	HIII 5F
S100305	10	HIII 5F	HIII 95M
S100309	10	HIII 95M	HIII 50M

These tests were all conducted with PVP production instrument panels and seats. The angle sled change from 15 degrees in S100212 to 10 degrees in S100217 resulted in ATD kinematics that better matched the kinematics observed in Test #090904. As a result, a sled angle of 10 degrees was maintained for the remaining sled tests. Once repeatability was established with S100219, the final two tests completed the baseline evaluations.

In comparing the sled pulse to that of the vehicle center of gravity (CG), acceptable correlation was observed once the vehicle pulse was shifted by 6ms. Figure 35 is a plot of the velocity time history of the first two sled tests compared to the measured MBD35 vehicle pulse of Test #090904 with the 6 ms time shift. To account for this observed difference, restraint systems were deployed 6 ms earlier on the sled to correspond to the equivalent deployment time anticipated for the vehicle test.
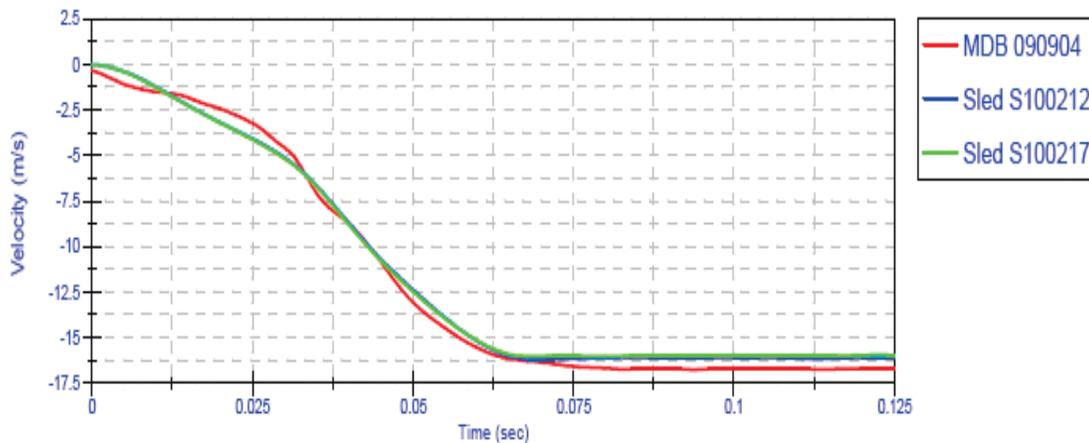
Figure 35 - Velocity Profile Comparison Between Vehicle CG and Sled Tests

6.7.2.2 TRC Sled Test Series #2

The tests in this series were designed to address two different objectives: the effects of sled buck reinforcement and interior hardware modification as well as first generation hardware development cycle. Tests S100420, S100421, S100426 and S100503 were conducted with PVP baseline restraint hardware to study the effect of adding:

- A reinforced instrument panel (IP) (S100420)

- A reinforced seat (S100421)

- A steering column load cell (S100426)

- A seat ramp (simulated with steel structure, shown in Figure 30) (S100503)

Understanding the impact of using a reinforced IP and reinforced seat (relative to the production versions used in the previous sled series) was important as it was anticipated that the remaining sled tests would be conducted with reinforced structures to enable reuse of test properties and to allow for the integration of the advanced restraint system hardware.

Tests S100427-S100430 were conducted as an initial hardware learning cycle with a subset of the first generation advanced restraint system. These tests incorporated the driver and passenger air bags, as well as the seat belt hardware, but did not include the seat ramp, knee air bags, or D-shape head side air bag. Table 12 includes the ATD configurations for the second sled test series.

Table 12 - Test Matrix for TRC Sled Test Series #2

Test Number	Driver ATD	Passenger ATD
S100420	HIII 50M	HIII 5F
S100421	HIII 50M	HIII 5F
S100426	HIII 50M	HIII 5F
S100503	HIII 50M	HIII 5F
S100427	HIII 5F	HIII 50M
S100428	HIII 95M	Ballast
S100429	Ballast	HIII 95M
S100430	HIII 50M	HIII 5F

6.7.2.3 TRC Sled Test Series #3

A third sled test series focused on the second generation hardware for the advanced restraint system. For these tests, the restraint system was "expanded" to include knee air bags and seat ramps. In addition, a D-shape curtain was mounted on the driver side and deployed in the fourth test of this series. The deployment times for the restraint system components were guided by the CAE studies, as well as results from the separate sled testing conducted by Takata. As the test matrix of Table 13 shows, all three ATDs in each seating position were evaluated.

Table 13 - Test Matrix for TRC Sled Test Series #3

Test Number	Driver ATD	Passenger ATD
S100706	HIII 5F	HIII 50M
S100707	HIII 95M	HIII 5F
S100708	HIII 50M	HIII 95M
S100709	HIII 50M	HIII 5F

6.7.2.4 TRC Sled Test Series #4

The fourth sled test series conducted prior to vehicle crash tests evaluated the optimized 2nd generation advanced restraint system hardware. In addition to the hardware changes from the previous test series, the knee air bags for both occupants were redesigned to improve their geometric coverage and to increase their inflated pressure, and the D-shape HSAB was modified to increase forward coverage and to decrease its interaction with the seat belt system. Again, all three ATDs were included in the test matrix (Table 14).

Table 14 - Test Matrix for Sled Test Series #4

Test Number	Driver ATD	Passenger ATD
S100816	HIII 50M	HIII 5F
S100817	HIII 5F	HIII 50M
S100818	HIII 95M	Ballast
S100819	HIII 50M	HIII 95M
S100830	HIII 50M	Ballast
S100831	HIII 95M	Ballast

6.8 ARS Interim Vehicle Crash Tests

Prior to conducting the final ARS vehicle crash tests, two "interim" vehicle crash tests (one MDB-to-vehicle and one vehicle-to-pole) were conducted with the second generation of ARS hardware. These two tests were added to confirm that the restraint design assumptions were robust despite limitations of the development sled environment (for example, the inability to simulate dynamic intrusion observed in the vehicle tests). It was also an important learning opportunity and sense-check with respect to the CAE model analyses which were relied upon heavily for optimizing the advanced restraint system for each occupant. One of the outcomes of these tests was, for example, that the coverage of the knee air bags was improved.

The ARS interim MDB-to-vehicle test (Test #100723) was conducted at a speed of 73.3 mph, with a HIII 50M (with THOR-Lx legs) driver and a HIII 5F (with THOR-FLx legs) right front passenger. In this test, the 5th passenger was moved one inch rearward from the full forward seating position to allow the knee air bag to deploy and get into position. This adjustment was necessary given the challenges of integrating the knee air

41

bags within the existing PVP architecture. This was the only vehicle test in which the passenger HIII 5F was not placed in the full forward position.

The second ARS interim vehicle crash test (Test #100813) was the 35 mph vehicle-to-pole test, a repeat of Test #090922. The driver was a HIII 50M (with THOR-Lx legs), while a HIII 5F with THOR-FLx legs was placed in the right front passenger seat.

6.9   ARS Component Development Summary

The final list of ARS components, and the tunable parameters used for the CAE optimization studies, are provided in Table 15. Through the component, sled, and interim vehicle crash testing, the development of each ARS component was such that the ARSC had high confidence that the ARS components would function to their predicted system potential during the final vehicle crash tests.

Table 15 - ARS Components with Fixed and Tunable Parameters

ARS Component	Fixed Parameter(s)	Tunable Parameter(s)
Driver and Passenger Air Bags with Active Vents (PVM)	Bag geometry/tethers Vent size Inflator output	PVM time to deploy
Knee Air Bags	Bag geometry/tethers Inflator output	Deploy/no deploy
Dual-Stage Switchable Load Limiting Retractor (IEA)	"High" torsion bar load spec "Low" torsion bar load spec	Time to switch (high→low)
Retractor Pretensioner	Pretensioner output/stroke	Deploy/no deploy
Lap Anchor Pretensioner	Pretensioner output/stroke	Time to deploy
Motorized Seat Ramp	Ramp specification	Activation/no activation

7   CAE Analysis

CAE analysis played a significant role within the ARS Project. CAE Design of Experiment (DOE) optimization studies were conducted with the following objectives:

- Determine the appropriate vent size for the DAB and PAB (fixed parameters)

- Determine the appropriate retractor torsion bar combination (fixed parameter)

- Determine the recommended settings for the tunable parameters for the final ARS configuration for each of the 24 load cases.

The CAE studies were also relied upon to quantify the performance difference between the baseline PVP restraint system and the final advanced restraint system for 14 of the 24 load cases, including all of the 95th male assessments.

The CAE analysis was carried out using LS-DYNA occupant simulation finite element (FE) code. Figure 36 provides the process flow for the CAE analysis conducted for the ARS Project.
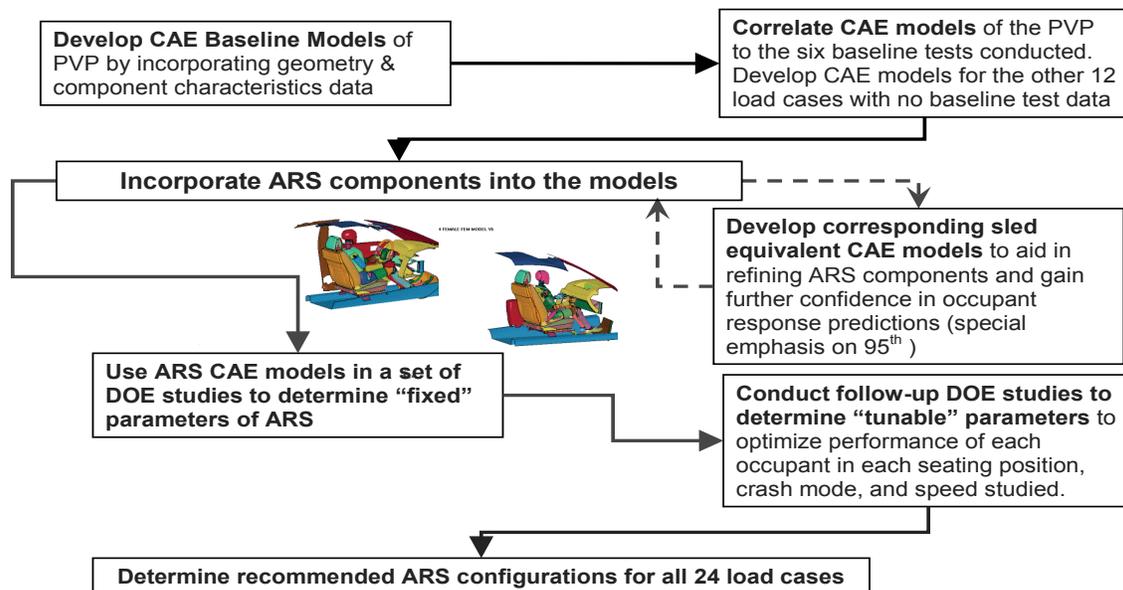
Figure 36 - CAE Process Flow

7.1   Development of CAE PVP Baseline Models

The baseline PVP models were developed in seven steps:

1. The geometry of the occupant environment(s) was defined

2. The load-deformation, stress-strain and displacement characteristics required to define occupant interaction with the vehicle interior were evaluated

3. CAE representations of the restraint system (air bags, seat belt restraints) were developed

4. The toepan, knee bolster and IP intrusion were defined

5. The steering wheel intrusion was defined

6. The vehicle pitch and yaw were defined

7. CAE models corresponding to each of the 24 load cases were completed. This involved:

   - Incorporating items 1-5 as appropriate, introducing the occupant (CAE ATD with THOR legs where appropriate) and positioning the occupant according to specifications

   - Applying crash pulse and executing the model

   - Debugging any errors and establishing candidacy of each model

In the baseline PVP CAE models of the driver, the interior environment was comprised of the seat, floor-pan, pedals, toepan, driver left side door trim, A- and B-pillars, IP and knee bolster, steering wheel and column, windshield, seat belts and accompanying hardware, and the air bag. In the baseline PVP CAE models of the passenger, the interior environment was comprised of the seat, floor-pan, toepan, passenger right side door trim, A- and B-pillars, IP and knee bolster, windshield, seat belts and accompanying hardware, and the air bag. Except for the seat belts and air bags, the surfaces of these components were meshed using information provided by the manufacturer of the PVP. Production air bags were used to determine the geometries and folds of the CAE air bag models.

Component level models were developed to help characterize occupant interactions with the vehicle interior. Through this development work, the following component characteristics were determined:

- Steering wheel rim stiffness

- Steering wheel (collapsible) column stiffness

- Material models for the CAE seat (foam and structure)

- Material models for the seat belts

- Knee bolster stiffness

- Passenger side glove box stiffness

Once these characteristics were determined, the component CAE models simulating physical tests were exercised under specific loading conditions. These model outputs were then compared with corresponding data from the component tests to assess their correlation.

In order to facilitate the introduction of dynamic intrusion in the CAE models, a coordinate-measuring machine was used for detailed pre- and post-test dimensional analysis of all vehicles. The data included X-Z sections of the intrusion profile from the

floor pan to the upper cowl at the center of the driver seating position and similar measurements at the center of the right front passenger seating position as well as a matrix of points on the driver and passenger toepans. Along with these measurements, the vehicle cross-car beam accelerations and steering wheel dynamic intrusion measurements were also recorded. This information was utilized to represent the toepan intrusions by a combined linear translation and inward rotation of two equivalent toepan planes for the driver and passenger. This information was also used to represent the steering wheel, driver knee-bolster and passenger knee-bolster intrusions in the model. Because the actual vehicle intrusion time histories for each of the discrete measurement points were not known, the intrusion representations in the model were assumed to be constant velocity. Overall, the dynamic intrusion representation in the model was simplified and represented a key adjustment parameter for correlating the model response.

The interior components were set for the corresponding ATD for each of the load cases (e.g., position of the seat, seat belt routing, seat back angle, etc.). Finally, the development of distinct models for each of the 24 load cases was completed with the introduction of the air bag and pretensioner deployment times, along with the retractor high / low torsion bar switch time.

7.2   Correlation of Baseline PVP CAE Models

The correlation of the baseline PVP CAE models was established by comparing ATD kinematics and time histories of head, chest, and pelvic accelerations, chest deflection, and femur and tibia loads. A correlation assessment was made for each of the six baseline vehicle crash tests. Appendices A and B include the peak IAVs measured in the baseline vehicle crash tests, along with the corresponding values predicted by the baseline PVP CAE models.

7.3   Incorporation of ARS Components in CAE Models

Component tests (e.g., pendulum tests, linear impactor tests) conducted under Task 6 of the ARS Project were simulated in the CAE models to assess the correlation of the ARS components to these test conditions. The component model correlation process ensured that the restraint components, by themselves, accurately represented the response of each restraint component under external load prior to introduction into the full system environment.

A test series was also conducted to study one of the tunable parameters in the advanced restraint system, the time to deploy the lap anchor pretensioner relative to the retractor pretensioner. Since the relative deployment times influence the pay-in from the retractor pretensioner and the lap anchor pretensioner, it was important that these functions be accurately simulated in the CAE model. To confirm the accuracy of the dual pretensioning function in the model, static testing with a seated, belted, 50th HIII ATD was conducted to quantify the level of pretensioning observed at the retractor relative to the level of pretensioning observed at the seat belt anchor at various deployment times. The data generated from the dual pretensioner static evaluation was subsequently used to update the pretensioner functions in the CAE models.

7.4   Development of Sled CAE Models

CAE models of the sled tests conducted at the TRC were developed to provide an opportunity to assess the function and correlation of the ARS component models at a "system-level." This was also an important learning cycle in developing and gaining confidence in the CAE models for the HIII 95M as the sled testing provided the only physical evaluation of the HIII 95M. The sled models were created by taking the corresponding vehicle crash model, matching the sled pulse in the x-direction and disabling motion in the y and z-directions, orienting the vehicle per the attitude in the sled test, disabling the dynamic intrusion functions in the model, and setting up the occupants per the sled test. Neither the restraint component models nor the vehicle environment stiffness characteristics were adjusted.

7.5   CAE DOE Optimization Studies to Determine ARS Fixed Parameters

CAE Design of Experiments (DOE) optimization studies were conducted to determine values for the following fixed parameters:

- Retractor "high" and "low" torsion bar specifications

- Vent size of the DAB

- Vent size of the PAB

The objective functions used in the optimization process were "Beta-AIS3+" and "Beta-AIS2+." The Beta functions calculated the ratio of the occupant injury measures (OIM-AIS3+ and OIM-AIS2+) for the advanced restraint system relative to the baseline PVP restraint system for each of the CAE DOE runs. This allowed for the CAE DOE runs to be rank ordered, with the goal being to minimize the Beta-AIS3+ and Beta-AIS2+ functions.

The first CAE DOE optimization study focused on identifying the appropriate torsion bar high/low specification for the ARS retractor.

At the time of this CAE study, the passenger CAE model was still under development. The selection of the appropriate torsion bars was therefore based on the CAE DOE results of the driver. For this analysis, the MDB-to-vehicle and vehicle-to-pole crash modes were studied at the higher speed test conditions. Table 16 lists the DOE variables that were considered for this analysis. The retractor and lap anchor pretensioners were deployed at the same time as air bag stage 1, and the study did not include a seat ramp or knee air bag.

Table 16 - DOE Variables for CAE Analysis to Determine ARS Retractor Torsion Bar Sizes (Deployment and Switch Times are Relative to Air Bag Stage 1)

Crash Mode	ATD	Torsion Bar Sizes (kN)	Air Bag Vent Size (∅ in mm)	Air Bag PVM Deploy Time (ms)	IEA Switch Time (ms)
MDB35	HIII 5F	4.55/2.45 4.20/2.10 3.85/1.75	0 20 25	30 40 50 60	10
	HIII 50M	4.55/2.45 4.20/2.10 3.85/1.75	0 20 25	30 40 50 60	33 43 53
	HIII 95M	4.55/2.45 4.20/2.10 3.85/1.75	0 20 25	50 60 70 90	Not Switched
Pole35	HIII 5F	4.55/2.45 4.20/2.10 3.85/1.75	0 20 25	30 40 50 60	10
	HIII 50M	4.55/2.45 4.20/2.10 3.85/1.75	0 20 25	30 40 50 60	33 43 53
	HIII 95M	4.55/2.45 4.20/2.10 3.85/1.75	0 20 25	50 60 70 90	Not Switched

The results from the CAE DOE study favored the larger air bag vent size (25 mm) and the lower torsion bar specification (3.85/1.75 kN). Subsequent sled testing supported the lower torsion bar specification, including its applicability to the passenger side. Modification to an existing retractor was necessary to achieve this lower specification. Any further reduction in torsion bar size was not considered practicable from a manufacturing and functionality perspective.

Based on these results, the retractor torsion bar specification was fixed, and further CAE analysis was conducted to determine the appropriate air bag vent sizes. For this, CAE DOE optimization studies were conducted for 12 of the 24 load cases. The higher speed MDB-to-vehicle and vehicle-to-pole crash modes for both the driver and passenger were used, and again, all three ATDs were studied. Table 17 lists the DOE variables for the driver side while Table 18 provides the DOE variables for the passenger side.

Table 17 - DOE Variables for CAE Analysis to Determine Driver Air Bag Vent Size
(Deployment and Switch Times Relative to Air Bag Stage 1)

Crash Mode	ATD	Air Bag Vent Size (number and diameter in mm)	Air Bag PVM Deploy Time relative to Air Bag Stage 1 (ms)	Knee Air Bag	LPT Deploy Time relative to RPT Deploy Time (ms)	IEA Switch Time relative to RPT Deploy Time (ms)
MDB35	HIII 5F	1 x 25 1 x 28 1 x 31	30 40 50	ON OFF	0 6	10
	HIII 50M	1 x 25 1 x 28 1 x 31	40 50 60	ON OFF	0 6	35 40 45
	HIII 95M	1 x 25 1 x 28 1 x 31	50 60 70	ON OFF	0 6	40 50 60
Pole35	HIII 5F	1 x 25 1 x 28 1 x 31	30 40 50	ON OFF	0 6	10
	HIII 50M	1 x 25 1 x 28 1 x 31	40 50 60	ON OFF	0 6	35 40 45
	HIII 95M	1 x 25 1 x 28 1 x 31	50 60 70	ON OFF	0 6	40 50 60

Table 18 - DOE Variables for CAE Analysis to Determine Passenger Air Bag Vent Size (Deployment and Switch Times Relative to Air Bag Stage 1)

Crash Mode	ATD	Air Bag Vent Size (number and diameter in mm)	Air Bag PVM Deploy Time Relative to Air Bag Stage 1 (ms)	Knee Air Bag	LPT Deploy Time Relative to RPT Deploy Time (ms)	IEA Switch Time Relative to RPT Deploy Time (ms)
MDB35	HIII 5F	2 x 64 2 x 68 2 x 72	30 40 50	ON OFF	0 6	10
	HIII 50M	2 x 64 2 x 68 2 x 72	44 54 64	ON OFF	0 6	10 25 43
	HIII 95M	2 x 64 2 x 68 2 x 72	60 70 80	ON OFF	0 6	45 55 65
Pole35	HIII 5F	2 x 64 2 x 68 2 x 72	30 40 50	ON OFF	0 6	10
	HIII 50M	2 x 64 2 x 68 2 x 72	44 54 64	ON OFF	0 6	10 25 43
	HIII 95M	2 x 64 2 x 68 2 x 72	60 70 80	ON OFF	0 6	45 55 65

Based on the results for these CAE analyses, the DAB vent size was fixed at 1 x 28 mm in diameter, and the PAB vents were fixed at 2 x 64 mm in diameter.

7.6   CAE DOE Optimization Studies to Determine ARS Tunable Parameters

To determine the final recommended advanced restraint system configuration for each of the 24 load cases, CAE DOE optimization studies were conducted for each load case. The DOE variables for the driver load cases are provided in Table 19 while those for the passenger load cases are listed in Table 20.

Table 19 - DOE Variables for CAE Analysis to Determine Recommended Driver ARS Configurations (Deployment and Switch Times Relative to Air Bag Stage 1)

ATD	Crash Configuration	Air Bag PVM Deploy Time (ms)	Knee Air Bag	Lap Anchor PT Deploy Time (ms)	IEA Switch Time (ms)
HIII 5F	MDB35	30 35 40	ON OFF	0 6	10
	MDB25	30 35 40	ON OFF	0 6	10
	Pole35	30 35 40	ON OFF	0 6	10
	Pole25	30 35 40	ON OFF	0 6	10
HIII 50M	MDB35	55 60 65	ON OFF	0 6	35 40 45
	MDB25	55 60 65	ON OFF	0 6	35 40 45
	Pole35	45 50 55	ON OFF	0 6	40 45 50
	Pole25	45 50 55	ON OFF	0 6	40 45 50
HIII 95M	MDB35	65 70 75	ON OFF	0 6	45 50 55
	MDB25	65 70 75	ON OFF	0 6	45 50 55
	Pole35	50 55 60	ON OFF	0 6	50 55 60
	Pole25	50 55 60	ON OFF	0 6	50 55 60

Table 20 - DOE Variables for CAE Analysis to Determine Recommended Passenger ARS Configurations (Deployment and Switch Times Relative to Air Bag Stage 1)

ATD	Crash Configuration	Air Bag PVM Deploy Time (ms)	Knee Air Bag	Lap Anchor PT Deploy Time (ms)	IEA Switch Time (ms)
HIII 5F	MDB35	35 40 45	ON OFF	0 6	10
	MDB25	35 40 45	ON OFF	0 6	10
	Pole35	30 35 40	ON OFF	0 6	10
	Pole25	30 35 40	ON OFF	0 6	10
HIII 50M	MDB35	44 49 54 59	ON OFF	0 6	33 38 43
	MDB25	44 49 54 59	ON OFF	0 6	33 38 43
	Pole35	44 54 64	ON OFF	0 6	25 35 45
	Pole25	44 54 64	ON OFF	0 6	25 35 45
HIII 95M	MDB35	65 70 75	ON OFF	0 6	50 55 60
	MDB25	65 70 75	ON OFF	0 6	50 55 60
	Pole35	60 65 70	ON OFF	0 6	50 55 60
	Pole25	60 65 70	ON OFF	0 6	50 55 60

The ranges for PVM deployment times and IEA switch times were selected based on the timing associated with the ATD's interaction with the air bag. The delay of 6 ms between the retractor pretensioner deployment and lap anchor pretensioner deployment represented that time at which the RPT had completed its webbing pay-in phase.

From an "optimization" standpoint, the recommended ARS configuration reflected a combination of the discrete values selected for the DOE study. Assuming the appropriate ranges have been selected for these variables, the true "optimal" selection may actually be somewhere in between the discrete values chosen.

In many of the load cases, the Beta optimization functions yielded very similar results for several of the potential ARS configurations. For these cases, the selection of the "recommended" ARS configuration was influenced by results and observations from physical testing, including sled and vehicle crash tests. In addition, the level of correlation for the CAE models varied for the different body regions. Confidence in the specific IAV predictions from the CAE models played a role in interpreting and weighing the Beta functions. Finally, the selection of the recommended ARS configuration was influenced if similar Beta functions yielded the flexibility to simplify the deployment strategy across different load cases.

In the original DOE matrices, the retractor pretensioner was always deployed at the same time as air bag stage 1, and the seat ramp was modeled in its "activated" state. In some of the lower-speed load cases, the calculated Beta functions for all of the proposed ARS configurations showed little to no improvement over the baseline PVP restraint system. This was not surprising given the good performance of the PVP system in the baseline vehicle crash tests. Subsequent CAE runs indicated that suppressing the RPT and not activating the seat ramp would yield lower Beta functions and be more likely to at least match the baseline performance of the PVP restraint system. Consequently, this strategy was adopted for several of the lower-speed load cases, taking advantage of the tunability of the advanced restraint system by suppressing the RPT and not activating the seat ramp in specific load cases.

Additional CAE runs beyond the DOE matrix were also conducted if one of the variables showed a very strong influence on the overall results and the "preferred" selection was at the high or low end of the range studied. In such a case, additional CAE studies were conducted with an additional discrete value beyond the variable range originally evaluated.

The physical sled and vehicle crash testing of the 5th percentile female were conducted with a HIII 5F retrofitted with THOR-FLx legs. The corresponding CAE evaluations were conducted using a virtual HIII 5F ATD with HIII legs since a THOR-FLx CAE model was not available at the time the simulations were conducted. During the course of the ARS Project, a contract was established with a second CAE supplier to develop a CAE model for the THOR-FLx legs. Although not used during the CAE DOE optimization studies, these models were eventually successfully integrated with the HIII 5F ATD model, and the baseline PVP and recommended ARS configurations were rerun with the THOR-FLx CAE models for the 8 load cases involving the 5th female. The results from these additional CAE runs were the basis for comparing the two restraint systems for the load cases that relied on CAE analysis.

There were no baseline PVP vehicle crash tests with the HIII 95M ATD, therefore, the assessment of the advance restraint system relative to the baseline PVP restraint system was based solely on CAE analysis. The correlated MDB-to-vehicle and vehicle-to-pole models for the HIII 50M were used, and the HIII 95M CAE occupant model obtained from Humanetics (formerly First Technology Safety Systems) was swapped with the HIII 50M. The baseline occupant performance for the HIII 95M in each of the load cases was established using the PVP restraint hardware, and then the models were run with the ARS components to determine the potential incremental benefit.

8   Final ARS Vehicle Crash Tests

8.1   ARS Crash Tests

The list of the final ARS vehicle crash tests is provided in Table 21. The longitudinal acceleration measured at the CG of the vehicle was used to calculate the delta-v. The ARS configurations and deployment strategies for both the driver and passenger in each test were set based on the CAE DOE optimization results.

Table 21 - ARS Vehicle Crash Test Matrix

Crash Configuration	Test Speed (mph)	Delta-V (mph)	Test Number	Driver	Passenger
MDB35	72.2	35.5	100916	HIII 5F	HIII 50M
Pole25	25.0	29.7	100923	HIII 50M	HIII 5F
MDB35	72.5	37.3	100930	HIII 50M	HIII 5F
Pole35	35.1	40.0	101007	HIII 50M	HIII 5F
MDB25	54.3	27.5	101014	HIII 50M	HIII 5F
MDB25	54.1	26.9	101108	HIII 50M	HIII 5F

A summary of the key ATD injury measurements is provided for all of the final ARS vehicle crash tests in Table 22 (driver) and Table 23 (right front passenger). As was the case with the baseline PVP restraint system, the advanced restraint system performed well, with all measured injury values below the established injury limits specified in FMVSS No. 208.

Table 22 - Summary of Driver ATD Injury Assessment for All Final ARS Vehicle Crash Tests

Injury Criteria	MDB35		MDB25		Pole35	Pole25
	HIII 5F (100916)	HIII 50M (100930)	HIII 50M (101014)	HIII 50M (101108)	HIII 50M (101007)	HIII 50M (100923)
HIC (15ms)	136	267	86	73	216	121
Neck NIJ	0.68	0.38	0.37	0.25	0.39	0.32
Chest Deflection (mm)	30	34	33	31	35	23
Chest Accel - 3ms (g)	38	47	30	32	37	27
Left Femur Fz (kN)	3.88	6.92	3.02	2.46	2.66	1.36

Injury Criteria	MDB35		MDB25		Pole35	Pole25
	HIII 5F (100916)	HIII 50M (100930)	HIII 50M (101014)	HIII 50M (101108)	HIII 50M (101007)	HIII 50M (100923)
Right Femur Fz (kN)	2.80	6.23	2.40	2.27	2.86	1.91
Left Upper Tibia Fz (kN)	2.61	3.14	2.22	1.28	1.90	0.90
Right Upper Tibia Fz (kN)	1.52	1.80	0.71	0.85	1.22	1.38
Left Lower Tibia Fz (kN)	3.27	4.75	3.34	2.23	2.57	1.05
Right Lower Tibia Fz (kN)	1.77	2.38	1.47	2.17	2.96	2.05

**Table 23 - Summary of Passenger ATD Injury Assessment for
All Final ARS Vehicle Crash Tests**

Injury Criteria	MDB35		MDB25		Pole35	Pole25
	HIII 5F (100930)	HIII 50M (100916)	HIII 5F (101014)	HIII 5F (101108)	HIII 5F (101007)	HIII 5F (100923)
HIC (15ms)	259	219	178	128	156	147
Neck NIJ	0.38	0.26	0.42	0.41	0.32	0.32
Chest Deflection (mm)	17	31	15	19	22	20
Chest Accel - 3ms (g)	46	39	41	30	41	30
Left Femur Fz (kN)	4.58	6.18	3.58	2.76	2.70	1.90
Right Femur Fz (kN)	2.65	2.53	1.30	2.05	2.56	2.37
Left Upper Tibia Fz (kN)	4.23	3.25	0.98	2.33	2.46	1.72
Right Upper Tibia Fz (kN)	2.88	3.31	0.88	1.10	2.42	1.14
Left Lower Tibia Fz (kN)	4.80	3.43	1.54	3.29	3.27	2.51
Right Lower Tibia Fz (kN)	2.69	3.83	No Data	1.80	2.91	1.38

MDB25 Test #101014 with the HIII 50M driver and HIII 5F passenger was repeated with different ARS configurations for both seating positions in an attempt to improve the performance of the advanced restraint system relative to the baseline.

8.2 Test Repeatability

In order to compare the performance of the baseline and advanced restraint systems, the test methodology must have an acceptable level of repeatability. This was examined for

both crash modes at both speeds in terms of the vehicle pulse and intrusion measurements.

8.2.1 MDB-to-Vehicle, 35 mph

The longitudinal and lateral velocity time histories as measured at the CG of the PVP for all of the higher speed MDB-to-vehicle crash tests are provided in Figures 37 and 38, respectively. The largest variation was noted in the lateral velocity, with the peak lateral velocity for the six tests ranging from 9–13 mph.
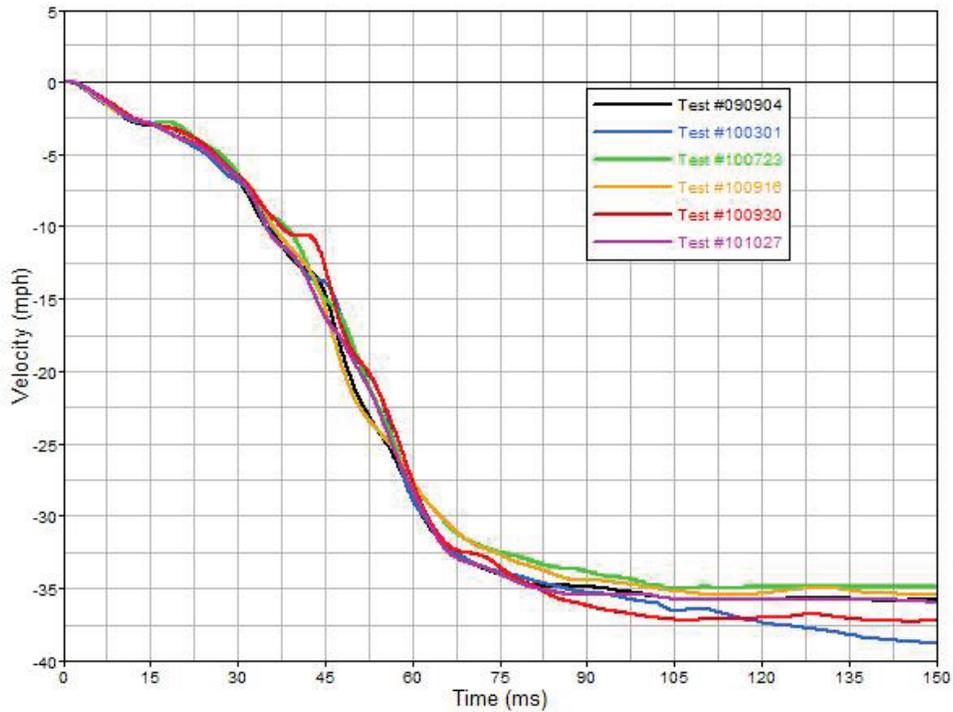
Figure 37 - Longitudinal Velocity Time History, MDB35
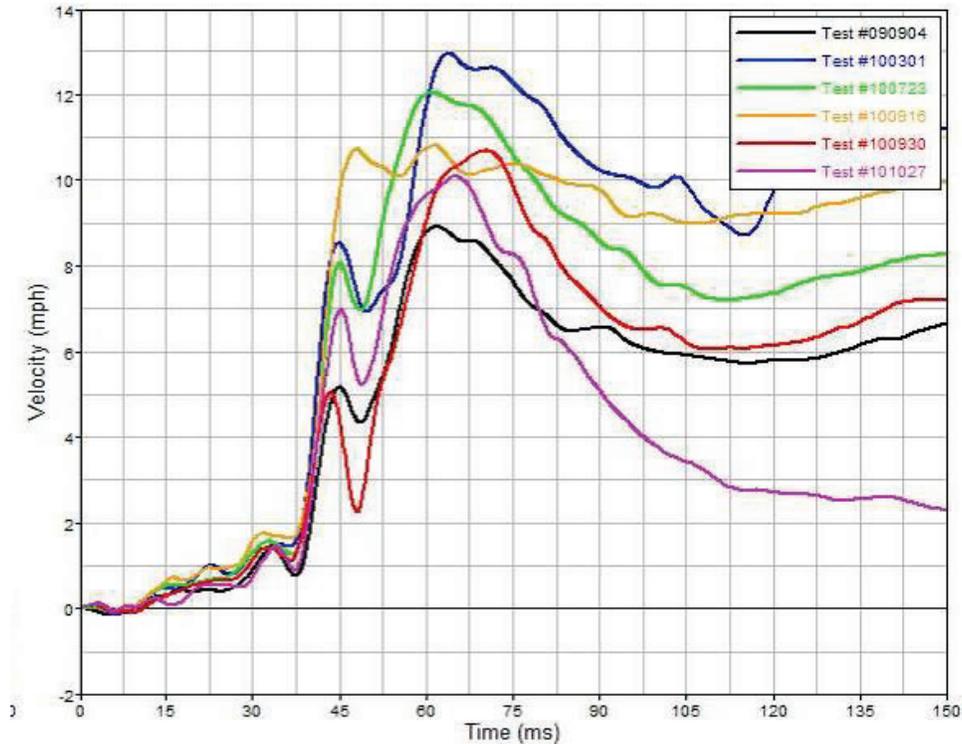
Figure 38 - Lateral Velocity Time History, MDB35

As mentioned earlier, the collection of detailed dimensional data was important for the development of the CAE models and also helpful in understanding the repeatability of the tests from an intrusion perspective. As part of the dimensional analysis, the intrusion was measured at the centerline of the driver and passenger seating positions, from the floor pan to the top of the dash panel. The locations of the measurement points used in the dimension analysis are shown in Figure 39. Figures 40 (driver) and 41 (passenger) show the pre- and post-test measurements in the X-Z plane for each of the six tests. Both sides show similar deformation patterns from test-to-test, with more variation noted on the passenger side at the upper measurements.

Figure 39 – Photograph of Measurement Points Used in Dimensional Analysis
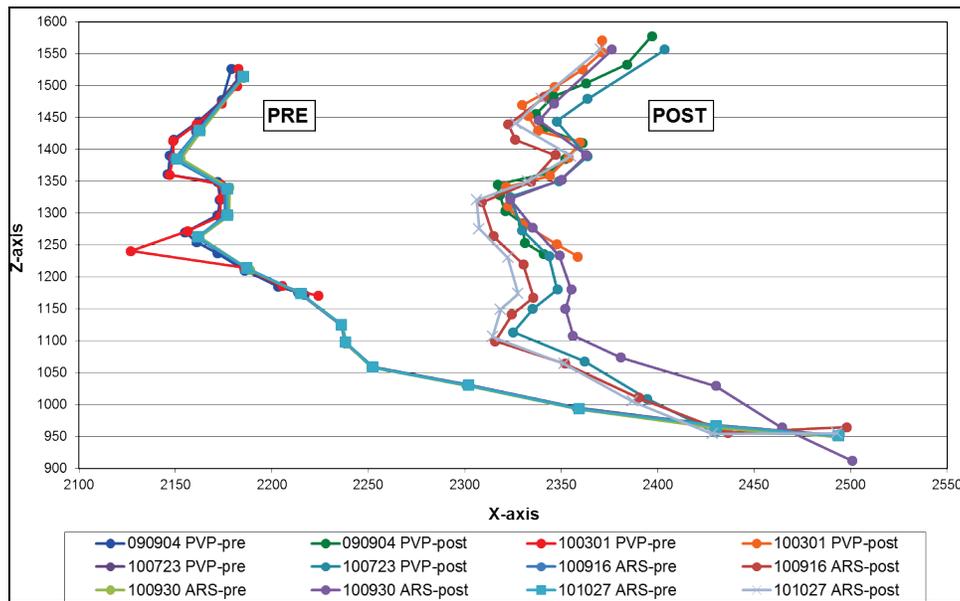
Figure 40 - Dash Panel Intrusion Profile – Driver Side, MDB35
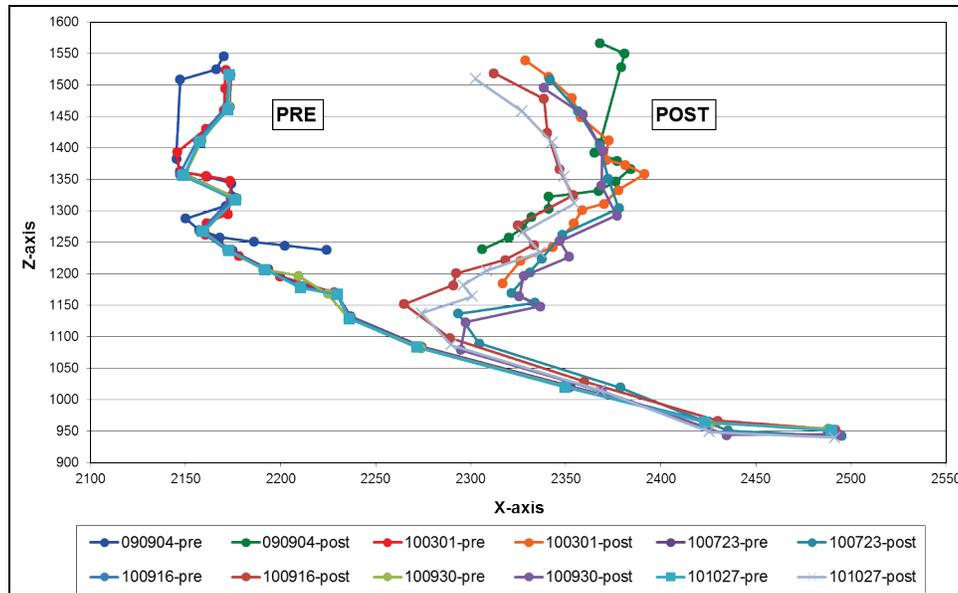
Figure 41 - Dash Panel Intrusion Profile – Passenger Side, MDB35

8.2.2 MDB-to-Vehicle, 25 mph

A similar analysis of the pulses for the lower-speed MDB-to-vehicle tests was conducted. The MDB25 longitudinal and lateral velocity time history plots are provided in Figures 42 and 43. Again, the lateral component showed more variability, ranging from 5 – 8 mph.
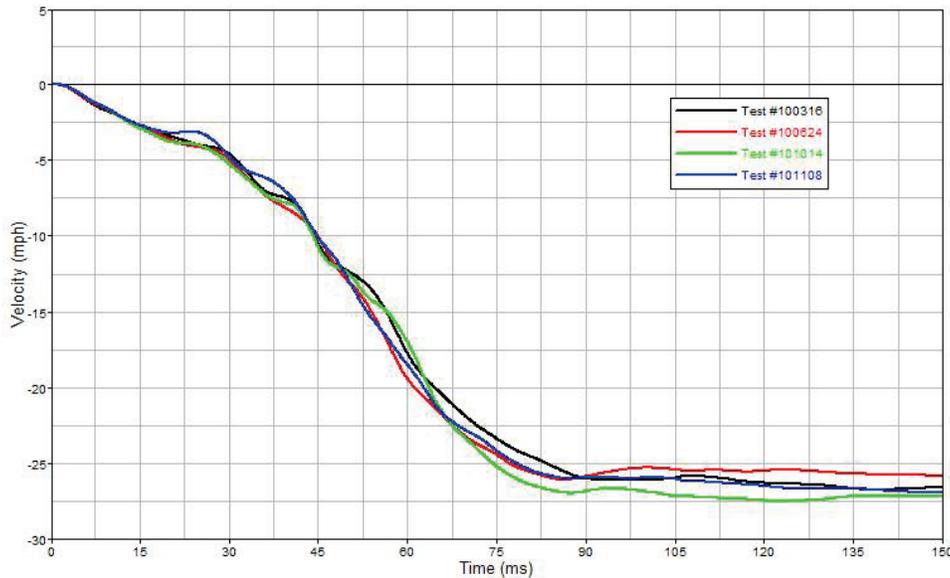
Figure 42 - Longitudinal Velocity Time History, MDB25
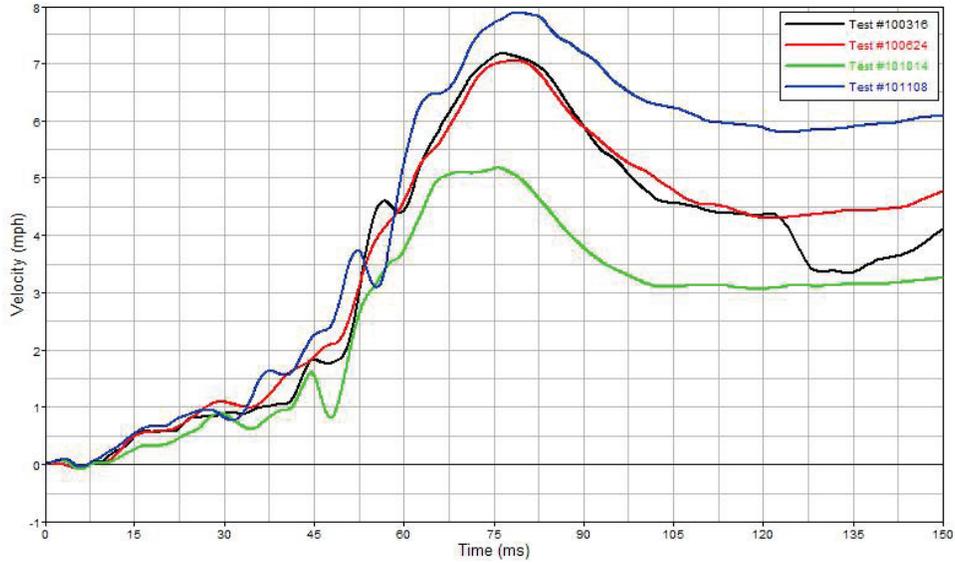
Figure 43 - Lateral Velocity Time History, MDB25

The MDB25 intrusion profiles on the driver and passenger sides are provided in Figures 44 and 45. The lower speed produced significantly less intrusion overall as shown in these plots.
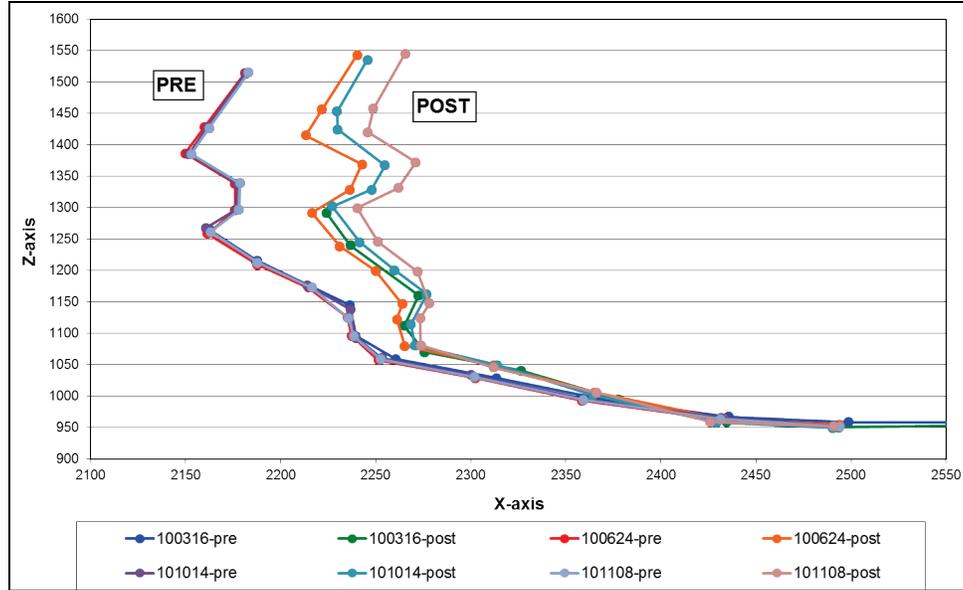
Figure 44 - Dash Panel Intrusion Profile – Driver Side, MDB25
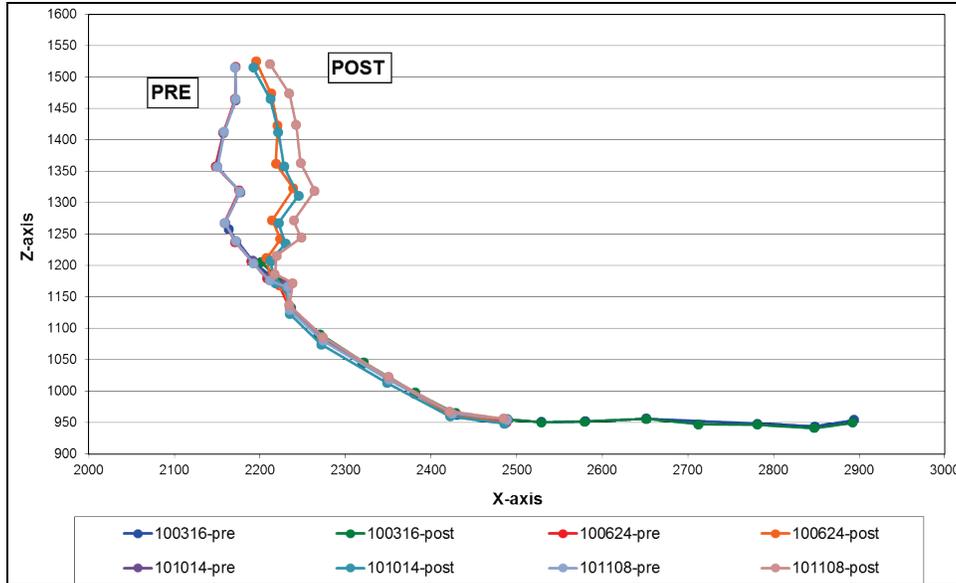
Figure 45 - Dash Panel Intrusion Profile – Passenger Side, MDB25

8.2.3 Vehicle-to-Pole, 35 mph

The longitudinal velocity time histories for the three 35 mph vehicle-to-pole tests conducted during the course of the ARS Project are provided in Figure 46. In addition, the dash panel intrusion profiles measured for the baseline test (Test #090922) and the final ARS test (Test #101007) are plotted in Figure 47 (driver side) and Figure 48 (passenger side). As was the case with the MDB-to-vehicle test, the higher speed Pole35 test condition resulted in significant intrusion.
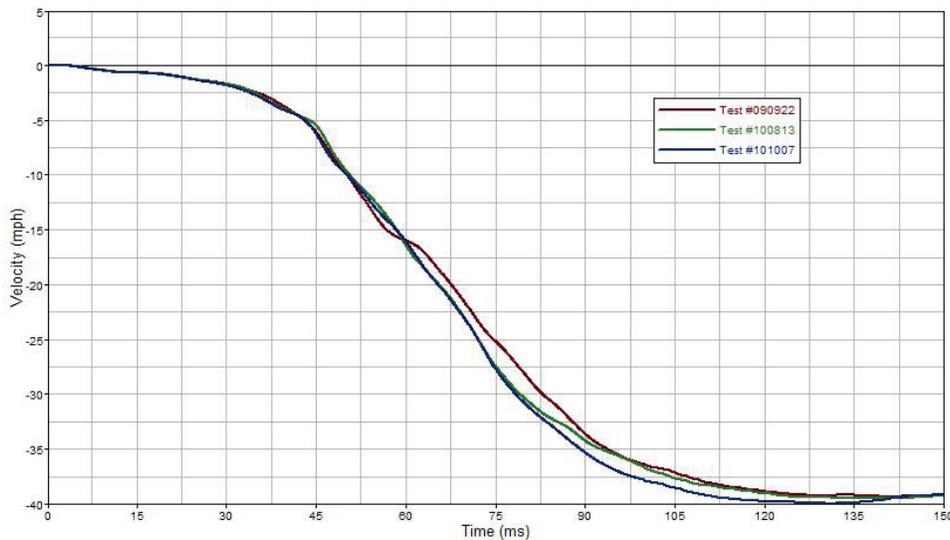
Figure 46 - Longitudinal Velocity Time History, Pole35
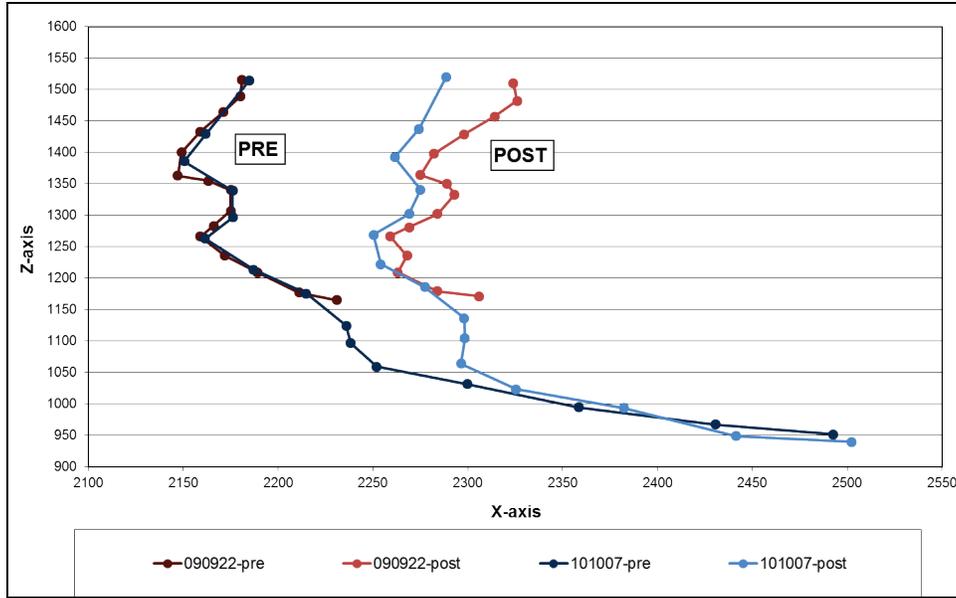
Figure 47 - Dash Panel Intrusion Profile – Driver Side, Pole35
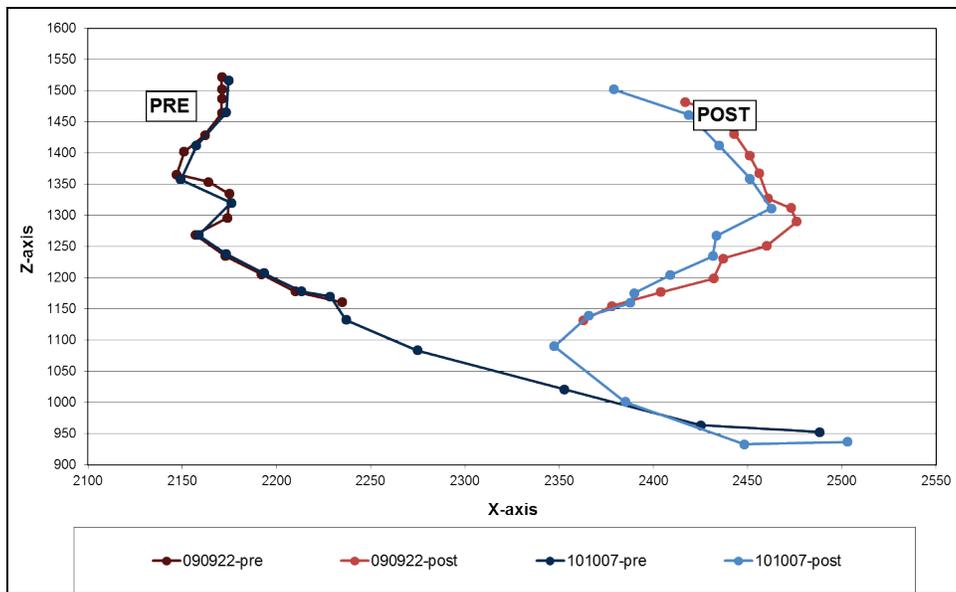
Figure 48 - Dash Panel Intrusion Profile – Passenger Side, Pole35

8.2.4 Vehicle-to-Pole, 25 mph

Two Pole25 (25 mph vehicle-to-pole tests) were conducted, Test #100322 (baseline) and Test #100923 (ARS). The longitudinal velocity time histories as measured at the PVP CG for these two tests is plotted in Figure 49, while the dash panel intrusion profiles are provided in Figures 50 and 51. On the driver side, the intrusion was in the 25-50 mm range, while the peak intrusion measured on the passenger side was approximately 100 mm.
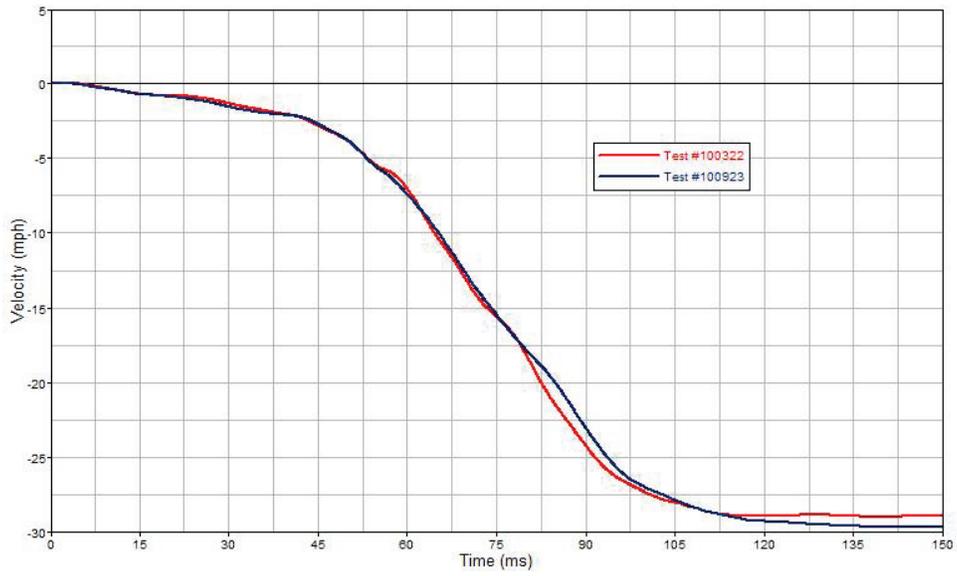
Figure 49 - Longitudinal Velocity Time History, Pole25
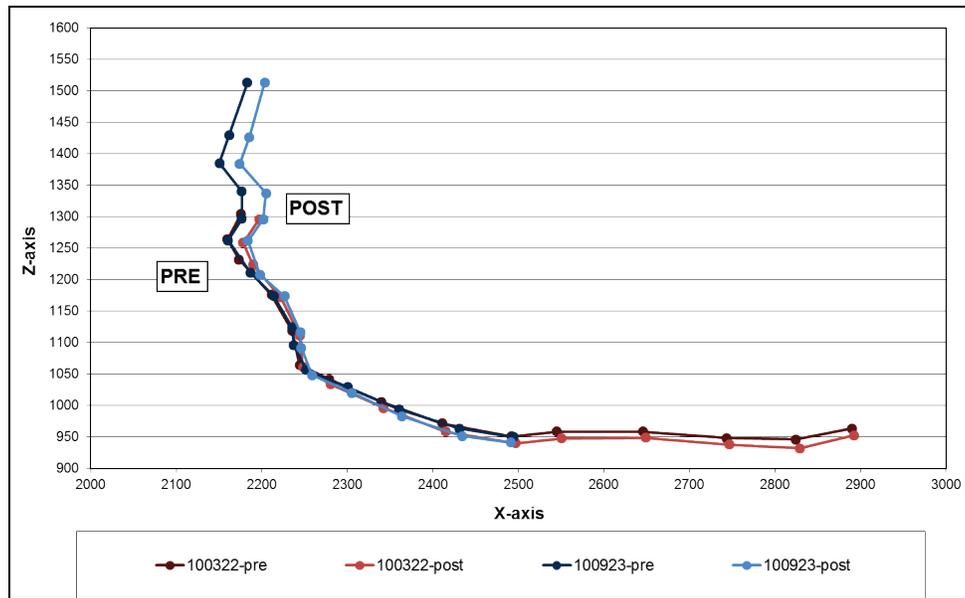
Figure 50 - Dash Panel Intrusion Profile – Driver Side, Pole25
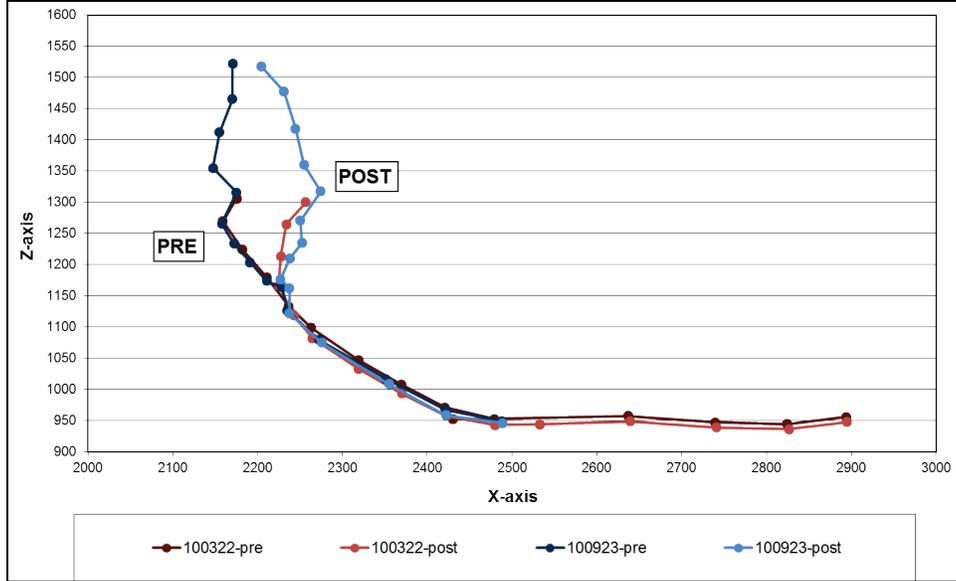
Figure 51 - Dash Panel Intrusion Profile – Passenger Side, Pole25

8.2.5 Repeatability Assessment

Overall, the repeatability of both test modes was deemed acceptable, allowing for a valid comparison of the advanced restraint system performance to that of the baseline in the tests conducted. Nevertheless, it should be noted that variation in local intrusion from test to test, as well as ATD leg position, can play a significant role in the measured femur and tibia loads. The dimensional analyses also showed that structural intrusion posed a significant ARS design challenge with respect to improving the lower extremity performance results, particularly for the higher speed load cases.

9   ARS Assessment

An assessment was made for each of the 24 load cases comparing the performance of the advanced restraint system relative to that of the baseline. For 10 of these load cases, the comparison was made directly from the ATD data collected in the vehicle crash test results. The remaining 14 load cases were assessed through CAE. This section summarizes the results for all 24 load cases and provides the recommended ARS configuration for each one.

9.1   Driver Side Summary

9.1.1 HIII 5F Driver

All testing and CAE analysis with the HIII 5F ATD was conducted at the full-forward seating position, with the seat at approximately the mid-height position according to the current FMVSS No. 208 seating procedure and the D-ring at the full-up position. The D-ring position was selected to be consistent with the manner in which the PVP was tested per FMVSS No. 208. This was then kept constant to allow for a direct comparison between the baseline and the advanced restraint systems.

No ARS deployable devices were activated earlier than the corresponding devices in the baseline PVP crash test (or simulation). All ARS and PVP configurations used an early retractor IEA switch time, corresponding to +10 ms after the initiation of the retractor pretensioner to utilize the lowest torsion bar setting.

Table 24 summarizes the recommended ARS configurations for the driver side 5th female occupant. All deployment times are relative to the "air bag stage 1" deployment time to facilitate comparison between load cases.

Table 24 - Recommended ARS Configurations, 5th Female Driver

ATD	Crash Configuration	Air Bag PVM Deploy Time (ms)	Knee Air Bag	RPT	LPT Deploy Time (ms)	Retractor IEA Switch Time (ms)	Seat Ramp
HIII 5F	MDB35	35	ON	ON	0	10	ON
HIII 5F	MDB25	35	OFF	OFF	0	10	OFF
HIII 5F	Pole35	35	ON	ON	0	10	ON
HIII 5F	Pole25	35	OFF	ON	0	10	ON

The common activation times for the PVM and IEA across all four load cases show that a single air bag and seat belt specification is sufficient for the HIII 5F in these crash modes. ARS discrimination is required relative to crash speed since the recommended ARS specification activates the KAB at the higher speed conditions and suppresses the KAB at the lower speed. Also, the MDB25 crash configuration was unique in that the

recommended ARS configuration did not include the deployment of the retractor pretensioner or the activation of the seat ramp.

Figures 52 and 53 summarize the combined OIM-AIS3+ and OIM-AIS2+ calculations for the driver side HIII 5F.

	MDB35	MDB25	Pole35	Pole25
Baseline	0.22	0.12	0.15	0.13
ARS	0.16	0.11	0.11	0.10
	Test	CAE	CAE	CAE
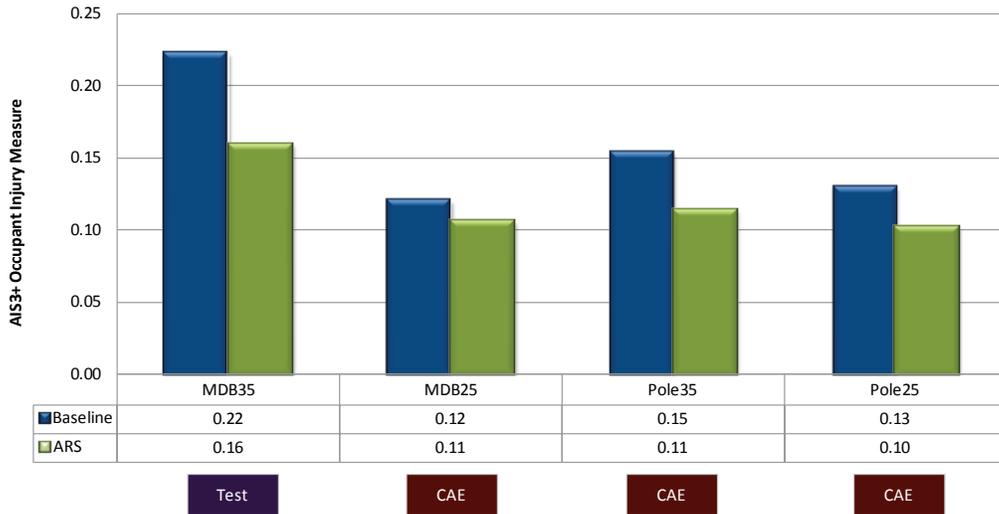
Figure 52 - OIM-AIS3+ Summary, HIII 5F Driver

	MDB35	MDB25	Pole35	Pole25
Baseline	0.72	0.47	0.50	0.45
ARS	0.60	0.43	0.45	0.41
	Test	CAE	CAE	CAE
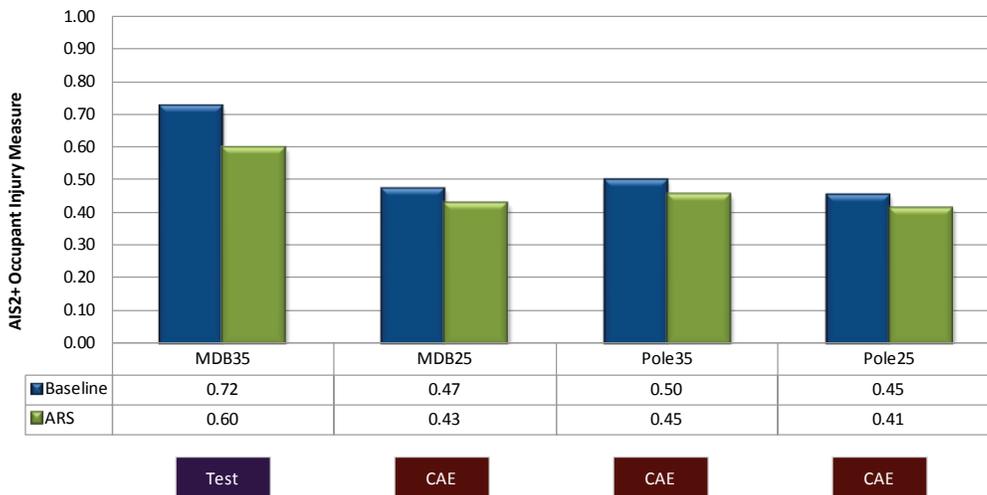
Figure 53 - OIM-AIS2+ Summary, HIII 5F Driver

For the MDB35 load case, the improvement in OIM-AIS3+ and OIM-AIS2+ was largely due to the reduction in femur and tibia loads attributed to the effectiveness of the KAB. As an example, Figure 54 shows a time history plot comparing the 5th driver left femur loads measured in the MDB35 PVP baseline tests (Test #100301 and Test #101027) to that measured in the final ARS test (Test #100916). With the KAB, contact with the knee occurs early, and the peak load is reduced relative to the baseline tests.
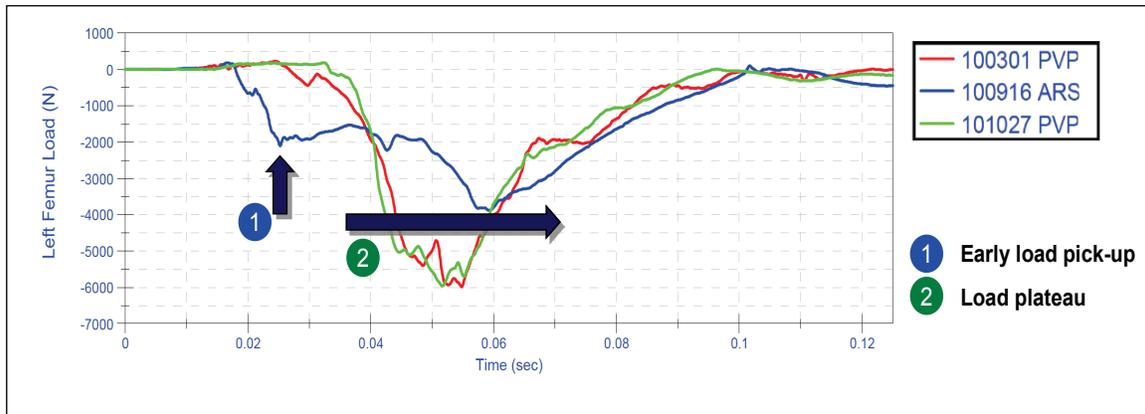
Figure 54 - Left Femur Axial Force Time History Plot, HIII 5F Driver, MDB35

In the MDB35 load case, the effectiveness of the DAB PVM was also demonstrated through reduction in the chest resultant deceleration and head deceleration, as illustrated in Figure 55.

Head Acceleration

Chest Acceleration
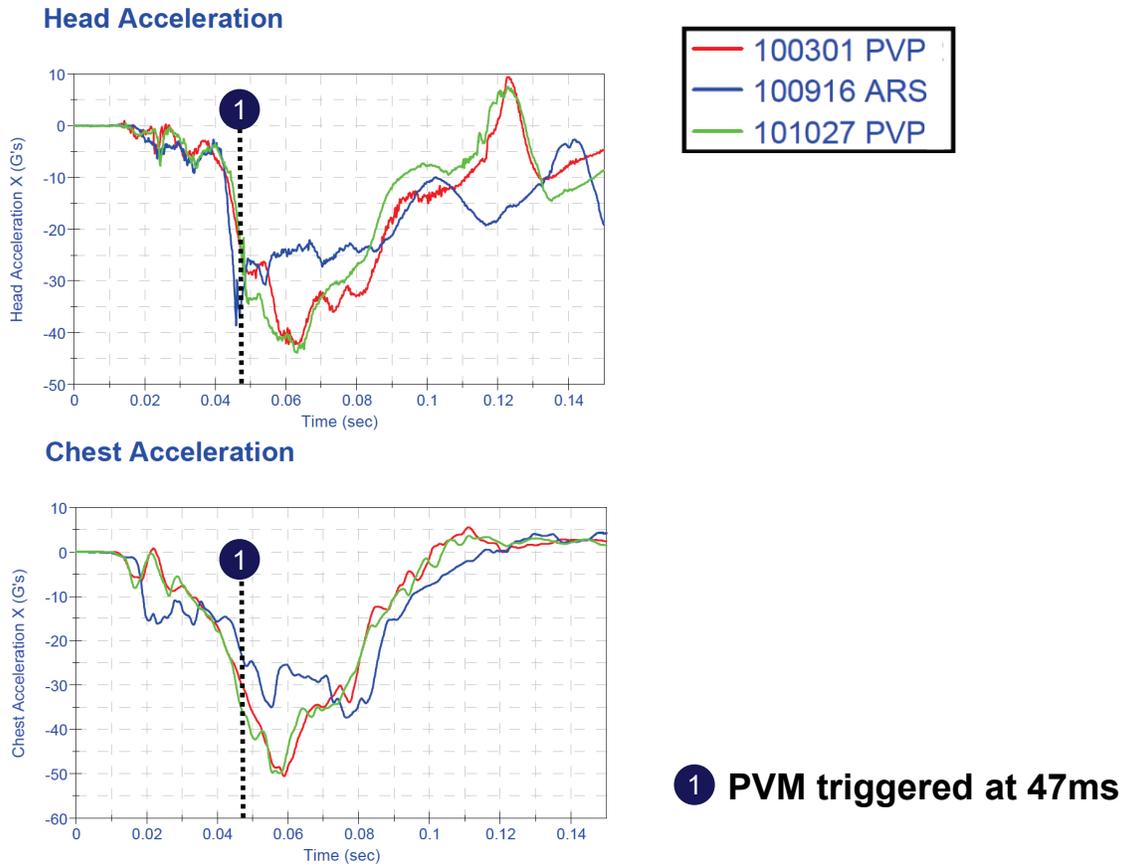
Figure 55 - Head and Chest Acceleration Time History Plots, HIII 5F Driver, MDB35

For the MDB25 load case, the lower extremity tibia loads were low with the baseline PVP restraint system. As a result, the recommended ARS configuration for the MDB25 load case included suppressing the KAB to avoid a potential increase in the already low tibia loads. For this load case, the overall occupant performance improvement came via a reduction in chest deflection.

For the vehicle-to-pole load cases, the IAVs associated with the baseline PVP system were generally very low, and so it was challenging to identify an advanced restraint system that could provide further injury reduction potential. The exception was the Pole35 load case in which the high femur loads predicted with the baseline PVP CAE model were effectively mitigated by the ARS KAB. This resulted in a 23-percent reduction in the OIM-AIS3+.

9.1.2 HIII 50M Driver

All testing and CAE analysis with the HIII 50M ATD was conducted at the mid-track, full-down seating position, and the D-ring at the full-up position.

No ARS deployable devices were activated earlier than the corresponding devices in the baseline PVP crash test (or simulation).

Table 25 summarizes the recommended ARS configurations for the driver side HIII 50M occupant. All deployment times are relative to the "air bag stage 1" deployment time to facilitate comparison between load cases.

Table 25 - Recommended ARS Configurations, HIII 50M Driver

ATD	Crash Configuration	Air Bag PVM Deploy Time (ms)	Knee Air Bag	RPT	LPT Deploy Time (ms)	Retractor IEA Switch Time (ms)	Seat Ramp
HIII 50M	MDB35	60	ON	ON	0	35	ON
HIII 50M	MDB25	55	OFF	OFF	0	30	OFF
HIII 50M	Pole35	50	ON	ON	6	40	ON
HIII 50M	Pole25	50	ON	ON	6	30	ON

For each of the four load cases, a unique ARS configuration was specified based on the optimization studies. There was more differentiation between the two MDB-to-vehicle load cases than there was for the two vehicle-to-pole load cases. For the vehicle-to-pole load cases, the same PVM activation time was specified, indicating that a common DAB deployment strategy could be used for the vehicle-to-pole crash mode. A general trend was the specification of a softer restraint system for the head and chest by selecting PVM and IEA switch times for the lower speed scenarios that were equal to or earlier than the corresponding higher speed scenarios. This is intuitive considering the lower occupant energy at the lower speed load cases. The MDB25 load case was unique in that the KAB, RPT, and seat ramp were not deployed.

Figures 56 and 57 summarize the combined OIM-AIS3+ and OIM-AIS2+ calculations for the driver side HIII 50M.
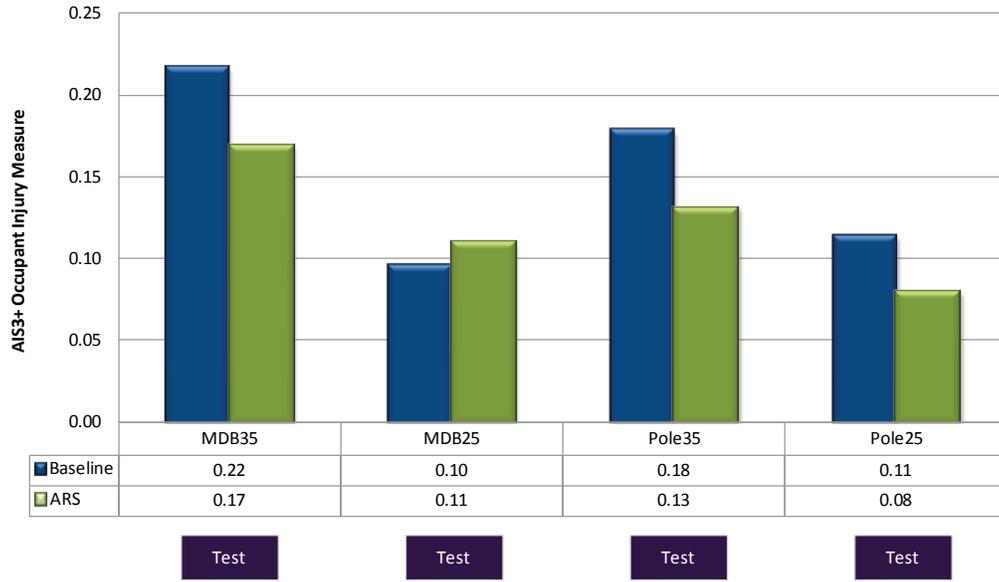
Figure 56 - OIM-AIS3+ Summary, HIII 50M Driver
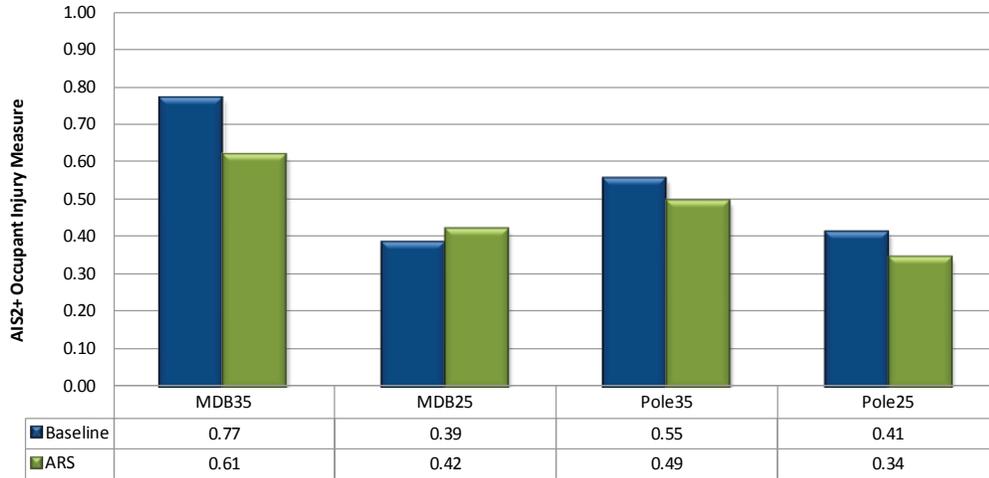
Figure 57 - OIM-AIS2+ Summary, HIII 50M Driver

For the MDB35 load case, a reduction in the OIM-AIS3+ and OIM-AIS2+ (22% and 20%, respectively) was achieved with the ARS system. The improvement was due to the reduction in chest deflection and lower tibia loads. The KAB was not effective at counteracting the effect of dynamic intrusion on the femur loads, contrary to its effectiveness on the sled simulation. The different performance in the barrier test relative

to the sled test demonstrates the effect of structural intrusion. The time history plots in Figure 58 show that the ARS KAB effectively limited the femur loading during sled testing but could not prevent strike-through in the corresponding MDB35 test.
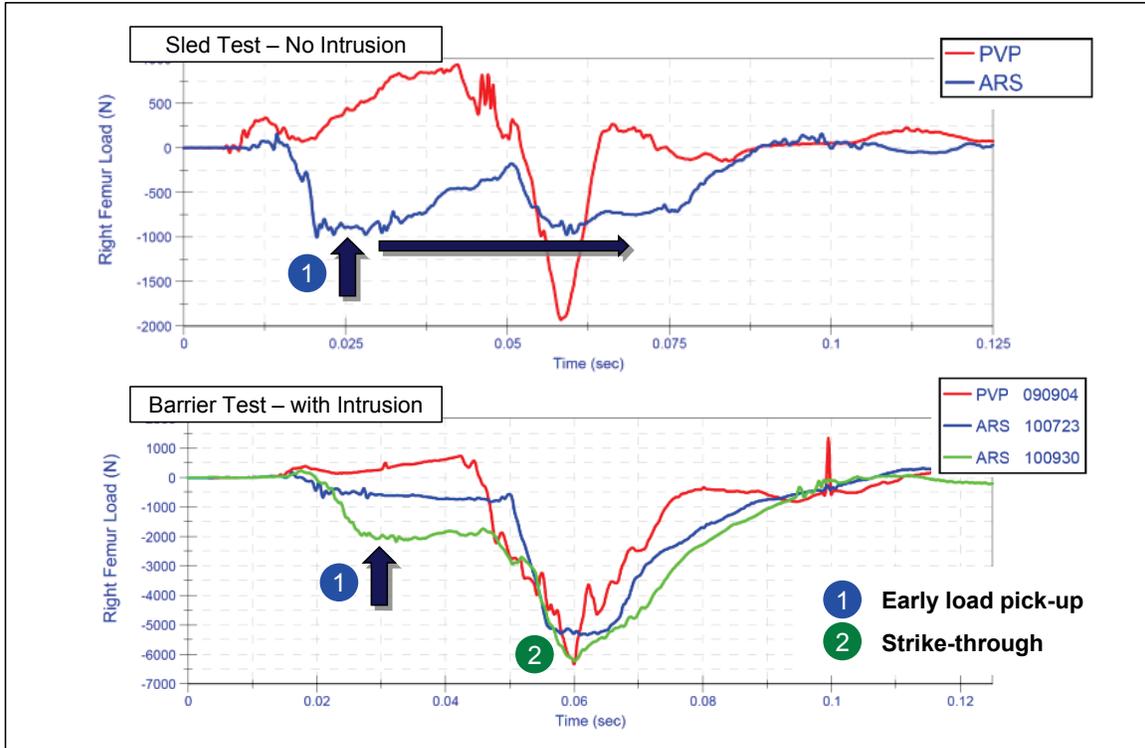
Figure 58 - Right Femur Axial Force Time History Plots, HIII 50M Driver, MDB35

For the MDB25 load case, the ARS system as tested did not provide improvement over the low-injury probability for the baseline PVP restraint system in Test #100316. Subsequent to the final ARS MDB25 crash test, a follow-up CAE study predicted that reduced chest deflection could be achieved in this crash mode by specifying a system that suppressed the deployment of the KAB, seat ramp, and RPT. One interesting observation was that for the MDB35 load case, the KAB stiffness was insufficient to counteract intrusion, while for the MDB25 load case, the femur and tibia load profiles indicate that the KAB stiffness may actually have been too high. The time history plots in Figure 59 show higher femur and tibia peaks with the ARS KAB (MDB25 Test #101014) versus the same measurements in the baseline PVP test (MDB25 Test #100316) without a KAB.
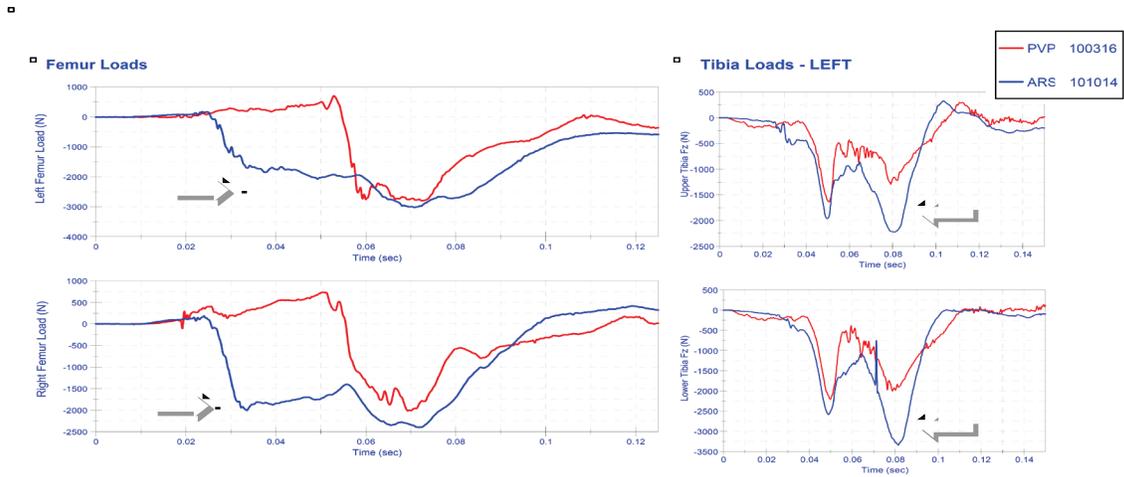
Figure 59 - Femur and Left Tibia Force Time History Plots, HIII 50M Driver, MDB25

For the vehicle-to-pole load cases, reductions in OIM were achieved with the ARS system (27% reduction in OIM-AIS3+ for Pole35 and 11% reduction in OIM-AIS3+ for Pole25). At the higher speed, reductions in chest deflection and chest G's were observed. Similar to the MDB35 case, the KAB was not effective at counteracting the effect of dynamic intrusion on the femur loads. At the lower speed, reductions in chest deflection were observed. In addition, with less intrusion, the KAB was effective in reducing the femur loads in the Pole25 test as shown in Figure 60.
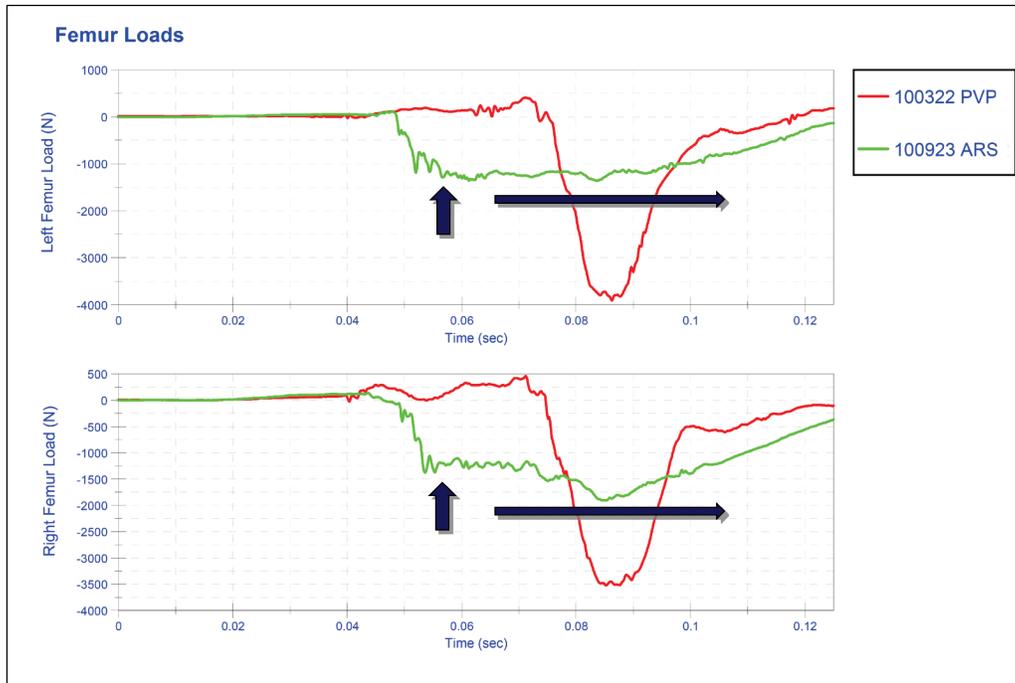
Figure 60 - Left and Right Femur Force Time History Plots, HIII 50M Driver, Pole25

9.1.3 95th Male Driver

All CAE simulations with the HIII 95M ATD were conducted at a nominal 95th seating position identified by the ARSC for this project. For the PVP, this was identified as the full-rear/full-down seating position. In addition, the D-ring was at the full-up position.

There are no established injury risk curves for the HIII 95M tibia loads and, thus, tibia loads were not assessed for the HIII 95M.

Table 26 summarizes the recommended ARS configurations for the driver side HIII 95M occupant. All deployment times are relative to the "air bag stage 1" deployment time to facilitate comparison between load cases.

Table 26 - Recommended ARS Configurations, HIII 95M Driver

ATD	Crash Configuration	Air Bag PVM Deploy Time (ms)	Knee Air Bag	RPT	LPT Deploy Time (ms)	Retractor IEA Switch Time ms)	Seat Ramp
HIII 95M	MDB35	75	ON	ON	6	55	ON
HIII 95M	MDB25	65	OFF	ON	0	45	ON
HIII 95M	Pole35	50	ON	ON	0	55	ON
HIII 95M	Pole25	50	ON	ON	0	55	ON

The CAE DOE results indicate that a common ARS configuration can be applied for the vehicle-to-pole crash mode. To achieve the optimal benefit of the ARS for the HIII 95M driver, pre-crash information would be needed to differentiate between the MDB-to-vehicle and vehicle-to-pole load cases, as well as the two different speeds associated with the MDB-to-vehicle crash modes. The MDB25 load case was unique in that the KAB was not deployed. The MDB35 load case was unique in that the LPT activation was staggered relative to the RPT. A general trend was the specification of a softer restraint system for the head and chest by selecting PVM and IEA switch times for the lower speed scenarios that were equal to or earlier than the corresponding higher speed scenario.

Figures 61 and 62 below summarize the OIM-AIS3+ and OIM-AIS2+ calculations for the driver side HIII 95M occupant.

	MDB35	MDB25	Pole35	Pole25
Baseline	0.21	0.17	0.25	0.21
ARS	0.20	0.14	0.19	0.14
	CAE	CAE	CAE	CAE
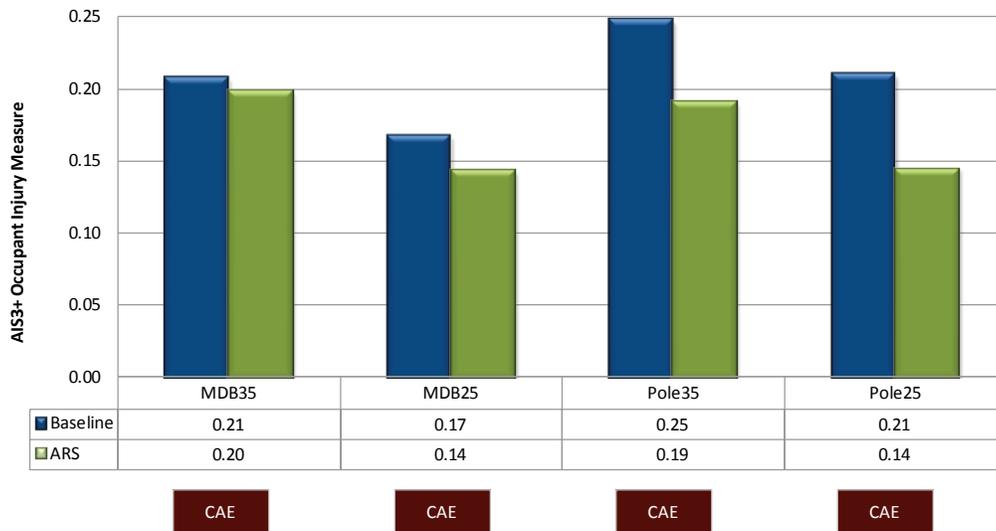
Figure 61 - OIM-AIS3+ Summary, HIII 95M Driver
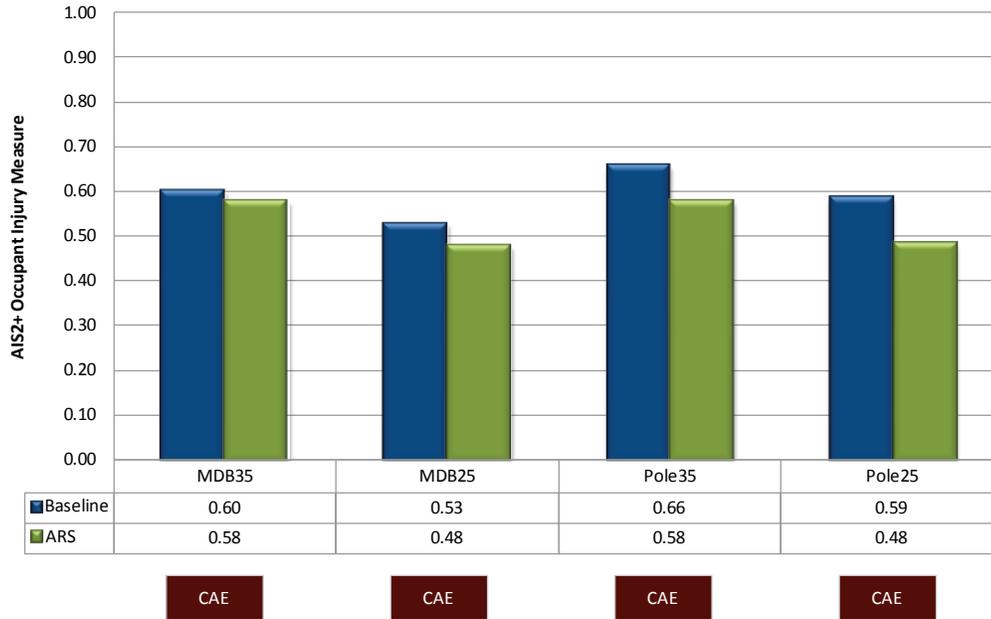
Figure 62 - OIM-AIS2+ Summary, HIII 95M Driver

For all load cases, the model predicted a reduction in OIM-AIS3+ and OIM-AIS2+ with the advanced restraint system relative to the baseline PVP restraint system. The largest reductions were observed for the vehicle-to-pole load cases, with 27% and 30% reductions in OIM-AIS3+ for the higher speed and lower speed load cases, respectively. The model predicted the ARS system would yield reductions in chest deflection for all load cases, while maintaining or reducing the generally low levels of injury for the other body regions relative to the baseline. The overall combined probabilities are higher than the corresponding HIII 5F and HIII 50M results, due to higher HIC and chest deflection predictions. The absolute injury measures must be viewed with caution considering no correlation could be performed tying the CAE model back to physical crash tests with intrusion. However, the relative comparisons of PVP and ARS performance are valid and the overall trend is that the ARS will provide incremental benefit relative to the baseline PVP restraint system.

9.1.4 Driver Summary

Table 27 summarizes the recommended ARS configurations for all 12 driver side load cases. All deployment times are relative to the "air bag stage 1" deployment time to facilitate comparison between load cases.

Table 27 - Recommended ARS Configurations, Driver

ATD	Crash Configuration	Air Bag PVM Deploy Time (ms)	Knee Air Bag	RPT	LPT Deploy Time (ms)	Retractor IEA Switch Time (ms)	Seat Ramp
HIII 5F	MDB35	35	ON	ON	0	10	ON
HIII 5F	MDB25	35	OFF	OFF	0	10	OFF
HIII 5F	Pole35	35	ON	ON	0	10	ON
HIII 5F	Pole25	35	OFF	ON	0	10	ON
HIII 50M	MDB35	60	ON	ON	0	35	ON
HIII 50M	MDB25	55	OFF	OFF	0	30	OFF
HIII 50M	Pole35	50	ON	ON	6	40	ON
HIII 50M	Pole25	50	ON	ON	6	30	ON
HIII 95M	MDB35	75	ON	ON	6	55	ON
HIII 95M	MDB25	65	OFF	ON	0	45	ON
HIII 95M	Pole35	50	ON	ON	0	55	ON
HIII 95M	Pole25	50	ON	ON	0	55	ON

The specified range of PVM deployment times and IEA switch times for each of the occupants highlights the potential benefit of pre-crash sensing technology that can discriminate among occupant sizes and seating positions for these load cases. The early activation of the PVM coupled with an early activation of the IEA created a "soft" restraint system tailored for the HIII 5F; such a system would almost certainly be ineffective at restraining the larger adult male occupants. Conversely, the relatively late PVM and IEA activations specified for the HIII 95M created a system that would likely be much too stiff for the HIII 5F.

There were some trends observed that were consistent across all three occupants, namely:

- The specification of a softer restraint system for the head and chest by selecting PVM and IEA switch times for the lower speed scenarios that were equal to or earlier than the corresponding higher speed scenario.

- Less differentiation in the ARS system was required for the vehicle-to-pole load cases compared to the MDB-to-vehicle load cases.

- For load cases where the baseline PVP restraint system yielded low IAVs, it was not practical to expect a reduction in overall injury with the advanced restraint system. For these cases, the general strategy was to suppress the KAB, and in some cases, suppress the RPT and seat ramp in an effort to match the PVP performance.

Figures 63 and 64 illustrate the effectiveness of the advanced restraint system across all occupants and load cases. Improvement was achieved in eleven of the 12 load cases at

both the AIS3+ and AIS2+ levels. The lone exception was the HIII 50M in the MDB25 load case. The data in Figures 62 and 63 represent the test results for this load case (Test #101108). A follow-up CAE study was conducted to investigate the possible benefit of suppressing the RPT and not activating the seat ramp (contrary to the conditions tested). The results from the CAE analysis suggested a marginal benefit relative to the baseline could be achieved with this configuration. The recommended ARS configuration in Table 25 for the 50th MDB25 loads case reflects the findings from the CAE follow-up study.
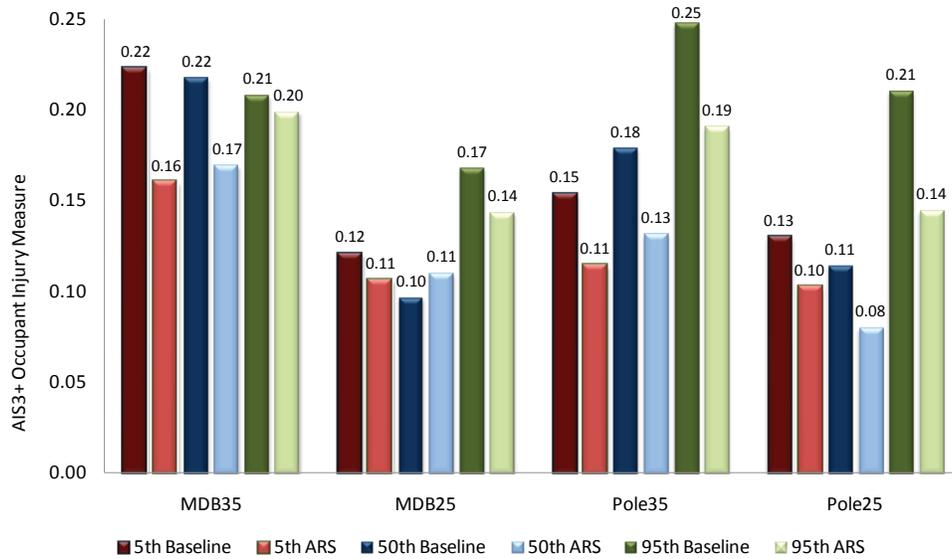
Figure 63 - OIM-AIS3+, PVP Versus ARS, All Drivers
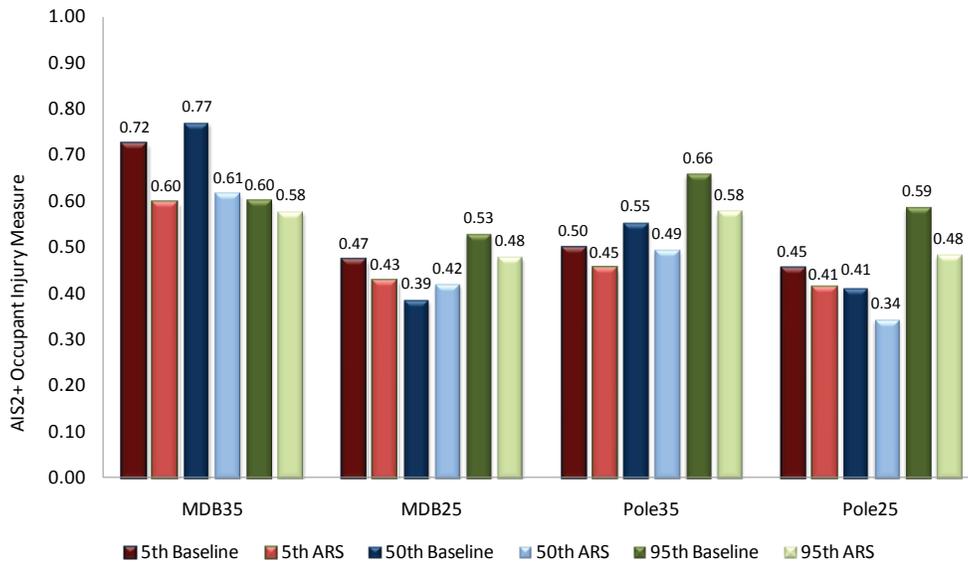
Figure 64 - OIM-AIS2+, PVP Versus ARS, All Drivers

The ability to improve the performance across a diverse set of load cases illustrates the potential benefit of an adaptive restraint system, where system parameters can be tuned to each load case separately.

While the benefits of the adaptive air bag and seat belt system were clearly demonstrated, knee air bag design and tuning challenges were highlighted as well. For the HIII 5F, the KAB was effective for the higher speed load cases but was suppressed for the lower speed cases because of the increase in lower extremity loads predicted if the KAB were to be activated. For the HIII 50M, the KAB was not effective for the higher speed load cases (too soft), nor for the MDB25 load case (too stiff). However, the KAB was effective for the Pole25 load case.

Given project constraints, the stroking steering column is a key component of the restraint system that was not tuned as part of the ARS. As an energy absorbing element in the overall driver side restraint system, it is conceivable that an advanced steering column whose energy management can be adapted to specific load cases could provide further reduction in the overall occupant injury probability.

9.2   Passenger Side Summary

9.2.1 HIII 5F Passenger

All testing and CAE analysis with the HIII 5F was conducted at the full-forward seating position, with the seat at approximately mid-height according to the current FMVSS No. 208 seating procedure, and the D-ring at the full-up position.

No ARS deployable devices were activated earlier than the corresponding devices in the baseline PVP crash test (or simulation). All ARS and PVP configurations used an early retractor IEA switch time, corresponding to +10 ms after the initiation of the retractor pretensioner to utilize the lowest torsion bar setting.

The ARS PAB used a high-output strategy for all load cases (5 ms delay between primary and secondary stages), resulting in earlier coupling of the ATD at the beginning of the restraint phase.

Table 28 summarizes the recommended ARS configurations for the passenger side HIII 5F occupant. All deployment times are relative to the "air bag stage 1" deployment time to facilitate comparison between load cases.

Table 28 - Recommended ARS Configurations, HIII 5F Passenger

ATD	Crash Configuration	Air Bag PVM Deploy Time (ms)	Knee Air Bag	RPT	LPT Deploy Time (ms)	Retractor IEA Switch Time (ms)	Seat Ramp
HIII 5F	MDB35	40	ON	ON	6	10	ON
HIII 5F	MDB25	40	OFF	OFF	0	10	OFF
HIII 5F	Pole35	30	ON	ON	0	10	ON
HIII 5F	Pole25	35	OFF	ON	0	10	ON

For each of the four load cases, a unique ARS configuration was specified based on the optimization studies. For the MDB-to-vehicle load cases, common PVM time-to-open (TTO) and IEA switch times were specified, indicating a common PAB deployment strategy and seat belt design could be used. The MDB25 load case employed the strategy of suppressing the KAB, RPT and seat ramp, which is consistent with other load cases where the baseline PVP performance left minimal opportunity for improvement. For both lower speed load cases, the KAB was suppressed to avoid inducing lower extremity loads higher than the very low baseline loads observed with the PVP system. This is consistent with the strategy for the HIII 5F driver side.

Figures 65 and 66 summarize the combined OIM-AIS3+ and OIM-AIS2+ calculations for the passenger side HIII 5F ATD.

	MDB35	MDB25	Pole35	Pole25
■ Baseline	0.14	0.06	0.17	0.07
□ ARS	0.12	0.09	0.10	0.09
	Test	Test	Test	Test
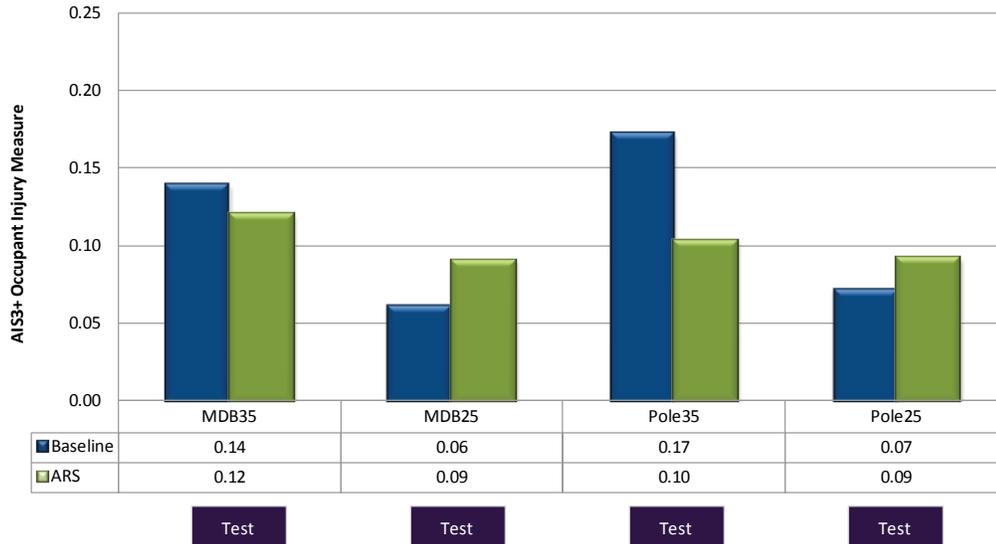
Figure 65 - OIM-AIS3+ Summary, HIII 5FPassenger
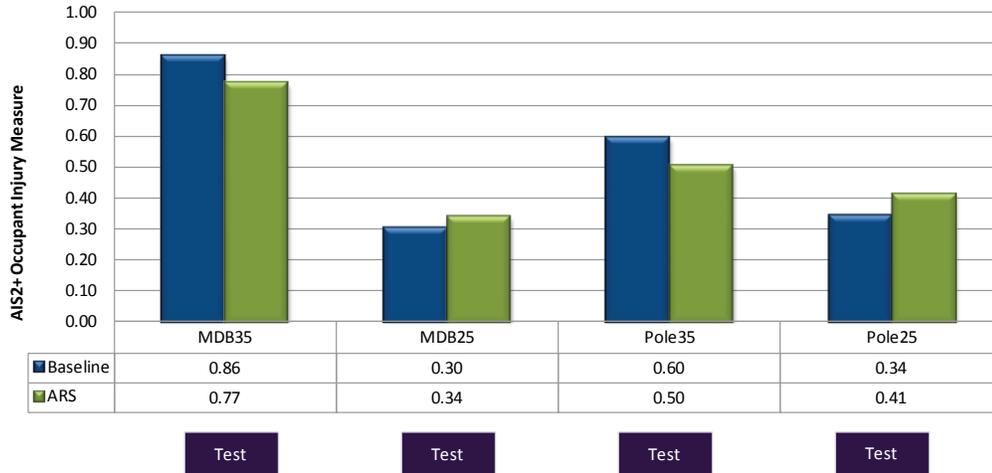
Figure 66 - OIM-AIS2+ Summary, HIII 5F Passenger

For the higher speed MDB and pole load cases, the advanced restraint system showed benefit relative to the baseline PVP restraint system primarily due to a reduction in HIC15. For both higher speed load cases, the ARS KAB was not effective at counteracting the effect of the dynamic intrusion, and so no improvement in lower extremity injury was noted.

For the MDB25 and Pole25 load cases, the baseline PVP injury values were low (OIM-AIS3+ of 6% and 7%, respectively), and the advanced restraint system was not able to show improved performance. Still, the occupant injury measure associated with the ARS remained at low levels (<10% OIM-AIS3+), and all injury levels associated with the ARS were below FMVSS No. 208 limits for the HIII 5F.

9.2.2 HIII 50M Passenger

All testing and CAE analysis with the HIII 50M ATD was conducted at the mid-track / full-down seating position and the D-ring at the full-up position.

No ARS deployable devices were activated earlier than the corresponding devices in the baseline PVP crash test (or simulation).

Table 29 summarizes the recommended ARS configurations for the passenger side HIII 50M occupant. All deployment times are relative to the "air bag stage 1" deployment time to facilitate comparison between load cases.

Table 29 - Recommended ARS Configurations, HIII 50M Passenger

ATD	Crash Configuration	Air Bag PVM Deploy Time (ms)	Knee Air Bag	RPT	LPT Deploy Time (ms)	Retractor IEA Switch Time (ms)	Seat Ramp
HIII 50M	MDB35	54	ON	ON	0	43	ON
HIII 50M	MDB25	54	OFF	ON	0	33	ON
HIII 50M	Pole35	54	ON	ON	0	35	ON
HIII 50M	Pole25	54	ON	ON	0	25	ON

For each of the four load cases, a unique ARS configuration was specified based on the optimization studies. A common PAB PVM deployment time strategy was used, indicating adaptivity in the air bag was not a discriminating parameter for performance optimization across the four load cases for the HIII 50M passenger. However, the adaptivity in the seat belt load limiter was a performance optimization discriminating parameter, considering a unique IEA switch time was specified for each of the load cases. The KAB deployment strategy was consistent with the HIII 50M driver side, namely, the KAB was suppressed for the MDB25 load case to avoid inducing lower extremity loads higher than the low loads recorded by the baseline PVP system.

Figures 67 and 68 summarize the combined OIM-AIS3+ and OIM-AIS2+ calculations for the passenger side HIII 50M ATD.

	MDB35	MDB25	Pole35	Pole25
Baseline	0.21	0.09	0.11	0.08
ARS	0.14	0.07	0.09	0.06
	Test	CAE	CAE	CAE
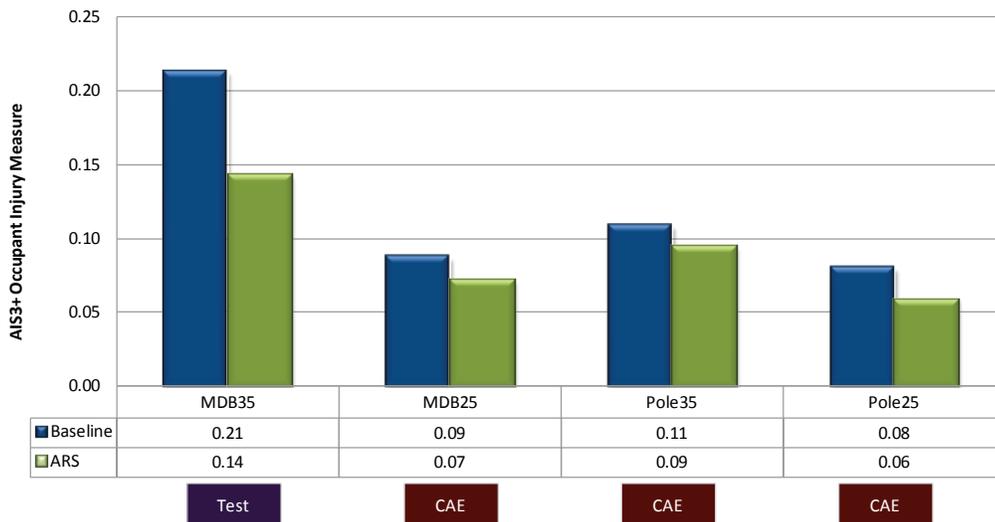
Figure 67 - OIM-AIS3+ Summary, HIII 50M Passenger
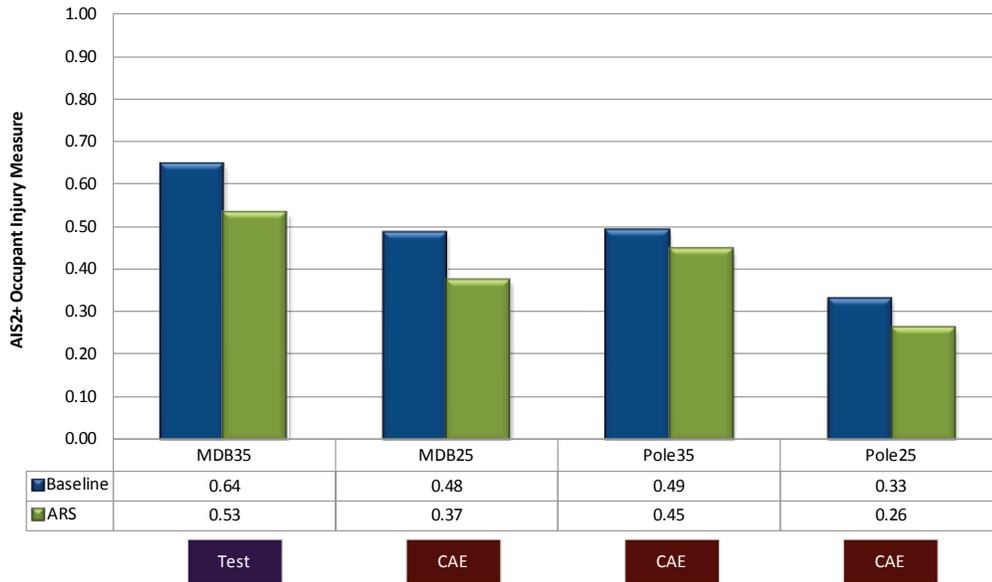
Figure 68 - OIM-AIS2+ Summary, HIII 50M Passenger

The OIM-AIS3+ and OIM-AIS2+ were reduced by the ARS for all load cases, and all injuries were below the limits established by FMVSS No. 208 for the HIII 50M. For the MDB35 load case, the overall benefit (33% reduction in OIM-AIS3+) was due to the reduction in HIC15 compared to the baseline PVP test result. For the other three load cases, the overall reduction was due to chest deflection reductions obtained as a result of tailoring the restraint system stiffness by utilizing the adaptivity in the PAB PVM and IEA seat belt. Due to dynamic intrusion for the higher speed load cases, the KAB did not mitigate lower extremity loads, which was consistent with the HIII 50M. driver side performance.

9.2.3 95th Male Passenger

All CAE simulations with the HIII 95 ATD were conducted at the full-rear/full-down seating position selected by the ARSC for this project. The D-ring was at the full-up position.

There are no established injury risk curves for the HIII 95M tibia loads and thus tibia loads were not assessed.

Table 30 summarizes the recommended ARS configurations for the passenger side HIII 95M occupant. All deployment times are relative to the "air bag stage 1" deployment time to facilitate comparison between load cases.

Table 30 - Recommended ARS Configurations, 95ᵗʰ Male Passenger

ATD	Crash Configuration	Air Bag PVM Deploy Time (ms)	Knee Air Bag	RPT	LPT Deploy Time (ms)	Retractor IEA Switch Time (ms)	Seat Ramp
HIII 95M	MDB35	70	ON	ON	0	60	ON
HIII 95M	MDB25	75	OFF	ON	0	50	ON
HIII 95M	Pole35	65	ON	ON	0	55	ON
HIII 95M	Pole25	65	ON	ON	6	55	ON

For each of the four load cases, a unique ARS configuration was specified based on the optimization studies. A common PVM deployment time and IEA switch time strategy was used for the vehicle-to-pole load case, indicating adaptivity in the air bag and seat belt were not discriminating parameters for performance optimization in this load case. The KAB deployment strategy was consistent with the HIII 95M driver and the HIII 50M passenger, namely, the KAB was suppressed for the MDB25 load case to avoid inducing lower extremity loads higher than the low loads associated with the baseline PVP system simulation.

Figures 69 and 70 summarize the OIM-AIS3+ and OIM-AIS2+ calculations for the passenger side HIII 95M occupant.

	MDB35	MDB25	Pole35	Pole25
Baseline	0.14	0.11	0.19	0.11
ARS	0.14	0.09	0.11	0.09
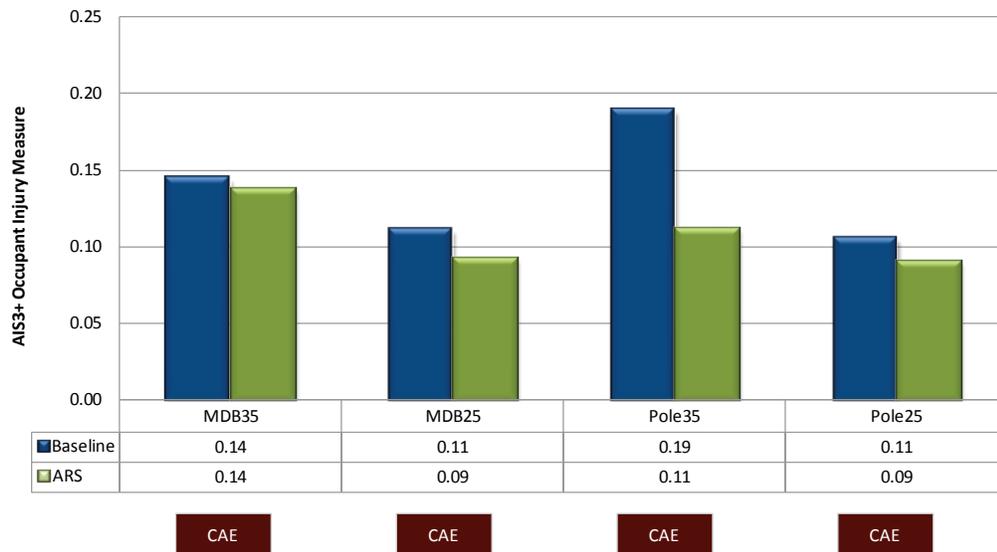
Figure 69 - OIM-AIS3+ Summary, HIII 95M Passenger
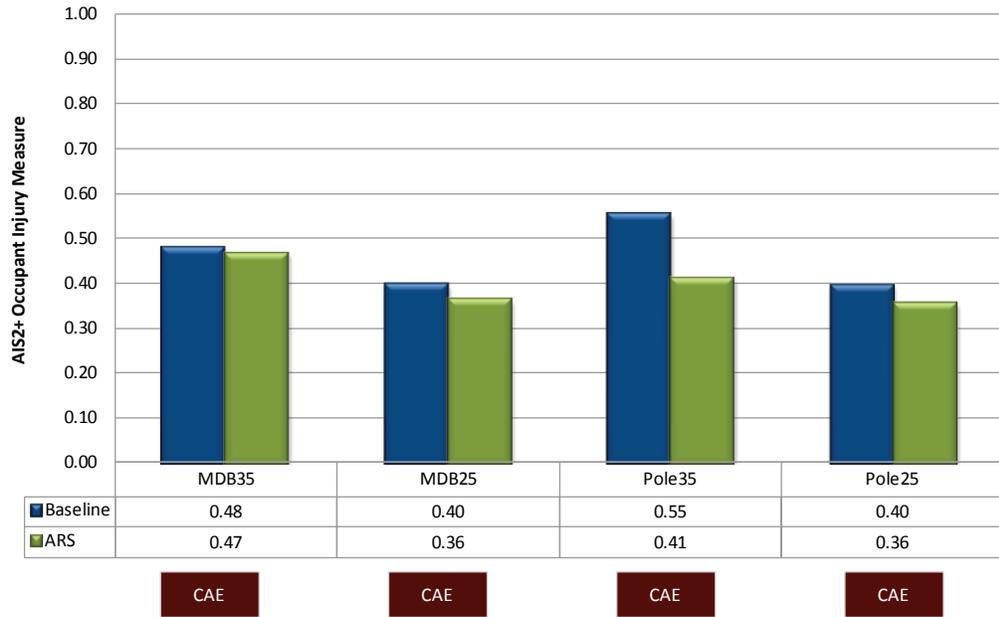
Figure 70 - OIM-AIS2+ Summary, HIII 95M Passenger

For all load cases, the CAE model predicted a reduction in OIM-AIS3+ and OIM-AIS2 with the advanced restraint system relative to the baseline PVP system. The CAE model predicted the ARS would yield reductions in chest deflection for all load cases, while maintaining or reducing the generally low levels of injury for the other body regions relative to the baseline. The largest improvement occurred in the Pole35 load case in which the ARS yielded a large reduction in HIC relative to the baseline PVP restraint system. The KAB was ineffective at counteracting the effect of intrusion in the MDB35 load case.

9.2.4 Passenger Summary

Table 31 summarizes the recommended ARS configuration for all twelve passenger side load cases. All deployment times are relative to the "air bag stage 1" deployment time to facilitate comparison between load cases.

Table 31 - Recommended ARS Configurations, Passenger

ATD	Crash Configuration	Air Bag PVM Deploy Time (ms)	Knee Air Bag	RPT	LPT Deploy Time (ms)	Retractor IEA Switch Time (ms)	Seat Ramp
HIII 5F	MDB35	40	ON	ON	6	10	ON
HIII 5F	MDB25	40	OFF	OFF	0	10	OFF
HIII 5F	Pole35	30	ON	ON	0	10	ON
HIII 5F	Pole25	35	OFF	ON	0	10	ON
HIII 50M	MDB35	54	ON	ON	0	43	ON
HIII 50M	MDB25	54	OFF	ON	0	33	ON
HIII 50M	Pole35	54	ON	ON	0	35	ON
HIII 50M	Pole25	54	ON	ON	0	25	ON
HIII 95M	MDB35	70	ON	ON	0	60	ON
HIII 95M	MDB25	75	OFF	ON	0	50	ON
HIII 95M	Pole35	65	ON	ON	0	55	ON
HIII 95M	Pole25	65	ON	ON	6	55	ON

As was the case with the driver, the specified range of PVM deployment times and IEA switch times for each of the occupants highlights the potential benefit of pre-crash sensing technology that can discriminate among occupant sizes and seating positions for these load cases.

Figures 71 and 72 summarize the OIM-AIS3+ and OIM-AIS2+ calculations for all passenger occupants.
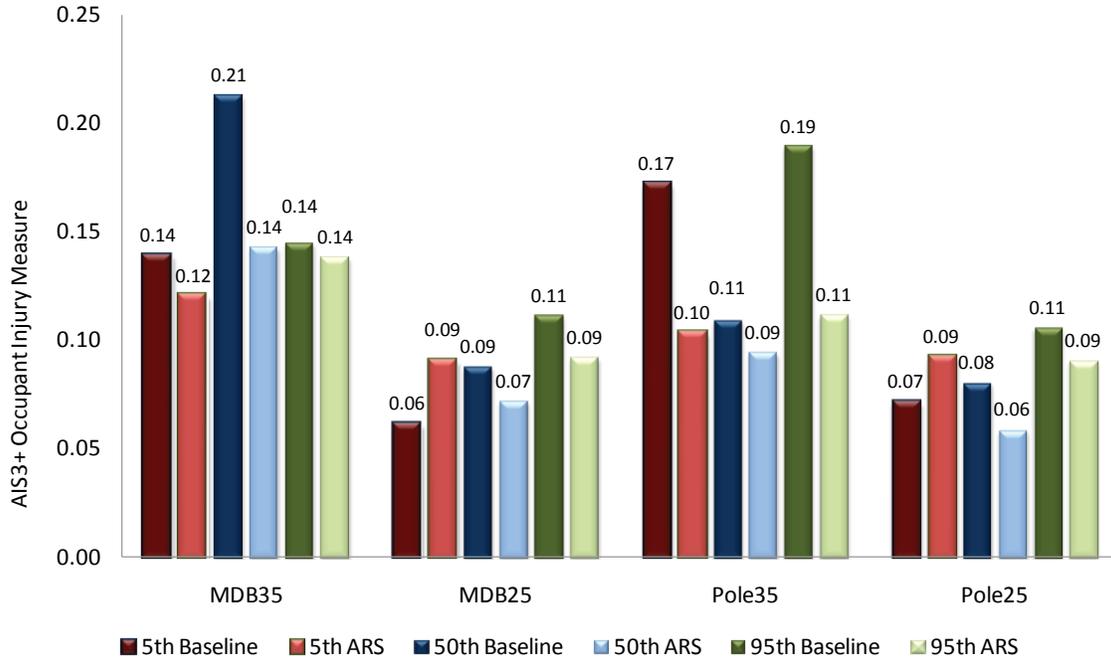
Figure 71 - OIM-AIS3+, PVP Versus ARS, All Front-Outboard Passengers
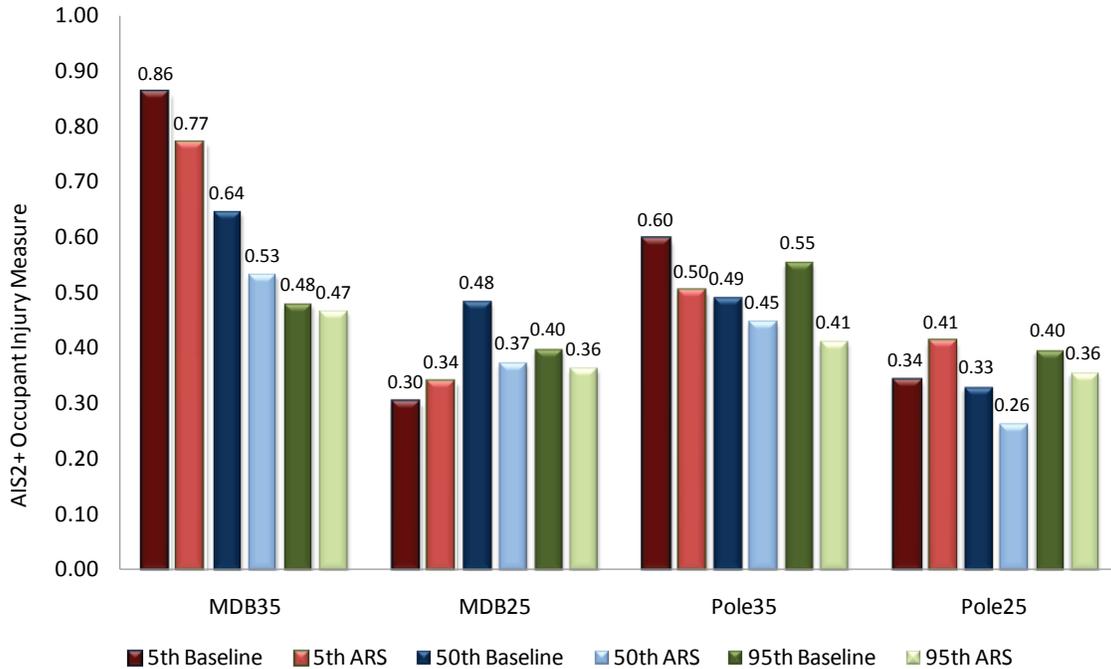
Figure 72 - OIM-AIS2+, PVP Versus ARS, All Front-Outboard Passengers

These figures illustrate the effectiveness of the advanced restraint system across all occupants and load cases. At the AIS3+ and AIS2+ levels, improvement was achieved for ten of twelve load cases. The two exceptions were the HIII 5F MDB25 and Pole25 load cases for which the baseline PVP result already predicted a low risk of injury. In these cases, the ARS still achieved an OIM-AIS3+ <10%. The ability to improve the performance across a diverse set of load cases illustrates the potential benefit of an adaptive restraint system, where system parameters can be tuned to each load case separately.

The passenger side KAB was generally not as effective as the driver side KAB. This could at least partly be attributed to the passenger side occupant compartment geometry, which placed the ATD's left knee in close proximity to the center console. The layout geometry was such that the ATD's left knee consistently loaded the inboard edge of the knee air bag cushion, which increased the chance for strike-through using a conventional KAB design.

10   Summary

Two unique crash test modes, a key deliverable of the ARS project, were identified through field data analysis, an investigation of anticipated pre-crash sensing and advanced restraint system capability, investigative CAE studies, and through discussions with NHTSA. The first crash mode simulated a vehicle-to-vehicle impact by using a MDB-to-stationary vehicle crash configuration, while the second crash mode simulated a vehicle-to-object impact with a centerline pole impact. The execution of the test protocol for the two modes was shown to be generally repeatable. These crash modes were successfully used to assess the potential benefit of an advanced restraint system capable of being tailored within a single project vehicle environment through the use of pre-crash information.

In the vehicle testing and CAE assessments, the baseline PVP restraint system performed well, making it challenging to demonstrate improved occupant performance with the advanced restraint system in all load cases. Nevertheless, the overall occupant injury reduction benefit with a tailorable advanced restraint system was demonstrated for both test modes at the higher impact speeds, whereas for the lower speed conditions, the baseline versus advanced restraint system performance was comparable with an overall benefit not clearly shown. Regional injury metrics for the head, chest and lower extremities were not in all cases lower than the measured baseline responses, and for higher energy tests, intrusion limited the ability of the advanced restraint system to improve the lower extremity performance results.

By scope and definition, this project is limited by the test and analysis conducted and crash injury data collected as well as conclusions drawn from prior engineering studies and field accident data. For example, the baseline PVP was the only vehicle architecture evaluated. Thus, the applicability of these results to other vehicles architectures across the fleet is unknown. Also, vehicle manufacturers' consider structural response, compartment / occupant packaging and interior component construction and these are tuned coincidently for several crash modes with the restraint performance tuned and optimized accordingly. Thus, the "retrofitting" of hardware onto the existing project vehicle architecture will limit the potential benefit of the restraint system configuration evaluated. In addition, only one seat adjustment position was investigated for each occupant size. A different seating adjustment for a given load case may have led to a different recommended ARS configuration, and the performance difference between the baseline PVP restraint system and the advanced restraint system may also have been different. This limits the extrapolation of the potential benefits of the advanced restraint system in terms of estimating the number of injuries prevented in the field. Significantly more research, test and field data analysis of baseline vehicle restraints systems available to consumers today is necessary to extrapolate and predict overall real-world benefit potential with advanced restraint systems.

The advanced restraint system was tailored for each load case under the assumption that the occupant, crash type, and crash speed could be discriminated. Pre-crash input and the sensor algorithms required for implementation in a vehicle were assumed and accounted for in the project pre-test set ups. However, the pre-crash sensing technologies and

software needed to achieve this discrimination, and an assessment of their capability and reliability, was beyond the scope of this project and requires further research.

In addition, the MDB-to-vehicle test procedure may not be applicable to the full range of light vehicles and may present some challenges to existing testing facilities. Further investigation is needed to determine whether refinements to the test method are warranted.

The ARS Project met its deliverables and also provided tangible occupant performance data through the use of unique test modes and advanced restraint system configurations. Furthermore, research data was collected which could provide a foundation for future research in this area.

11   References

Insurance Institute for Highway Safety. (2009). *Status Report, 44*(2), p. 3.

National Highway Traffic Safety Administration. (2008). "Consumer Information; New Car Assessment Program, Docket No. NHTSA-2006-26555, Final Decision Notice." *Federal Register* 73:134 (11 July 2008) p. 40016.

DOT HS 811 794A
July 2013

U.S. Department
of Transportation

**National Highway
Traffic Safety
Administration**

NHTSA
www.nhtsa.gov